Phenotypic Models of T cell Activation

Melissa Lever

Linacre College

University of Oxford

A thesis submitted for the degree of

Doctor of Philosophy

Michaelmas 2015

Acknowledgements

The path to completing a PhD is diverging and intricate, not too dissimilar to the signal transduction network of my study. I would like to express my gratitude to the many people and institutions that have helped me along the way.

I thank the Systems Biology DTC for facilitating my venture into biology, and the EPSRC for providing funding.

I would also like to thank my supervisor Omer Dushek for providing immense support, guidance and energy for the project at all times. I would also like to thank my co-supervisor Anton van der Merwe for providing indispensable expertise on the biological and experimental aspects on the project. Thanks also go to my co-supervisor Philip Maini for his mathematical guidance. I thank the Dunn School of Pathology for the stimulating work environment and the members of the Dushek and van der Merwe labs for their support and lively company. Special thanks go to Hong-Sheng Lim for tirelessly teaching me how to tackle the unpredictable world of wet lab experiments.

My time at Oxford would not have been complete without the fantastic assortment of people, met through Linacre College and beyond, that I have become friends with along the way. I have been further enriched through a diverse assortment of extra-curricular activities, and a special mention goes to the Oxford Ashtanga community and the Samatha sangha.

Last, but certainly not least, I thank my parents for their unwaivering support and love.

Contributions

The experimental results in this paper were produced in collaboration with Hong-Sheng Lim (HSL) and Ann Tivey (AT). The contributions they have made to the figures in this thesis are mentioned below:

Measurement of binding kinetics	Fig. 4.3, Fig. 4.3, Table 4.1.	HSL, AT and ML
Transduction of Jurkat and Primary T cells	Fig. 4.4.	HSL and ML
Stimulation of Primary T cells	Fig. 4.5 c,d, Fig. 4.7.	HSL
Peptide immobilisation	Fig. 4.6 c,d.	HSL
Stimulation of Jurkat T cells	Fig. 4.8 a,b, Fig. 4.9.	HSL

All figures in Chapter 2 are adapted from the paper: Phenotypic models of T cell activation. Lever et al. *Nature Reviews Immunology* 14, September 2014.

Abstract

T cells are important immune cells that initiate and regulate immune responses to cell surface antigens. The productive binding of T cell receptors (TCRs) to cell surface antigens initiates a signal transduction cascade within the T cell that results in T cell effector functions. It is established that the dose of antigen and the binding parameters between TCRs and antigen determines the functional response of the T cell. Although much progress has been made to identify the molecules that constitute the intracellular signalling network, it remains unclear how these molecules interact with each other to convert antigen concentration and binding paramters into a downstream response. A mathematical model of T cell activation can provide insight into this network, however despite extensive study, there is still no conclusive model.

We have taken a phenotypic modelling approach to study T cell signalling. We begin by reformulating the existing models of T cell activation in the literature under a consistent framework so that they can be categorised. This analysis reveals that detailed, quantitative studies of T cell activation are required to test the models. We address this by using a high affinity T cell receptor system to generate dose-response data. The antigens have a 10^5 range in affinity for the TCR and are presented over a very wide range of concentrations. The dose-response assays show that there is an optimal affinity at low antigen dose, and the dose-response profiles can be seen to decrease at high antigen doses. We then generate simple a model that can exhibit these phenotypes, which we term the kinetic proofreading with limited signalling coupled to an incoherent feed forward motif model.

The structure of this model has implications for the structure of the T cell signalling network. The model indicates that there is a mechanism that causes activated TCRs to become inert on a timescale of around ten minutes, which we attribute to their internalisation and down-modulation. The incoherent feed forward motif suggests two parallel inhibitory and activatory pathways within the T cell that both act on a downstream molecule. Further research must be done to identify the molecules involved in this motif.

Contents

List of Figures

List of Abbreviations

A	alanine
AP1	activator protein-1
APC	antigen presenting cell
ATF	activating transcription factor
β_{2M}	β2 microglobulin
BCL10	B cell leukemia/lymphoma
C	cysteine
Ca^{2+}	Calcium
CAR	chimeric antigen receptor
CARMA1	(CARD)-containing MAGUK protein
CBM	CARMA1-BCL10-MALT1
CDR	complementary determining region
C_N	amount of bound TCR in the signalling-competent state at equilibrium
Csk	c-terminal Src kinase
C_T	amount of bound pMHC-TCR complex at equilibrium
DAG	diacylglycerol
DC	dendritic cell
DMSO	dimethyl sulfoxide
DNA	deoxyribonucleic acid
DTT	dithiothreitol
EC_{50}	ligand dose required for half the $E_{\max}$
$E_{\max}$	maximal response from a ligand in a dose-response assay
E. coli	*Escherichia coli*
EDC	1-ethyl-3- (3-dimethylaminopropyl) carbodiimide

ELISA . . . . . enzyme-linked immunosorbent assay

EDTA . . . . . ethylenediaminetetraacetic acid

ERK . . . . . extracellular signal-regulated kinase

FBS . . . . . fetal bovine serum

FFL . . . . . feed forward loop

FPLC . . . . . fast protein liquid chromatography

G . . . . . glycine

GADS . . . . . GRB2-related adapter downstream of Shc

GRB2 . . . . . growth factor receptor-bound protein 2

GTP . . . . . guanosine triphosphate

H . . . . . histidine

I . . . . . isoleucine

IκB . . . . . inhibitor of κB

IS . . . . . immunological synapse

IKK . . . . . inhibitor of NF-κB kinase

IL . . . . . interleukin

IFN-γ . . . . . interferon-γ

IP$_3$ . . . . . inositol 1,4,5-triphosphate

ITAM . . . . . immunoreceptor tyrosine-based activation motif

Itk . . . . . IL-2-induced tyrosine kinase

JNK . . . . . Jun amino-terminal kinase

$K_{\mathbf{D}}$ . . . . . dissociation constant = $k_{\text{off}}/k_{\text{on}}$

$k_{\mathbf{off}}$ . . . . . off-rate

$k_{\mathbf{on}}$ . . . . . on-rate

L . . . . . leucine

LAT . . . . . linker for activation of T cells

LB . . . . . lysogeny broth

M . . . . . methionine

MALT1 . . . . . mucosa-associated lymphoid tissue lymphoma translocation protein

MAPK . . . . . mitogen activated protein kinase

MAPKK . . . . . mitogen activated protein kinase kinase

MAPKKK . . . . . mitogen activated protein kinase kinase kinase

MIB2 . . . . . mind bomb-2

MIP-1β . . . . . macrophage inflammatory protein-1β

NaCl . . . . . sodium chloride

MHC . . . . . major histocompatibility complex

Nck1 . . . . . noncatalytic tyrosine kinase

NF-κB . . . . . nuclear factor-κB

NHS . . . . . N-hydroxysuccinimide

NFAT . . . . . nuclear factor of activated T cells

PBMC . . . . . peripheral blood mononuclear cell

PBS . . . . . phosphate buffered saline

PenStrep . . . . . penicillin streptomycin

PI3K . . . . . phosphoinositide 3-kinase

PIP$_2$ . . . . . phosphatidylinositol 4,5-bisphosphate

PKCθ . . . . . protein kinase Cθ

PLC-γ1 . . . . . phospholipase C-γ1

pMHC . . . . . peptide-MHC

PMSF . . . . . phenylmethanesulfonylfluoride

P_T . . . . . total number of pMHC

Q . . . . . glutamine

R . . . . . arginine

RasGRP . . . . . Ras guanyl nucleotide-releasing protein

RNA . . . . . Ribonucleic acid

RU . . . . . response units

S . . . . . serine

scFv . . . . . single-chain variable fragment

SEM . . . . . standard error of the mean

SFK . . . . . Src familiy kinase

SH2 . . . . . Src homology 2

SHP . . . . . SH2-containing phosphatase

SLP-76 . . . . . SH2 domain-containing leukocyte protein of 76kDa

SMAC, c/p/dSMAC . . . . supra-molecular activation complex, central/distal/peripheral-SMAC

SOS . . . . . son of sevenless

SPR . . . . . surface plasmon resonance

τ . . . . . dissociation time $= 1/k_{\text{off}}$

T . . . . . threonine

T_T . . . . . total number of TCR

TAK1 . . . . . TGF-b activated kinase

TCR . . . . . T cell receptor

TRAF . . . . . TNF receptor-associated factor

V . . . . . valine

W . . . . . tryptophan

WT . . . . . wild-type

ZAP-70 . . . . . ζ-chain-associated protein of 70kDa

KING LEAR
Speak.
CORDELIA
Nothing, my lord.
KING LEAR
Nothing!
CORDELIA
Nothing.
KING LEAR
Nothing will come of nothing: speak again.

— Shakespeares's *King Lear*

1 Introduction

Thymus derived lymphocytes, known as T cells, are integral to the immune system. They initiate and regulate immune responses to cell surface antigens and thus can play helpful or unhelpful roles in many clinically relevant processes. These include targeting infections and cancer, as well as allergy, autoimmunity and transplant rejection [1]. T cells detect antigen through T cell receptors (TCRs) on their surface, which are clonotypic. The development of TCR amino acid sequence takes place in the thymus, where a diverse repertoire of non-reactive TCRs is generated. T cell precursors are hematopoietic stem cells that migrate from the bone marrow to the thymus. They undergo a developmental program that involves the semi-random expression of TCRs coupled to selection processes. The TCR genes are assembled from separate variable (V), diversity (D) and joining (J) segments to eventually encode a TCR complex. T cells are then positively selected if the TCR they express can bind to antigen presented by thymic cortical epithelial cells. However if it binds too strongly to antigen they will be negatively selected. The T cells that are selected to leave the thymus will then circulate between the blood and lymphatic system and reside in secondary lymphoid organs [2]. The collective T cell functional response includes changes in gene expression and metabolic reprogramming to result in cell differentiation, proliferation and effector functions, amongst other responses [3]. The precise type of response depends on the strength of TCR stimulus, the subset to which the T cell belongs and the environment within which the T cell is activated [4].

There are many types of T cell, and a major classification is whether a T cell is CD4+ or CD8+, which corresponds to the co-receptor type that the T cell expresses. T cells expressing the CD4 co-receptor can be classified into T helper cells and regulatory T cells (Treg). T helper cells provide help to B cells, which are antibody producing lymphocytes. Once a T helper cell has detected antigen presented by a B cell, the T cell will become activated and secrete cytokines that cause the B cell to proliferate and its progeny to undergo affinity maturation and class-switching of the antibody that they express [4]. T helper cells also activate CD8+ T cells and macrophages [5]. Treg cells by contrast do not activate cells and instead suppress the activity of other T helper cells [5]. T cells that express the CD8 co-receptor are termed cytotoxic T cells. Once a cytotoxic T cell has detected antigen, it will secrete cytotoxic granules that can induce target cells to undergo cell death [4]. Prior to encountering antigen, a T cell is termed a naive cell, which can be CD4+ or CD8+. Antigenic peptides are presented to naive cells by dendritic cells (DCs), which are a type of antigen presenting cell (APC). Once a naive T cell detects an antigen to which it is specific, a signal transduction cascade is initiated within the naive cell. It will then undergo a developmental program to become either an effector or a long-lived memory T cell [6].

A T cell will become activated by presented antigen through the productive engagement of its TCRs with peptide antigens bound to a major histocompatibility complex (pMHC) presented on the surface of an APC. T cells are restricted by the type of MHC molecule they can bind to, which are either MHC class I and MHC class II. The restriction of T cells to MHC class is enforced by the co-receptor during thymic selection. CD4+ T cells recognise MHC class II and CD8+ T cells will recognise MHC class I. The precise response of a T cell will depend on the subset to which the T cell belongs (naive/effector/memory CD4+ or CD8+) and the context of the interaction, which is affected by a host of co-stimulatory and co-inihibitory ligand interactions between the T cell and APC [7].

The signalling machinery within the T cell conveys information of the pMHC-TCR interaction and the local environment to the downstream functional response of the T cell. The signalling cascade has been extensively studied and has yielded the discovery of

many of the molecules that lie in this signalling network. Much progress has been made in understanding which of these molecules interact with each other, the mechanism of their interactions and their spatio-temporal relationship within the signalling cascade [1, 8, 9]. However, this signalling network is not yet completely characterised.

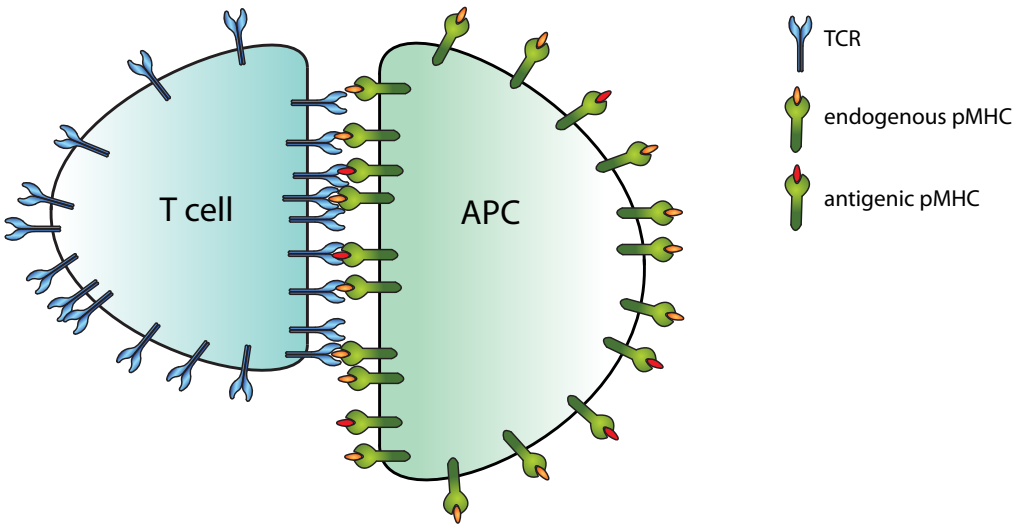

Figure 1.1: Schematic of T cell interacting with an antigen presenting cell: T cells detect antigen presented on an antigen presenting cell (APC) through the engagement of the T cell receptor (TCR) with antigenic peptide presented on the major histocompatibility complex (pMHC). There are around 10,000 TCRs on a T cell surface [10, 11]. Typically a small number of pMHCs on an APC will be antigenic, compared to around 10,000 much weaker binding endogenous pMHCs [12, 13]. A productive interaction results in T cell activation, which can include functional responses such as differentiation, proliferation, cytokine production, and the secretion of cytotoxic effector molecules.

The aim of this thesis is to extend our understanding of the signalling network within T cells through a mixture of theory and experiment. The approach is to develop a minimal model of the T cell signalling network, aided by experiments, to help provide insight into the structure of the signal transduction cascade. In Chapter 2, I outline the experimental method to quantitatively examine how the strength of the pMHC-TCR interaction determines the downstream T cell response. In Chapter 3, I review and synthesise the experimental and mathematical work in the literature that has been done to

explore the phenotype and mechanisms of T cell activation. In Chapter 4, the results of the experiments described in Chapter 2 are shown. In Chapter 5, I show the development of a model that captures the phenotype of T cell activation and reveals the structure of the signal transduction cascade within the T cell. The conclusions are presented in Chapter 6. In the remainder of this Chapter I present the biological background to the system to be studied and explain the motivation for using a phenotypic modelling approach to aid in the understanding of this system. .

1.1 The T cell receptor

1.1.1 The TCR-CD3 complex

The TCR complex relays information from the APC to the T cell by initiating a signal transduction cascade. It consists of the disulphide linked TCR$\alpha\beta$ heterodimer and the associated CD3 subunits. The extracellular portion of the TCR consists of membrane-distal variable (Vα and Vβ) and membrane-proximal constant (Cα and Cβ) immunoglobulin superfamiliy domains. The region that binds to pMHC primarily consists of three complementary-determining regions (CDRs) on each of the Vα and Vβ domains [14, 15]. The TCR contains a transmembrane region and short cytoplasmic segments [16]. The TCR is non-covalently linked with the CD3 complex that has comparatively longer cytoplasmic regions [17, 18]. It consists of the CD3 -δ, -ϵ,-γ and -ζ-chains that associate as dimers ($\epsilon\delta$, $\gamma\epsilon$ and $\zeta\zeta$). Each of the CD3-$\delta/\epsilon/\gamma$-chains contain an immunoreceptor tyrosine-based activation motif (ITAM) on their cytoplasmic domain and the ζ-chain contains three ITAMs, to give a total of ten ITAMs on the TCR-CD3 complex (Fig. 1.2) [4]. The TCR-CD3 complex is unique in possessing a multiplicity of ITAMs, which can be compared to other lymphoid receptors that only contain one-two ITAMs, such as the B cell receptor that contains two. A reason for this abundance could be because different T cell functions, such as development vs effector functions, propagate from distinct ITAMs [19]. The three ITAMs on the ζ-chain have been shown to affect the qualitative response of the transduced signal. The ITAMs have been found to be sequentially phosphorylated by Lck from the membrane-distal to membrane proximal ITAM

[20], and ZAP-70 has been found to bind to these phosphorylated ITAMs with increasing affinities, also from membrane-distal to membrane proximal [21–24]. A quantitative analysis of this ITAM configuration has revealed an emergent ultrasensitivity in the signal response and an increase in potency compared to a configuration that lacks multiple ITAMs, sequential phosphorylation or differential affinities for ZAP-70 [25]. Multiple ITAMs have also been shown to be necessary for T cell development in the thymus because they amplify the signal through the TCR [26, 27].

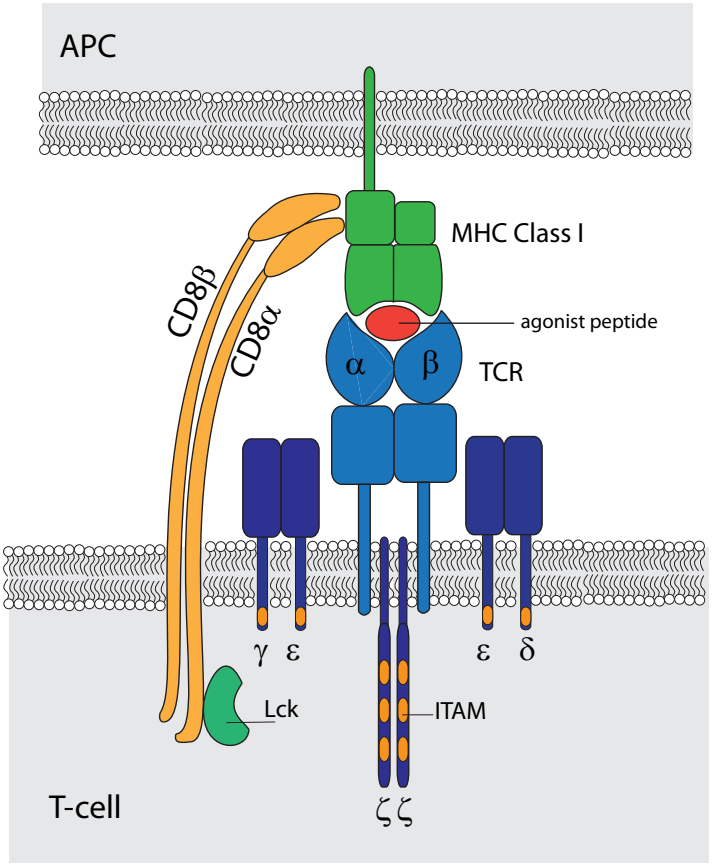

Figure 1.2: TCR-CD3 complex and CD8 coreceptor from CD8+ T cell bound to pMHC: The TCR$\alpha\beta$ heterodimer binds to peptide presented on MHC Class I. The TCR-CD3 complex consists of TCR$\alpha\beta$ and the CD3-δ,-ϵ,-γ and-ζ-chains that contain ITAMs. A signal is transduced through the TCR by the phosphorylation of ITAMs by the kinase Lck. Lck constitutively associates with co-receptors and phosphorylates ITAMs.

1.1.2 The pMHC complex

There are two classes of MHC molecule, and the type of peptide to which a MHC binds relates to the origin of the peptide. The MHC class I molecule associates with peptides that are the result of proteasomal degradation of proteins derived from the cytosol of the cell. These peptides can be derived from self or from intracellular pathogens, and so are often derived from cancer or a virus. The MHC class I molecule consists of an integral membrane heavy chain subunit that noncovalently associates with the $\beta 2$ microglobulin (β_{2M}). The length of peptide that they present is usually 8-10 amino acids. MHC class I molecules are present on almost all nucleated cells in the body [4].

MHC class II molecules associate with peptides that have been endocytosed by the APC. The molecule consists of a heterodimer of α and β transmembrane subunits. MHC class II molecules are displayed by B cells, macrophages, monocytes, DCs and endothelium. The length of peptide presented on MHC class II can have lengths of between 12-24 amino acids [4].

The presentation of antigens does not always follow this pattern however, and this is termed cross presentation. One instance of this is where exogenous proteins are presented by MHC class I molecules. The other case is when endogenous proteins are presented by MHC class II molecules when they have been degraded through autophagy and other processes [28].

There are usually two or three residues on a peptide that anchor it to the MHC for optimal binding. These residues occur with high frequency at specific positions for a given MHC allele and are termed anchor residues [29].

1.1.3 Engineering high affinity T cell receptors

The natural affinity of TCRs for pMHCs is in the range of 1-100μM K_{D} ($K_{\mathrm{D}} = k_{\mathrm{off}}/k_{\mathrm{on}}$) [16]. This low affinity has been a hindrance to methods that attempt to utilise TCRs to detect the expression of specific antigens on target cells. Such applications include detecting quantitative changes in pMHC expression, identification of cross-reactive pMHCs, and immunotherapies that target tumour pMHCs [30, 31]. One method of addressing this is through using multimeric forms of soluble TCR$\alpha\beta$ heterodimers,

which results in an increase in avidity, and therefore dissociation time, of the TCR-pMHC interaction [30]. Another approach is through affinity maturation, which can be engineered by phage display. In this method, soluble TCRs are produced in a stable form by introducing an interchain disulfide bond at the interface between the TCR constant domains (dsTCRs). The soluble dsTCRs are fused to the M13 pIII capsid protein. Libraries of the dsTCRs are then generated by randomising the CDR loops of the dsTCRs. The resulting mutagenised library is displayed to the specific pMHC, and the high affinity dsTCRs are selected. This is repeated over several rounds to produce the desired high affinity TCRs [31]. This directed evolution can result in TCRs with pM K_{D} to their cognate pMHC [32].

1.2 Triggering through the T cell receptor

1.2.1 TCR proximal molecules

Proximal to the TCR-CD3 complex are the co-receptors CD4 and CD8 that augment TCR signalling. Co-receptors stabilise the pMHC-TCR interaction by binding to distinct residues on the MHC molecule from the TCR. They enhance activation by recruiting the co-recepter associated protein tyrosine kinase Lck to the proximity of the TCR-CD3 complex [33, 34]. Lck is a Src familiy kinase (SFK) and it contains several tyrosines that regulate its status of activation. The phosphorylation of an activating tyrosine on its catalytic domain stabilises an open conformation to enable full kinase activity. Phosphorylation of this activatory tyrosine is regulated by transphosphorylation by Lck itself, and it is thought to be dephosphorylated by the transmembrane phosphatase CD45 and cytosolic phosphatases Src homology 2 (SH2)-containing phosphatase (SHP-1) and SHP-2. There is a negatively regulating tyrosine on the C-terminal which is phosphorylated by C-terminal Src kinase (Csk) and dephosphorylated by CD45 [9]. Lck can also interact with ITAMs independently of co-receptors. It is likely that in resting T cells an equilibrium is formed between the different phosphorylation states of Lck [35]. There is disagreement over what percentage of Lck is constitutively active, as well as the extent to which Lck is activated following pMHC-TCR engagement [36,

37]. The phosphorylation of the TCR complex following pMHC engagement results in a downstream signalling cascade that ultimately results in T cell activation, which is discussed in more detail below.

The magnitude of T cell activation through the TCR is modulated by receptors on the T cell surface that bind to ligands on the APC. For example, the costimulatory receptor CD28 and the homologous inhibitory receptor CTLA4 both bind to CD80 [38, 39] and CD86 [40] on the APC.

1.2.2 The mechanism of TCR triggering

Upon engagement of TCR with antigenic pMHC, biochemical changes occur in the cytoplasmic tail of the CD3 chains, including phosphorylation of tyrosine residues in ITAMs by SFKs Lck and Fyn. This process is termed TCR triggering, and there are various theories as to what the primary mechanism of this process could be. Some mechanisms propose that the ITAM motifs become more accessible through conformational change of the TCR-CD3 complex upon pMHC engagement [41]. One theory prosposes that the tyrosines on ITAMs are buried in the inner leaflet of the plasma membrane and become accessible following pMHC engagement. However, the many reports that ITAMs are constitutively phosphorylated contradicts this [42].

Other mechanisms of TCR triggering propose a redistribution of the TCR-CD3 complex with respect to kinase and phosphatase proteins associated at the membrane. One such model is the kinetic segregation model, which posits that bulky phosphatases, such as CD45, are excluded from the pMHC-TCR contact interface due to their large ectodomains. This allows phosphorylation of ITAMs by tyrosine kinases to be maintained, which would be sufficient for TCR triggering [41].

1.2.3 TCR triggering to LAT assembly

TCR triggering begins with the phosphorylation of the two tyrosines in ITAMs of the TCR-CD3 complex by Lck and Fyn. The phosphorylated tyrosines serve as docking sites for the cytoplasmic tyrosine kinase ζ-chain-associated protein of 70kDa (ZAP-70), which binds through its tandem SH2 domains. ZAP-70 is then phosphorylated by Lck, followed

by transautophosphorylation, which activates it. Although the TCR-CD3 complex has no intrinsic enzymatic activity, the recruitment and activation of ZAP-70 allows the TCR-CD3 complex to phosphorylate target molecules. These include key adaptor molecules linker for activation of T cells (LAT) and SH2 domain-containing leukocyte protein of 76kDa (SLP76). These molecules facilitate the spatio-temporal organization of effector molecules to activate multiple branching signalling pathways [1]. LAT is a transmembrane protein that contains 9 tyrosines on its cytoplasmic domain. The phosphorylation of LAT allows key molecules to bind, including phospholipase C-γ1 (PLC-γ1), phosphoinositide 3-kinase (PI3K), and adapter molecules growth factor receptor-bound protein 2 (GRB2) and GRB2-related adapter downstream of Shc (GADS). GADS binds to SLP-76 and recruits SLP-76 to the phosphorylated LAT complex through its SH2 domain [43]. The N-terminal region of SLP-76 contains 3 tyrosines that when phosphorylated, allow the molecules VAV1, noncatalytic tyrosine kinase (Nck1) and interleukin-2 (IL-2)-induced tyrosine kinase (Itk) to bind via their SH2 domains. PLC-γ1 is then activated by Itk [1].

The dependency of ZAP-70 for T cell activation has been examined in a recent study using mice that express a mutant form of ZAP-70 that can have its catalytic activity blocked by a small-molecule inhibitor [44]. It was found that naive, effector and memory CD8+ cells require ZAP-70 activity for activation, however Tregs do not need it to perform suppressive activity.

1.2.4 Immunological synapse formation

Naive T cells in lymph nodes rapidly scan APCs for antigen, encountering an APC every 3 minutes [45]. Upon antigen recognition, TCR signalling causes the termination of migration and a stable interaction is formed between the T cell and APC by an adhesion domain that consists of adhesion molecules and integrins [46]. This results in the formation of the immunological synapse (IS), which consists of an assembly of pMHC-TCR, co-stimulatory/inhibitory and adhesion interactions at the contact interface between the T cell and APC. Early imaging studies found that the microtubule-organizing center and the Golgi apparatus were directed to the interface between the T cell and APC [47]. This cytoskeletal rearrangement is thought to be necessary for sustained signalling

from the TCR [48]. It was later found that molecules within the IS are organised into distinct domains, which are called supra-molecular activation complexes (SMACs). The central-SMAC (cSMAC) is enriched with TCRs. The peripheral-SMAC (pSMAC) forms a ring around the cSMAC and is dominated by adhesion molecules including leukocyte function-associated antigen-1 (LFA-1). Outside the pSMAC is the distal-SMAC (dSMAC) that consists of molecules with large ectodomains, such as CD45 [49]. Later studies conducted at a higher resolution found that despite the high concentration of TCRs in cSMAC, pMHC-TCR signalling takes place in the pSMAC, where the TCRs form microclusters. After engagement, TCR microclusters translocate to the cSMAC [50].

1.3 Diversification of signalling pathways from LAT

The phosphorylation and activation of PLC-γ1 by Itk at the LAT signalsome propagates several signalling pathways that result in changes in gene expression, amongst other effects. These are the Calcium pathway, the mitogen activated protein kinase (MAPK) pathway, and the nuclear factor-κB (NF-κB) signalling pathway.

1.3.1 The Calcium signalling pathway

Once PLC-γ1 is activated, it hydrolyzes phosphatidylinositol 4,5-bisphosphate (PIP_2) to produce inositol 1,4,5-triphosphate (IP_3) and diacylglycerol (DAG). The production of IP_3 leads to the Calcium (Ca^{2+}) signalling pathway: IP_3 triggers release of Ca^{2+} stores from the endoplasmic reticulum (ER) into the cytoplasm. The resulting decrease of Ca^{2+} concentration in the ER triggers an influx of Ca^{2+} into the cell. The result is to elevate the intracellular Ca^{2+} concentration, which leads to activation of calcineurin and its target transcription factor nuclear factor of activated T cells (NFAT). The phosphatase activity of calcinuerin is activated by its binding of Ca^{2+}-calmodulin. The subsequent dephosphorylation of NFAT reveals the nuclear localisation sequence and the NFAT proteins then translocate to the nucleus [51]. NFAT interacts with other transcription factors to bring about transcription of genes important for T cell activation, regulation and differentiation [52]. The most well studied of these is the interaction of NFAT and

activator protein-1 (AP-1) to produce transcription of genes for production of IL-2 [1]. AP-1 refers to dimeric transcription factors composed of Jun, Fos or activating transcription factor (ATF). It has been shown that NFAT activity in the absence of AP-1 results in a lack of IL-2 production and anergy, which is where the T cell is resistant to activation [1].

1.3.2 The MAPK signalling pathway

The MAPK signalling pathway is dependent on Ras, which is a guanyl nucleotide-binding protein. It is only active in the guanosine triphosphate-bound (GTP-bound) state, which is enabled by guanine nucleotide exchange factors son of sevenless (SOS) and Ras guanyl nucleotide-releasing protein (RasGRP). Ras is suppressed by GTPase-activating proteins. RasGRP is recruited to the membrane by binding to DAG via its C1 domain, which is necessary for its function [53]. RasGRP is then phosphorylated by PKCθ. SOS is constitutively bound to GRB2, through which it is recruited to LAT [1]. Once Ras is activated, it activates the serine-theronine kinase Raf-1, which is a MAPK kinase kinase (MAPKKK). Raf-1 then phosphorylates and activates MAPK kinases (MAPKKs). The MAPKKs in turn phosphorylate and activate MAPKs, which include the MAPK's extracellular signal-regulated kinase 1 (ERK1) and ERK2, p38 and Jun amino-terminal kinase (JNK) [53]. The MAPKs phosphorylate a range of proteins in the cytosol and the nucleus to bring about changes in protein function and gene expression [54]. Significant targets of MAPKs are transcription factors for cytokine and cytokine receptor expression including AP-1 and early growth response family members [55]. As noted previously, the Ca^{2+} and MAPK signalling pathways are integrated through the binding of NFAT to AP-1 in the nucleus [1].

1.3.3 The NF-κB signalling pathway

The third important signalling pathway is the NF-κB pathway, which propagates from the activation of protein kinase Cθ (PKCθ) that follows from the production of DAG. PKCθ can also be activated through an alternative pathway that is dependent on the engagement of the cell surface costimulatory receptor CD28 by CD80 or CD86. However, it is possible for the NF-κB pathway to be activated independent of CD28 costimulation [56]. The

classical NF-κB pathway proceeds as follows: the production of DAG stimulates PKCθ and it is recruited to the IS and activated. Activated PKCθ can phosphorylate caspase recruitment domain (CARD)-containing MAGUK protein (CARMA1), which causes it to undergo a conformational change and cluster. Clustered CARMA1 nucleate the formation of a B cell leukemia/lymphoma (BCL10) polymer, which binds to mucosa-associated lymphoid tissue lymphoma translocation protein (MALT1) to form very large CARMA1-BCL10-MALT1 (CBM) complex. Formation of CBM complex leads to the recruitment and activation of inhibitor of NF-κB kinase (IKK). The exact mechanism of this is unknown but it is thought to involve polyubiquitination of IKKγ by the ubiquitin ligases TNF receptor-associated factor (TRAF6), TRAF2 or mind bomb-2 (MIB2) [56, 57]. IKKβ is then phosphorylated by TGF-b activated kinase (TAK1), which enables it to phosphorylate inhibitor of κB (IκBα). This initiates the proteasomal degradation of IκBα, which allows the NF-κB heterodimer to translocate to the nucleus and activate gene transcription. NF-κB is responsible for T cell proliferation and differentiation [56]. It has been found to bind to the promoter for IFN-γ alongside NFAT [58].

The core DNA motif that NFAT recognises resembles half the DNA motif that κB binds, which means that there are some κB binding motifs to which NFAT can also bind [59]. This has been demonstrated with the crystal structure of NFAT bound to the IL8 promoter that showed NFAT dimers to bind the κB site at distinct contacts to the NF-κB dimer [60].

1.3.4 PI3K pathway

An alternative pathway for the metabolism of phosphoinositides is mediated by phosphoinositide-3 kinases (PI3Ks), which are lipid kinases that act by phosphorylating membrane phosphatidylinositol (PtdIns) and its by-products on the 3'-OH position of the inositol ring. The resultant products are PtdIns-3-phosphate, PtdIns-4,5-biphosphate (PIP_2) and PtdIns-3,4,5-triphosphate (PIP_3). Mammalian PI3Ks comprise a p110 subunit, which is catalytic, and a p85 subunit through which it associates with the plasma membrane. The p85 subunit contains an SH2 domain that binds to phosphorylated adaptor molecules, such as LAT, as well as 3'-phosphoinositides that it has generated. Molecules can bind to PIP_2

and PIP_3 through their PH domains, which are globular domains of Ĩ20 amino acids that bind phospholipids with high affinity and specificity [61, 62]. This includes Ikt, the serine/threonine kinases Akt, and phosphoinositide-dependent protein kinase 1 (PDK1). Akt is fully activated when it is phosphorylated by PDK1 and mTOR complex 2 (mTORC2), a complex that contains the serine/threonine kinase mTOR and other proteins. This allows Akt to translocate from the membrane to the cytosol and nucleus where it can regulate signalling pathways that control cell proliferation, metabolism and differentiation[63] .

PI3K is activated following TCR-pMHC engagement, although the mechanism is unclear. Its activation precedes the calcium flux through the T cell [64, 65]. It has been found after a T cell comes into contact with an APC, PIP_3 accumulates at the contact zone and it is also found throughout the plasma membrane [64, 65]. The production of PIP_3 is sustained for 6-9 hours [65]. Inhibition of PI3K has been found to only mildly affect IS formation and IL-2 production, indicating that it operates on a distinct pathway to these processes [65]. The PI3K pathway has been found to influence the expression of the transcription factor Forkhead box P3 (FOXP3), which is a marker for Treg cells. It has been found that sustained activation of this pathway results in upregulation of expression of FOXP3, which is reversed when PI3K is inhibited [66]. The pathway also effects the Forkhead box O (FOXO) transcription factor FOXO1, which promotes cell cycle arrest. Activation of the PI3K pathway results in exclusion of FOXO1 from the nucelus to the cytosol, which is dependent on Akt [67].

1.3.5 Cytoskeletal rearrangement and the inside-out integrin signalling pathway

T cells rapidly scan the lymph node for antigen presented by other cells. On encountering antigen, migration is decelerated [68] which is allows the T cell to form a conjugate with the APC and an immunological synapse to sustain signalling. This 'stop signal' [69] is initiated by TCR triggering and is brought about by reorganization of the cytoskeleton [68]. Actin polymerisation takes place at the T cell-APC interface to generate a lamellapodial sheet, which is an actin projection, over the surface of the APC. This is mediated actin nucleating factors, one of which is the actin related protein 2/3 (Arp2/3)

complex. Once activated, Arp2/3 stimulates the growth of branched actin arrays [3]. The nucleation activity of Arp2/3 is enhanced by nucleation promoting factors such as Wiskott-Aldrich syndrome protein (WASp) and WASp family-verprolin homologous protein 2 (WAVE2). The activation of Arp 2/3 occurs at the LAT/SLP-76 signalsome, where Nck recruits WASp. The guanine nucleotide exchange factor VAV1 activates the Rho family GTPases, including Cdc42 and Rac1. WASp is activated by the GTPase Cdc42, and WAVE2 regulated by Rac1 [70].

TCR triggering results in an increase in cell adhesion, which is mediated primarily by the integrin LFA-1. This is an example of inside-out signaling, where the signalling mechanisms originate inside the cell and are transmitted to the extracellular domain of the receptor [71]. The PLCγ pathway results in LFA-1 upregulation by activating the GTPase Ras proximity 1 (Rap1). Rap1 belongs to Ras superfamiliy of GTPases. Its activation through the PLCγ pathway follows from the production of DAG from the PLCγ mediated hydrolysis of PIP_2. DAG recruits serine-threonine kinases such as PKCθ to phosphorylate the guanine nucleotide exchange protein RapGEF2 to trigger activation of Rap1 [72]. Rap1 is active in the GTP-bound state and inactive when GDP-bound. Conversion to the active state is mediated by guanine nucleotide exchange factors that enable Rap1 to release GDP in order to bind to GTP. The hydrolysis of bound GTP is accelerated by guanine nucleotide exchange factors (GEFs) [73]. PKCs can directly affect integrin signalling by phosphorylating the beta-chain of LFA-1, which alters the interaction of LFA-1 with cytoskeletal proteins [72] . It has been found in Treg cells that the activation of Rap1 is not dependent on ZAP-70 catalytic activity, which indicates redundancy in the integrin pathway. It was found that the phosphorylated tyrosines on ZAP-70 can serve as a scaffold for GEFs to activate Rap1 [44].

TCR triggering also results in the polarisation of the microtubule organising centrer (MTOC), the microtubule skeleton and Golgi apparatus to the IS. This enables the secretion of cytokines and cytotoxic granules towards to the APC, which travel along microtubules and are directed towards target cell. These processes have been found to be dependent on Lck, Fyn, ZAP-70, LAT, SLP-76, VAV1 and the Calcium flux [74].

1.4 Functional effects of signal transduction through the TCR

The signalling cascades described above demonstrates how information of the engagement at the cell membrane between TCRs and pMHCs is relayed to the T cell nucleus through a complex set of interactions mediated by signalling proteins. This signal transduction cascade is not linear but instead branches and diversifies via adaptor proteins such as LAT. Furthermore, there are many negative and positive feedback loops along the signalling pathways that can alter the signal amplitude [75]. These signalling processes culminate in the nucleus, where transcription of genes is activated to produce cytokine secretion and other functional responses, the magnitude of which corresponds to the sensitivity and specificity of the T cell functional response to antigen.

1.4.1 Upregulation of expression of genes and surface molecules

As described above, various transcription factors are activated in response to distinct pathways. The MAPK pathway regulates the transcription factors AP1 and Egr familiy members, the Calcium pathway leads to the activation of NFAT, and the activation of PKCθ results in the activation of NF-κB. These transcription factors induce the expression of genes encoding for cytokines and cytokine receptors. The activation of PLCγ leads to the integrin signalling pathway and the upregulation of LFA-1 on the cell surface.

There are also transcription factors that are activated that control T cell development. For example, the PI3K pathways regulates FOXP3 expression, which is a marker for Treg cells. The activation of the mTOR complex mTORC1 results in the activation of transcription factors that influence T cell differentiation, including T-bet and Eomesodermin (Eomes). T-bet promotes Th1 cell development in CD4+ cells and cytotoxic effector functions in CD8+ cells [76]. Eomes has been associated with differentiation into memory subsets in CD8+ cells [76]. The mechanism of how mTORC1 is activated is currently unclear, but it is known to be regulated in response to increase in expression of L amino acid reporters after TCR engagement [72].

1.4.2 Metabolic reprogramming

T cell activation results in metabolic reprogramming of the cell. The activation of naive T cells results in clonal expansion of antigen specific T cells and differentiation into effector cells. Effector cells utilise aerobic glycolysis for energy, while naive, memory and Treg cells rely on oxidative phosphorylation [77]. The metabolic demands of effector cells are high in order to support the production of effector functions, growth and proliferation [78]. The supply of glucose to the cell is therefore increased to meet this demand by upregulating surface expression of glucose transporter GLUT1 [77].

Transcription factors have been identified that control the reprogramming of metabolism during effector T cell differentiation. It has been found that the transcription factor Myc is necessary for the increase in expression of glucose and glutamine transporters following TCR engagement. It also upregulates transferrin receptors, which are necessary for iron transport into the cell. The expression of Myc is digital, and the percentage of cells positive for Myc increases with the affinity of the pMHC-TCR interaction, as well as the dose [78]. The transcription factor IRF4 has been found to regulate the expression of molecules required for aerobic glycolysis. Its level of expression is determined by the affinity of the pMHC-TCR interaction, as well as the dose [79]. Effector T cells must increase their uptake of amino acids in order to support protein synthesis and other cellular processes. The uptake of leucine in particular is important because leucine availability regulates mTORC1 [80]. The uptake of leucine, which is a large neutral amino acid (LNAA) is mediated by System L amino-acid transporters that transport LNAAs across the plasma membrane. This process is controlled by triggering through the TCR, as well as the prescence of IL-2 . Uptake of leucine is necessary for mTORC1 activity as well as the functioning of metabolic machinery for naive cells to become effector cells. The transport activity of System L amino acid transporters is dependent on calcineurin mediated signalling pathways [80].

These studies highlight how cell metabolism is altered in response to TCR signalling and can support and modulate T cell activation, proliferation and differentiation. That the expression of metabolic transcription factors such as Myc and IRF4 depends on the

strength of TCR stimulus demonstrates how a clonal expansion of high affinity effector cells emerge during an immune response [81].

1.4.3 Downregulation in expression of genes and surface molecules

T cell activation also results in the downregulation of certain genes and surface molecules. The activation of Akt in the PI3K pathway results in exclusion of FOXO1 from the nucelus to the cytosol [67]. FOXO proteins promote cell cycle arrest, which is partly mediated by the its promotion of the synthesis of cell cycle inhibitory factors and through the inhibition of expression of cyclin D1 [67], which is required for progression since the G1 phase of the cell cycle. The exclusion of FOXO1 also turns off the expression of cytokine receptors for IL-7 because FOXO1 induces the expression of the IL-7Rα chain [63]. There is also a reduction in the expression of cell adhesion molecule CD62L, chemokine receptor CCR7 and sphingosine-1-phosphate receptor S1P1, since FOXO1 drives the transcription of transcription factor KLF2 that drives the expression of these surface molecules [63]. These surface molecules are important for the trafficking of naive cells, since naive cells will migrate between the blood and lymphatic system to lymph nodes by aid of chemokine receptors such as CCR7 and the adhesion molecule CD62L [82]. The egress from lymph nodes is controlled by S1P1 and loss of S1P1 is associated with retention in lymphoid organs [83]. The loss of these molecules enables activated T cells to migrate to peripheral tissues.

The expression of CD62L is also reduced through its proteolytic cleavage from the cell surface. This is mediated by ERKs, which phosphorylate the metalloprotease TACE/ADAM17 than then cleave CD62L proximal to the cell membrane which results in its shedding from the surface [82].

1.5 The phenotype of T cell signaling

Experiments that sought to characterise the T cell response utilised T cells with a defined TCR, which were mixed with APCs incubated with a panel of peptides at various doses. It was found that single amino acid mutations in a stimulatory peptide (that maintained MHC binding) could completely abolish the T cell response, as determined by proliferation or cytokine secretion, even at high pMHC doses [84]. It had also been found that as few as 1-10 agonist pMHCs could induce a T cell response [85]. These, and later experiments, have established that the T cell response is both sensitive and specific to presented pMHC [86]. Although it was initially postulated that the specific peptide sequence is what determined the T cell response, a large body of accumulating data now suggests that the peptide sequence determines the TCR-pMHC binding parameters, and it is these parameters that the T cell signalling machinery has evolved to discriminate.

Experimental work using panels of different TCRs and pMHCs has aimed to establish the relationship between the TCR-pMHC binding parameters - which include the off-rate constant (k_{off}), on-rate constant (k_{on}), and dissociation constant ($K_{\text{D}} = k_{\text{off}}/k_{\text{on}}$) - and the T cell response. Dose-response assays have shown that the potency (EC_{50}, defined as the concentration of pMHC producing half-maximal response) correlates with the K_{D} [87–90] and more recently, the maximal efficacy ($E_{\max}$, defined as the maximal response) has been shown to correlate to k_{off} [91]. Interestingly, studies examining the T cell response at a fixed pMHC dose showed that an optimal T cell response is observed as a function of k_{off} (or the dissociation time $\tau = 1/k_{\text{off}}$) [92–94] and that this optimum disappears at high pMHC concentrations [95]. There is also evidence that T cells respond digitally in an all-or-none fashion above a threshold pMHC dose but that they still maintain information about the pMHC quality when responding. Studies have also examined effects of co-presenting pMHC ligands and found that antagonism is possible, which is mediated, at least in part, by TCR cross-talk [96, 97].

These experimental studies highlight that the relationship between the TCR/pMHC binding parameters and pMHC dose to the T cell response is complex and have motivated

the construction of many mathematical models that aimed to reproduce the observed T cell phenotypes to pMHC. Over 10 models [91, 93, 98–103] have been published that explain various aspects of the T cell response. However, it is not clear how each model is related. This is in part because these models have been formulated using different mathematical frameworks, often making different biochemical assumptions, and providing different model outputs, making the models difficult to compare. For these reasons, it is difficult to know which models are consistent with a given experimental dataset and which are not.

1.5.1 Digital nature of T cell activation

Although the activation of signalling proteins at the level of a population of T cells shows an analogue response, single cell analysis has revealed that many proteins in the signal transduction cascade are activated in a digital manner [104]. This means that as the strength of TCR affinity and dose is increased, the number of responding cells that have activated a given protein increases, and the number of activated proteins per cell remains the same. In this case, the signal transduction pathway from TCR to signalling protein has converted an analogue input to a digital output. Experiments have shown that the activation of Ras [105] and ERK [102] are digital, as well as the activation of transcription factor Myc [78] and the nuclear translocation of NFAT [106]. Protein kinase D 2 (PKD2), which integrates DAG and PKC signalling, has also shown to be digital [107]. There is evidence that the nuclear translocation of NF-κB may be digital, since it has been found to be so in D10 T cells, which are a murine CD4+ cell line. In addition, the phosphorylation of IκBα, which is necessary for the translocation of NF-κB is digital in both CD8+ and CD4+ primary cells. However, another study reports an analogue response in memory CD4+ cells [106]. Since these proteins influence the expression of genes that encode for cytokines, it must be considered whether cytokine secretion is analogue or digital. The secretion of IL-2 [106, 108] and TNF-α [108] are secreted digitally in naive and memory CD4+ T cells. There is mixed evidence for the secretion of IFN-γ from cytotoxic T cells. It has been found to be secreted in an analogue manner [91], but it has also shown to respond with a good threshold but a poor switch. This

means there is a threshold of activation for the secretion of IFNγ, but the amount of γ increases with per cell with pMHC dose.

These studies highlight that there is a digital nature of T cell activation, but this is not something that has been considered in this thesis. This is due to the experimental methods that are used, whereby cytokine secretion is measured from a population of cells. This means that even if cytokines are secreted digitally, the response will appear analogue on a population level. The mathematical modelling conducted in this thesis therefore represents the signal transduction cascade of a population of cells.

1.6 Thresholds of activation

The sensitivity of a T cell to a given pMHC will vary across different T cell subsets. This threshold for activation is a function of the pMHC affinity, dose, and the duration of stimulation. As well as differences across T cell subsets, there are also differences in threshold for various markers of activation for a given T cell.

One marker for the sensitivity of a T cell is the expression of surface molecule CD5. This molecule has been shown to correlate with the sensitivity of a T cell to endogenous pMHC [109–111].The survival of CD8+ T cells and most probably CD4+ T cells in the periphery has been shown to be dependent on the binding to endogenous pMHC [112]. Increased CD5 expression has be shown to correspond to higher transcription of the gene that encodes for nuclear receptor Nur77, which is associated with improved readiness for activation and functional differentiation[112]. T cells that are more reactive to endogenous pMHC may therefore have increased sensitivity to foreign pMHC.

1.6.1 Thresholds for different markers of activation

The initial triggering of the TCR that precedes sustained signal transduction to the nucleus only needs a short duration of stimulation to be activated. The phosphorylation of the TCR, ZAP-70, ERK and Calcium influx all occur within minutes of TCR engagement [**Tkach2013**]. These early events happen before the formation of an IS. The activation of Lck and ZAP-70 has been shown to decrease after formation of the IS [113]. For sustained signalling of more downstream molecules, TCR engagement of a longer duration is

necessary. A sustained Calcium signal, as well as PI3K activity, has been shown to persist for 10 hours, and this is dependent on continuous TCR signalling. [114]. Downstream effector functions, such as IL-2 secretion and cell proliferation are similarly dependent on continuous signalling through the TCR for hours [114].

It has been found that there are different thresholds of pMHC dose for different cytokines. Th1 CD4+ cells need a lower concentration of pMHC to secrete IFN-γ than they do for IL-2 [115].

1.6.2 Thresholds for different subsets

The experimental evidence for thresholds for different T cell subsets is quite conflicting, owing to differences in experimental design and different markers of activation used. It has been shown that naive CD8+s need only 2 hours of stimulation to perform several rounds of division and acquire cytotoxic effector functions both *in vitro* and *in vivo* [116]. Another study has found that 24 hours of stimulation is sufficient for naive CD8+ cells to differentiate into effector and memory cells. Memory cells have been shown the have lower thresholds of activation for certain markers compared to naive cells. Memory cells have faster kinetics for IFN-γ and IL-2 secretion than naive cells *in vitro* when presented with a single type of pMHC, and they secrete a greater magnitude of cytokines. The same study showed that they have equal thresholds to undergo proliferation *in vitro* [117]. Another study has shown that *in vivo*, memory T cells proliferate more than naive cells from the same stimulus. However this study used polyclonal antigen presentation [118]. A more recent study has in fact shown that memory CD8+ T cells require a higher antigen threshold than naive *in vitro*. The results showed that low doses of monoclonal pMHC presentation to naive cells is sufficient for them to enter the cell cycle while memory cells do not activate effectors of cell cycle. Memory cells also had lower amounts of activated of ZAP-70 and Myc [119].

Teeg cells have been shown to have a greater sensitivity to endogenous pMHC than other cell types, which could indicate that they have a lower threshold for activation than other subsets [112].

1.6.3 Implications for modelling

A consequence of these different thresholds for various markers of activation and across T cell subsets means that it is difficult to make a general model of T cell activation. The work covered in this thesis focuses on cytokine secretion and NFAT translocation as readouts for activation, and hence cannot account for the activation of molecules more proximal to the TCR that have been shown to have different thresholds for activation. The results of this thesis are also specific to CD8+ effector cells, and so may not be relevant to CD8+ naive and memory cells or CD4+ cells.

1.7 Motivation for using a phenotypic modelling approach

Biological systems can be considered on different scales of organisation, which can be ordered into the following categories,

organism
organ
tissue
cell
molecule
atom.

This scheme of organisation can be considered hierarchical, such that the smaller 'parts' in one level are contained within the larger 'whole' in the level above [120]. The choice of which level to use when trying to understand an aspect of a biological system depends on the nature of the question being asked. To understand and predict how T cells process information regarding the concentration and binding parameters of a pMHC, one approach could be to consider the system on a molecular level and build a model of the molecular interaction network. A problem with this approach, however, is that a vast amount of knowledge of the T cell signal transduction cascade (molecular concentrations, rate parameters, interactions), much of which is currently unknown, is required to build such a model. The consequence is to have a model with many unknown parameters that must be fit to the data. This means that there is much uncertainty in the model.

The approach I have taken in this thesis is to develop a phenotypic model, which can be considered a coarse-grained version of the molecular interaction network. It could thus be placed on a level between 'molecule' and 'cell' in the above hierarchy. A phenotypic model is an abstraction of the complex interactions at the molecular level, such that the 'molecules' and 'connections' in the phenotypic model represent multiple signalling steps at the molecular level. The benefit of taking this approach is that there a fewer parameters to be fit, and so one can have more confidence in the model. Although this approach to modelling is not conventional, it can be argued that even with molecular level models, abstractions and approximations will have to be arbitrarily made at some point (such as omitting protein states and molecular interactions deemed not crucial) in order to limit the model complexity.

An assumption that I have made is that a phenotypic model can offer insight into the structure of the lower level molecular interaction network. Scientists and philosophers generally agree that properties of a higher level in a system are constrained by properties of the parts in a lower level [120, 121]. Consistent with this principle, it can be supposed that the structure of the lower level is constrained by the properties of a higher level. Therefore, assuming the phenotypic model is an unique descriptor of the data, the form of the phenotypic model must be informative of the molecular interaction network. The structure of the phenotypic model could be representative of 'modules' that contain within them many molecular interactions, analogous to how a circuit board contains many small components but can be summarised by larger interacting modules [122].

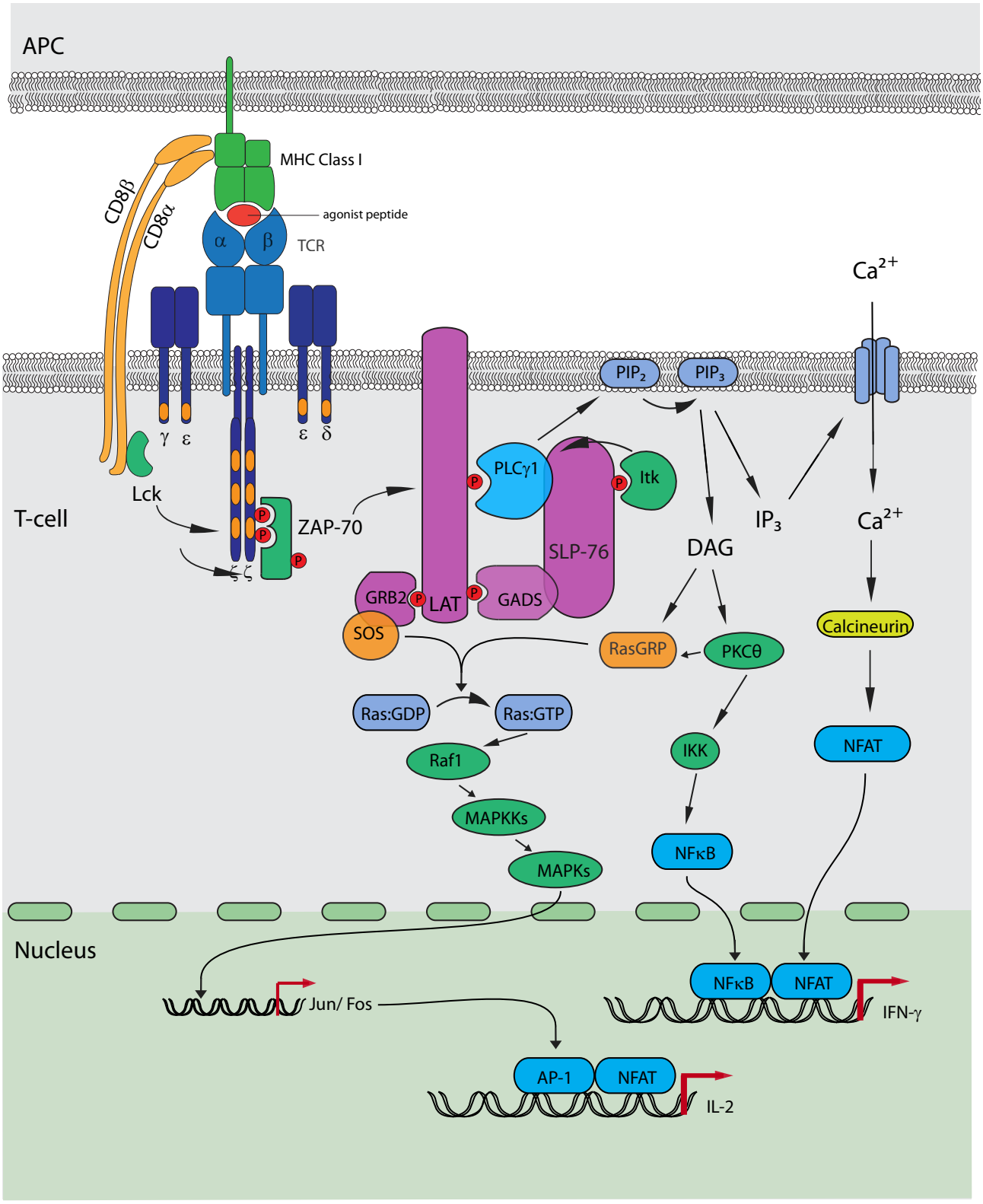

Figure 1.3: An overview of the T cell signal transduction cascade from TCR engagement to transcriptional activation: Following from initial TCR triggering, ZAP-70 is recruited to the TCR complex to enable downstream phosphorylation of signalling molecules including LAT. From LAT, the signal is diversified by branching into the Calcium signalling pathway, the MAPK pathway and the NF-κB pathway. These pathways lead to the nucleus where transcription factors are activated to enable cytokine secretion, proliferation and differentiation.

1.8 Summary of thesis

The aim of this thesis is the generation of a mathematical model that reduces the complex signal transduction within the T cell to a simpler form. This is a phenotypic model of T cell activation that represents the signal transduction cascade from TCR engagement to cytokine secretion. This model is informed by a quantitative dataset that I have generated as well as existing models in the literature.

Chapter 2: Materials and methods

In this Chapter, I outline the design of an assay to map out the phenotype of T cell activation. The assay involves stimulating T cells with pMHC that have a very broad range of affinity for the TCR expressed by the T cells.

Chapter 3: Analysis of existing models of T cell activation

The development of mathematical models of T cell activation has been hindered by the fact that models are difficult to relate to each other, in part because they have been formulated using different biochemical assumptions. Experiments are often conducted with limited pMHC affinities and doses, which makes them hard to compare to mathematical models. In this chapter, I summarise the experimental results on T cell activation and then synthesise the mathematical models in the literature under a consistent framework so that they can be compared.

This chapter is adapted from the published paper: Phenotypic models of T cell activation. Lever et al. *Nature Reviews Immunology* 14, September 2014.

Chapter 4: Experimental results

Motivated by the results of Chapter 3, I measured T cell activation in response to stimulation by pMHCs that span a wide range of affinity and concentration. Surprisingly, I find that none of the models described in Chapter 3 are sufficient to explain my experimental data.

Chapter 5: Modelling

I dedicate this Chapter to the formulation of a novel phenotypic model of T cell activation that can explain the experimental data shown in Chapter 4.

Chapter 6: Discussion

Finally, I discuss the themes of this thesis and the conclusions of the research.

2
Materials and methods

2.1 1G4 high affinity T cell receptor

The 1G4 TCR has been isolated from the 1G4 cytoxic lymphocyte clone that recognises the NY-ESO-1:157-165 antigen. The NY-ESO-1:157-165 peptide (SLLMWITQC) is a cancer testis antigen and is found on a variety of tumours [123].

The TCR used in all experiments is a high affinity version of the 1G4 T cell receptor, termed the 1G4 c58c61 TCR. It is specific to the cancer testis antigen NY-ESO-1/HLA-A2 (SLLMWITQC). The high affinity receptor was generated through directed evolution of the 1G4 WT TCR by phage display [32]. The TCR was obtained from Adaptimmune Limited, UK.

2.2 pMHCs

2.2.1 Peptides

The peptides used were ordered from Genscript, USA with $> 95\%$ purity, and consisted of the cognate peptide sequence SLLMWITQV and mutants of this sequence. Mutations to the peptide sequence were not done at anchor residues to reduce the possibility of mutations affecting peptide loading on the MHC.

2.2.2 MHC mutants

Amino acid substitutions of the HLA-A2 molecule were made by performing either overlapping PCR mutagenesis or QuikChange II site-directed mutagenesis (Strategene). Mutations were made to amino acids that should not affect peptide loading. Mutations on the MHC were chosen to lie within 6 $\mathring{A}$ of contact with the TCR, and involved the mutation of a residue to either an alanine (A) or to a glycine (G) if the residue was already an alanine. These mutations act to remove the associated side chains at that residue. The MHC mutants consisted of either H151A and E154A $\{151,154\}$, R72A and R75A $\{72,75\}$, and A69G and E154A $\{69,154\}$.

2.3 Protein purification, refolding and biotinylation

2.3.1 pMHC molecules

The HLA-A2 heavy chain and β_2-microglobulin (β_{2M}) components of the MHC complex were expressed as independently in *Escherichia coli* (E. coli), refolded in vitro and then purified by fast protein liquid chromatography (FPLC). This method of protein expression has been used for other T cell stimulation studies that stimulated T cells with plate-bound pMHC [91, 124]

Expression: E. coli was transformed with the plasmid for either the HLA-A2 heavy chain or the β_{2M} subunits. The E. coli was inoculated into 10ml LB media with 100μg/ml ampicillin and incubated overnight in a shaker. The overnight culture was then transferred to 1-2l of LB with 100μg/ml ampicillin and incubated at 200rpm and 37° until the media reached an $O.D_{600}$ = 0.6. Expression of recombinant protein was induced by adding 0.5 ml 1M IPTG to every litre of LB. Following 4-5 hours of incubation, cells were pelleted by centrifugation at 3000rpm 4°C. 20ml of lysis buffer was added to the pellets and they were incubated at 37°C for 15 minutes. A 2× wash buffer containing the detergent Triton-X100 was added to the lysis buffer, and the mixture was sonicated until homogeneous. The cell lysate was then centrifuged at 15000 rpm for 30 minutes at 4°C. The pellet was then resuspended by sonication in 1× wash buffer and centrifuged at 4°C and 15000 rpm for 15 minutes. The washing steps of sonication and centrifugation were repeated until

the pellet was a chalky colour and the supernatant clear. The pellet was then resuspended in resuspension buffer and centrifuged at 4°C and 15000 rpm for 15 minutes. Finally the pellet was resuspended in 8M urea solution and rotated at 4°C overnight.

Refolding: The heavy chain and β_{2M} subunits were refolded with peptide at a ratio of 1mg peptide:2.6 mg β_{2M}:3.2 mg heavy chain for every 100ml of refold buffer. The peptide was added dropwise to refold buffer that had been cooled to 4° C, followed by the β_{2M} and finally the heavy chain. The refold solution was stirred at 4° C for 40 hours. The samples were then concentrated using Centricon®Plus-70 (Millipore) such that 100ml of refold buffer was concentrated to approximately 700μl.

Biotinylation: The HLA-A2 heavy chain was tagged with a short C-terminal biotin-protein ligase recognition sequence, which can then be enzymatically conjugated to biotin with the BirA enzyme (biotinylation). To biotinylate the refolded pMHC, 1μl of each protease inhibitor pepstatin (1mg/ml), leupeptin (1mg/ml), and PMSF (100mM) were each added to 700 μl of concentrated refold solution. 100μl each of Biomix buffers A, B and C (Avidity) were then added to the refold solution. Finally, 1 μl of BirA enzyme (3mg/ml) (Avidity) was added and the refold solution was left at room temperature overnight.

FPLC: The samples were spun through Spin-X®centrifuge tube filters (Sigma). The samples were then separated by size-exclusion chromatography using a Superdex 75 10/300 GL column (GE Healthcare), with HBS-EP as the running buffer. The appropriate fractions were collected and the OD was measured.

Recipes:

- **Triton wash buffer:**

  Tris pH 8.0 50mM, NaCl 100mM, Triton X100 0.5%, DTT 10mM, EDTA 1mM

- **Lysis buffer:**

  Tris pH 8.0 50mM, NaCl 50mM, 100mg/ml Lysozyme 25μl/20ml.

- **Resuspension buffer:**

  Tris pH 8.0, NaCl 100mM, DTT 10mM, EDTA 1mM.

- **Urea solution:**

  Urea 8M, Tris pH 8.0 10mM, NaH_2PO_4, EDTA 0.1mM, DTT 10mM.

- **Refold buffer:**

  Tris pH 8.0 1M, L-arginine hydrochloride 400mM, EDTA 2mM, Reduced glutathione 5mM, Oxidised Glutathione 0.5mM, PMSF 0.1mM.

- **HBS-EP**

  HEPES pH 7.4 10mM, NaCl 150mM, EDTA 3mM, 0.005% TWEEN 20.

2.3.2 T cell receptors

The TCR α and β chains were expressed as inclusion bodies in E. coli and then refolded *in vitro*. The soluble TCR was then purified by dialysing the refold mixture, followed by anion exchange chromotography and then size-exclusion chromotography, as described in Boutler et al., 2003 [125].

2.4 pMHC:TCR binding properties

Binding parameters were measured by surface plasmon resonance (SPR) using a Biacore 3000 (GE Healthcare). Biacore has been used to determine binding kinetics between pMHC and TCR in other studies [90, 94, 124]

HBS-EP was used as the running buffer and experiments were performed at 37°C. A CM5 sensor chip (GE Healthcare) was used to immobilise pMHC. This was achieved through activating the carboxymethylated dextran matrix on the chip with a mixture of 1-ethyl-3- (3-dimethylaminopropyl) carbodiimide (EDC) and N-hydroxysuccinimide (NHS) to give reactive succinimide esters. Streptavidin was flowed over the surface and the amino groups on the steptavidin molecules reacted spontaneously with the esters to link them covalently to the dextran matrix. Biotynlyated pMHC were diluted to around 1-5μg/ml and then flowed over flow cells 2, 3, and 4 on the chip until an immobilisation of approximately 250 response units (RU) was reached. This low RU was chosen to minimsie mass transport effects. Flow cell 1 was kept empty as a negative control.

TCR were diluted to a starting concentration of $\approx$ 1-10$\times$ higher than the K_{D} of the pMHC.

2.4.1 Low affinity pMHC

For low affinity interactions ($K_{\mathrm{D}} \geqslant 0.1\mu$M), which tend to reach equilibrium within the timescale of Biacore experiments, the affinity was measured by equilibrium binding. 10μl of TCR was injected at a flow rate of 30μl/min and then the chip was flushed with HBS-EP for 5 minutes. This was repeated for at least eight TCR concentrations going from the lowest concentration to the highest.

The RU trace was normalised against the control in the BIAevaluation software and then exported to Prism (GraphPad). The K_{D} was obtained by extracting the equilibrium binding RU for each TCR concentration and then fitting to the Langmuir binding isotherm:

$$\text{bound} = \frac{C^A \times B_{\text{max}}}{C^A + K_{\mathrm{D}}}, \tag{2.1}$$

where 'bound' is the RU at equilibrium, C^A is the TCR concentration and B_{max} is the maximum binding (RU).

The k_{off} was found by fitting a one-phase decay to the dissociation part of the trace,

$$Y = (Y_0 - \text{plateau})e^{-k_{\text{off}}t} + \text{plateau}, \tag{2.2}$$

for each TCR concentration and taking the average. The k_{on} could then be calculated since $k_{\text{on}} = k_{\text{off}}/K_{\mathrm{D}}$.

2.4.2 High affinity pMHC

Affinity was determined by kinetic analysis for pMHC that had superphysiological affinity. Prior to TCR injection, running buffer was injected for 4 hours to see if there were any anomalies in the baseline RU trace. 325μl of TCR was injected at a flow rate of 30μl/min and then the chip was flushed with HBS-EP for 6 hours.

The k_{off} was found as described in Section 2.4.1. The k_{on} was found by fitting the association kinetics equation to the RU trace:

$$Y = Y_{\text{max}}(1 - e^{-k_{\text{ob}}t}), \tag{2.3}$$

where,

$$Y_{\text{max}} = \frac{[TCR]B_{\text{max}}}{[TCR] + K_{\text{D}}}, \tag{2.4}$$

$$k_{\text{ob}} = k_{\text{on}}[TCR] + k_{\text{off}}. \tag{2.5}$$

B_{max} is the maximal binding at equilibrium, at maximal TCR concentration. The known parameters are $[TCR]$, which the concentrations of TCR used in the Biacore assay, and k_{off}, which is fit as described in Section 2.4.1. The parameters B_{max} and k_{ob} are unknowns to be fit. The k_{on} can then be calculated and subsequently, the K_{D} can then be calculated.

2.5 Cell culture

2.5.1 T cells

The jurkat cells used were E6.1 Jurkat T cells expressing an NFAT-luciferase construct, which were obtained from Professor Oreste Acuto, University of Oxford, UK. Primary T cells were isolated from previously identified HLA-A2 negative donors according to University policy.

Luciferase reporters for NFAT have been used in the following studies [59, 126].

2.5.2 Cell culture conditions

Jurkats were cultured in DMEM supplemented with 10% FBS and 1% PenStrep and incubated at 37° in a humidified 10% $C0_2$ atmosphere. Primary cells were cultured in the same conditions as jurkats with the addition of IL-2 at 50IU/ml. 293T cells were cultured in RPMI supplemented with 10% FBS, 1% PenStrep and incubated at 37° in a humidified 5% $C0_2$ atmosphere.

2.5.3 Cell freezing and thawing

Cells were frozen after washing and resuspended in culture medium supplemented with 10% DMSO at a concentration of approximately 10×10^6 cells/ml. Cells were stored in 1.5ml Nunc™ Cell Culture Cryogenic Tubes (Thermo Scientific) at -80°C.

Cells were thawed by incubating the cryogenic tubes in a waterbath at 37°C. Once cells were thawed they were pipetted slowly into media pre-warmed to 37°C.

2.6 Cell transfection and T cell transduction

2.6.1 Production of lentvirus for T cell transduction

293T cells were cultured in RPMI +10% FBS +1% PenStrep (R_{10}) in T_{150} flasks and split the day before transfection such that they would be 50% confluent on the day of transfection. Serum and antibiotic-free RPMI was warmed to 37°C and X-tremeGENE transfection reagent (Roche) was warmed to room temperature. 174μl of X-tremeGENE transfection reagent was added slowly to 3ml of RPMI in a 15ml centrifuge tube and mixed by inverting the tube 4 times. The mixture was incubated at room temperature for 20 minutes.

A DNA mixture was prepared of lentivector (in LAL reagent endonuclease-free H_2O), pRSV.EV, pMDLg/p.RRE, pVSV at a ratio of 15:18:18:7μg. 1ml of RPMI/X-tremeGENE mix was added to DNA slowly, gently pipetted and then added back to the remaining RPMI/X-tremeGENE mix. The mixture was inverted 4 times to mix and then incubated at room temperature for 30min. The culture media of the 293T cells was removed and replaced with the RPMI/X-tremeGENE/DNA mix. The flask was tilted gently to ensure the mixture covered the cells and left to sit for 1 minute. 22ml of RPMI was added to the flask without touching the cells, and the flask was incubated at 37°C 5% CO_2 overnight.

The culture media from the 293T cells was transferred to a 50ml centrifuge tube and spun at 1400rpm for 6 minutes at 4° to pellet any cell debris. The supernatant was syringe filtered with a 0.45μm nylon filter into a fresh 50ml tube and kept on ice. The supernatant was then transferred to a sterile 38.5ml thin wall ultracentrifuge tube (Beckman Coulter) and made up to 31ml with fresh, cold R_{10} and centrifuged at 10000$\times$g for 18hr at 4° with the brake off. The supernatant was removed and the pellet was resuspended in the remaining volume ($<$2ml) and then made up to 2ml with R_{10}. The lentivirus could be frozen at -80°C.

2.6.2 Transduction of Jurkat cells

Three million jurkat cells were pelleted and 2ml of lentivirus was added to them. The solution was placed in a 6 well plate and centrifuged at 3000rpm for 1-2 hours. The plate was then incubated at 32°C for 3.5-6 hours and then incubated at 37°C 10% CO_2 for 3 days.

2.6.3 Isolation of CD8$^+$ T cells from blood

Blood was transferred from at least three heparinized tubes into three separate 50ml centrifuge tubes under a laminar flow hood. 10ml of PBS was added to the tubes to give a 1:1 ratio of blood:PBS. The diluted blood was underlayed with Ficoll (GE Healthcare). The mixture was spun at 1600 rpm for 30 minutes with the brake off in order to fraction the blood in layers going from top to bottom of: plasma, platelets, PBMC, Ficoll, and red blood cells. The plasma was pipetted off and discarded. The buffy coat layer containing PBMCs was aspirated from the all tubes and transferred to a new 50ml tube. PBS was added to the PBMCs to make a 50ml volume, and the tube was spun at 1200rpm for 10 minutes with the brake on. The PBMCs were washed for a second time and then resuspended in 30ml PBS.

CD8$^+$ cells were isolated by using the Dynabeads®CD8 Positive Isolation Kit (Life Technologies) according to manufacturer's instructions. CD8$^+$ cells were then washed, counted and then stimulated with pre-washed ($3\times$ in R_{10}) Dynabeads®Human T-Activator CD3/CD28 beads (Life Technologies) at a ratio of 3 beads per cell. Cells were plated at 1ml of cells per well at 1×10^6 cells/ml in a 24 well plate in DMEM 10% FBS 1% PenStrep + IL-2 (50units/ml) and incubated at 37° 10% CO_2 overnight.

2.6.4 Transduction of primary CD8+ T cells

1ml of concentrated lentivirus was added per well of stimulated CD8+ T cells and fresh IL-2 (50units/ml) was added. Cells were incubated at 37°C 10% CO_2. Cells were counted and resuspended in fresh media + IL-2 on days 5, 7, 10 and 13 post transduction. Cell concentration was at $0.8 - 1 \times 10^6$ cells/ml up to day 5, and 1×10^6 cells/ml from then on. Beads were removed with a magnet on day 5. Cells were resuspended and fed with IL-2 every 3 days thereafter.

2.6.5 Flow cytometry analysis of transduction efficiency

Cells were washed $2\times$ in PBS and then stained with 0.1μg/ml biotinylated 9V monomers in PBS for 1 hour on ice. They were then washed $2\times$ in PBS and stained with streptavidin-RPE (AbD Serotec) for 1 hour on ice. Cells were then washed $2\times$ in PBS and analysed

by flow cytometry using a FACSCalibur ™(BD Biosciences). Flow cytometry data was analysed using the software Flowjo.

2.7 Stimulation assays

2.7.1 Plate stimulation

In all stimulation experiments, cells were stimulated with immobilised pMHC presented on a plate, as has been done in other experiments [91, 99, 124].

Cells were split the day before a stimulation experiment. On the day of stimulation, streptavidin plates (Sigma) were washed 2× with PBS 0.05% TWEEN 20 (Sigma) and then 1× with PBS. They were then incubated at 37° with PBS 1% BSA for 1 hour. The pMHC were serially 2-fold diluted in PBS with a starting concentration of 10-30μg/ml. The diluted pMHC were then added to the streptavidin plates in volumes of 100μl and incubated at 4° C for 90 minutes. Following incubation, the plates were washed 3× with PBS.

Cells were washed, resuspended in culture media and then added to the plates in numbers of 40,000 per well in volumes of 100μl. The plates were spun at 200 rpm for 4 minutes to ensure that cells came into contact with the bottom of the plate, and then were incubated at 37° and 10% $C0_2$ for the required stimulation time.

2.7.2 Control for pMHC immobilisation

The amount of pMHC immobilised was checked by immobilising pMHC on streptavidin plates as described in (2.7.1), incubated with a mouse anti-HLA antibody, clone W6/32 (AbD Serotec) diluted 1:100 in PBS on ice for 1 hour. After washing the plate 3× with PBS, a goat anti-mouse IRDye 800CW Infrared dye (LI-COR) was used at a 1:5000 dilution in PBS for 90 minutes in the dark. The plate was washed 3× with PBS and then fluorescence was measured using an Odyssey®Infrared Imaging system. Flourescence intensity was quantified using the Odyssesy ®Infrared Imaging system application software.

2.7.3 NFAT assay

The jurkat cell line used has a firefly luciferase reporter for NFAT (Nuclear Factor of Activated T-cells), which is a marker of T -cell activation. The luciferase monomer can be catalysed into oxyfluoroluciferin with the substrate 5'-fluoroluciferin. This reaction produces a bright luminescence which can be measured.

After stimulating the jurkats for 16 hours, the cells were lysed and the luciferase reaction was catalysed using the ONE-Glo™ Luciferase Assay System (Promega). The One-Glo™ reagent was added to the cell media at a 1:2 ratio and after 5 minutes of incubation at room temperature, luminescence was read using the PHERAstar FS plate reader. Measurements were corrected for background luminescence by substracting luminescence from unstimulated cells.

2.7.4 Cytokine secretion assays

For stimulation assays on jurkats, IL8 secretion was detected. The supernatant was taken after 16 hours of stimulation and IL8 secretion was measured with a human IL8 ELISA kit (BD Biosciences). For assays on primary cells, IFN-γ and MIP-1β secretion was detected after 4 hours of stimulation using a BD OptEIA ™ human INF-γ ELISA set (BD Biosciences).

Measurements of these cytokines have been taken in other experiments that examine T cell activation; for example IFN-γ [91, 124], MIP-1β [127, 128] and IL-8 [94].

2.7.5 Cell death assay

Cells were stimulated as in Section 2.7.1, but cell numbers were at 100,000 cells per well. After 16 hours of stimulation, cells were removed by gently pipetting them out of each well. A second attempt to remove cells was made by washing each well with PBS. Cells were placed into eppendorfs and washed $2\times$ with PBS. CD69 staining of cells was performed using 5μl Alexa Fluor®647 anti-human CD69 antibody (BioLoegend) per sample and incubating for 60 minutes on ice in the dark. Cells were washed $2\times$ in PBS and resuspended in Annexin-V buffer (HEPES pH 7.4 10mM, NaCl 140mM, $CaCl_2$ 2.5mM) at a concentration of 1-5$\times 10^6$cells/ml. Cells were stained with PE Annexin-V (BD

Biosciences) at a concentration of 5μl per 100μl cells and incubated at room temperature in the dark for 15 mins. Cells were then analysed by flow cytometry using a FACSCalibur ™ (BD Biosciences). Flow cytometry data were analysed using the software Flowjo.

2.8 Development of mathematical models

Mathematical models of T cell activation were formulated using the principle of mass action in the form of ordinary differential equations analysed at steady state. The models were simulated using Matlab®.

3

Synthesis of models of T cell activation

3.1 Introduction

A variety of models exist that attempt to reproduce the phenotype of T cell activation as a function of pMHC-TCR binding parameters. These models have been motivated by numerous experiments that have shown that these binding paramters determine the magnitude of T cell response [87–95, 129–134] and that the relationship is complex. This relationship can be investigated by performing dose-response experiments, where T cells are presented with titrated doses of pMHCs and the downstream response, such as cytokine secretion, cell killing, or proliferation, is quantified several hours after stimulation (Fig. 3.1).

The outcome of these quantitative T cell assays has been to show different associations between pMHC-TCR binding parameters and the resultant activation. Experiments have shown that the dissociation time ($\tau = 1/k_{\text{off}}$), and therefore the dissociation constant ($K_{\text{D}} = k_{\text{off}}/k_{\text{on}}$), correlate with the potency of the response [87–89, 99] (Fig. 3.1b). The potency is also known as the EC_{50}, which is the pMHC dose required to give half the maximal response. The maximal response to a pMHC, called the maximal efficacy $E_{\max}$, has been found to positively correlate with the dissociation time [90, 91, 134]. Other experiments have shown that T cell activation at a fixed dose shows an optimum when plotted against dissociation time [92–94]. This optimum has also been observed *in vivo* [131, 135]. One study has found that the optimum is dose-dependent, such that it is

lost at high pMHC doses [95], shown in Fig. 3.1c. A few experiments have shown that there is also an optimum as a function of pMHC dose, where there is an inhibition in the response at high pMHC doses [103, 127, 136, 137].

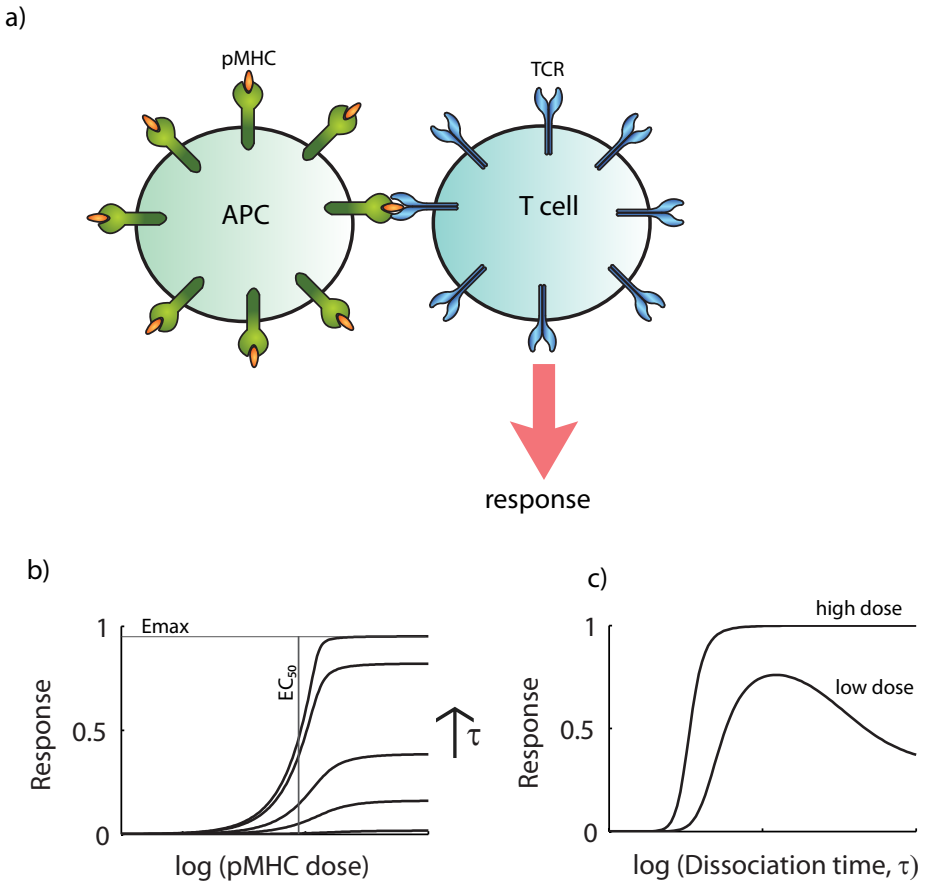

Figure 3.1: Relationship between TCR-pMHC binding parameters and T cell activation: **a)** A schematic of T cell activation assays to investigate how pMHC-TCR interactions determine the functional response of the T cell. The functional response is quantified several hours after stimulation (for example, by detecting cytokine production). The $E_{\max}$ is the maximal response from a pMHC, and the EC_{50} is a measure of potency that corresponds to the pMHC dose needed to give half the $E_{\max}$. **b)** The results of quantitative experiments can be visualised by plotting T cell response against pMHC dose, and **c)** by plotting T cell response over pMHC dissociation time.

These phenotypes of T cell activation have motivated the development of a variety of models [91, 95, 98–103, 138, 139] that aim to reproduce them. However despite extensive study, there is still no definitive model that can describe all the data. A barrier

to progress in model development is that it is difficult to compare and categorise the existing models due to them being formulated under different biochemical assumptions and assuming different end points of activation.

In this Chapter, the models are categorised according to their different assumptions and are synthesised to produce a representative model for each category. These models are titled the occupancy, kinetic proofreading, kinetic proofreading with limited signalling, kinetic proofreading with sustained signalling and kinetic proofreading with negative feedback, models. These models are phenotypic models, as opposed to mechanistic models. A mechanistic model captures T cell signalling events from T cell receptor triggering through to transcriptional regulation, which requires assumptions on which proteins are involved, their concentrations, their interaction network and their rate parameters. A phenotypic model, by contrast, uses a minimal set of assumptions to reproduce the experimental data. The advantages of this method is that it produces model that has typically few unknown parameters and is easier to interpret, since there is a simpler relationship between the model assumptions and the phenotype they produce. The mathematical framework is based on standard biochemical reactions in the steady state, which is a reasonable assumption for comparisons with prolonged T cell activation assays (lasting 4 hours). The phenotypic models make no explicit assumptions about the mechanism of TCR triggering, and are largely consistent with all known mechanisms of TCR triggering [41].

The mathematical derivations of these models are in the appendix and the results are summarised in Box 1.

3.2 Occupancy model

The occupancy model (also known as the affinity model [91]) assumes that T cell activation is proportional to the number of occupied TCRs at equilibrium. Upon a pMHC binding a TCR, the TCR immediately achieves a signalling-competent state. The parameters consist of the biomolecular binding rate (k_{on}) and the unbinding rate (k_{off}).

3.2.1 Phenotype of model and experimental support

The occupancy model predicts that the $E_{\max}$ is independent of the TCR-pMHC binding parameters (Fig. 3.2a.), which means that any pMHC can elicit the maximal response from the T cell provided that it is presented at high enough concentrations. This clearly is not a feature of the experimental data, for example, Fig. 2a in [91] shows the response of several low affinity pMHCs to plateau at high doses, and look unlikely to ever each the same magnitude of the high affinity pMHCs. The model does however predict that EC_{50} is correlated with K_{D}. The majority of the evidence in support of the occupancy model has come from studies that have found a strong correlation between K_{D} and EC_{50} [87–89, 99].

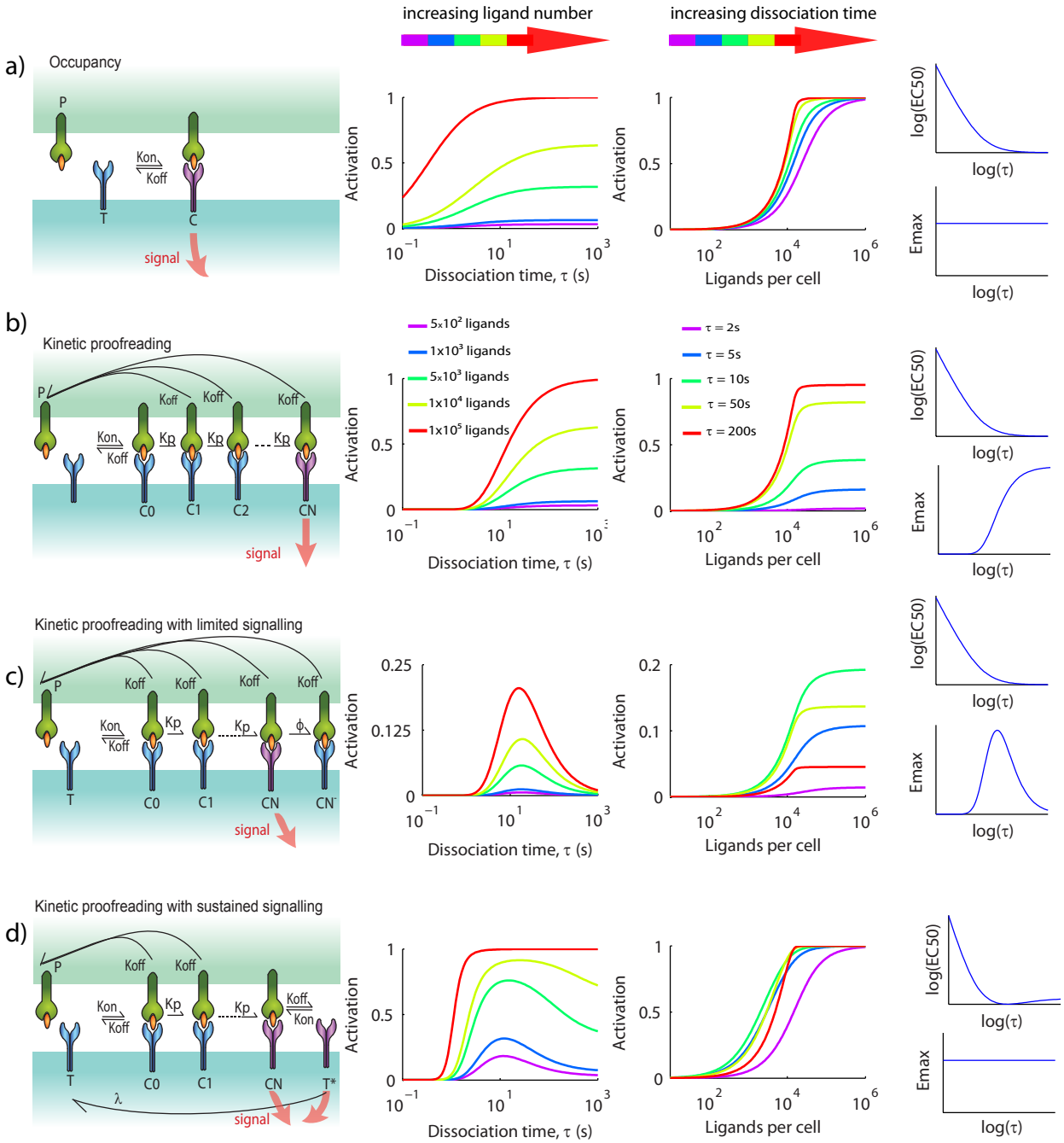

Figure 3.2: Phenotypic models of T cell activation: Left: Schematics of the models. **Centre-left:** Model predictions for T-cell activation as a function of ligand dissociation time (τ) at a fixed ligand dose. **Centre-right:** Dose-response predictions for ligands of increasing dissociation time (τ). **Right:** Predicted relationship between EC_{50} (top) and $E_{\max}$ (bottom) over the dissociation time (τ) for each model.
All models were simulated using the derived analytical results. The centre plots were normalised by $E_{\max}$ so that activation was in the range [0 1]. Parameters used: number of TCRs $T_T = 1.5708 \times 10^4$, $k_{\text{on}} = 3.1831 \times 10^{-5} s^{-1}$, $k_{\text{p}} = 1\ \text{s}^{-1}$, $N = 10$, $\phi = 0.09\ \text{s}^{-1}$, $\lambda = 0.001\ \text{s}^{-1}$

3.3 Kinetic proofreading model

The kinetic proofreading model was proposed to explain how T cells could discriminate between pMHCs based on the dissociation time between the pMHC and TCR [98]. The model posits that T cell activation is proportional not to the total number of occupied TCRs, but to the fraction of TCRs that have been bound by pMHC for sufficient duration to allow the TCR to achieve a signalling-competent state. In this model, biochemical modifications to the TCR that are required to achieve the signalling-competent state (e.g. tyrosine phosphorylation by Lck, binding by ZAP-70) are initiated upon pMHC binding and are immediately reversed upon pMHC dissociation. The delay between pMHC binding and TCR signalling allows T cells to discriminate pMHC ligands based on their dissociation time for the TCR.

3.3.1 Phenotype of model and experimental support

The implication of this model is that in a dose-response assay the $E_{\max}$ will be dependent on the pMHC dissociation time (Fig. 3.2b.). It follows that the model predicts that pMHCs with small dissociation time cannot attain responses equivalent to pMHCs with large dissociation time by simply increasing their concentrations. This has been found experimentally [90, 91, 134]. This allows the kinetic proofreading model, but not the occupancy model, to exhibit antigen discrimination based on the dissociation time. The kinetic proofreading model also predicts that the EC_{50} will be directly related to K_{D} as in the occupancy model, so all of the experimental support for the occupancy model also supports kinetic proofreading.

3.4 Kinetic proofreading with limited signalling

The models discussed so far make the assumption of reversible binding between pMHCs and TCRs, which allows a single pMHC to serially bind and trigger multiple TCRs. Why then do these models not exhibit an optimum in signalling as a function of pMHC dissociation time, as had been predicted by serial triggering models [91, 140–144]? Serial triggering models predict that because a pMHC can serially rebind TCRs, an intermediate

dissociation time that enables the triggering of multiple TCRs is optimal. Although the kinetic proofreading model and the serial triggering model make the same biochemical assumptions, they use different end points as predictors of T cell activation. The serial triggering model predicts that it is the rate of formation of signalling-competent TCRs that governs T cell activation, while the kinetic proofreading model predicts that it is the number of bound signalling-competent TCRs. The serial triggering model can be accommodated into the current framework by assuming that each TCR can only produce one 'packet' of signal, such that the duration of signal from a productively engaged TCR is limited. This model is termed the kinetic proofreading with limited signalling model, which is an extension of the kinetic proofreading model that posits that a TCR will be in a signalling-competent state for a limited period of time before becoming inert.

3.4.1 Model phenotype and experimental support

The kinetic proofreading with limited signalling model predicts that activation shows an optimum when plotted over dissociation time (Fig. 3.2c.). This optimum occurs at all pMHC doses so the $E_{\max}$ also shows an optimum. The reason for the persistence in the optimum, even at high pMHC doses, is because T cell activation is dependent on a continuous (steady-state) signal: when a pMHC with a long dissociation time binds to a TCR, it will remain bound to a TCR in an inert state which prevents the serial binding of the TCR that is required for continuous signalling. There is evidence for an optimal dissociation time from *in vivo* [130, 131, 135] studies as well as *in vitro* [92–94]. Like the occupancy and the kinetic proofreading model, the limited signalling model also predicts a direct relationship between EC_{50} and K_{D}.

3.5 Kinetic proofreading with sustained signalling

While the kinetic proofreading with limited signalling model predicts an optimal dissociation time for all pMHC doses, several models predict that the optimal dissociation time does not persist at high doses [93, 95]. These models assume that rather than the signal from the TCR being limited, it instead sustains signalling for a period of time following pMHC dissocation. The possibility of a sustained signalling state was inferred from

experimental data [93] and may be mechanistically related to the idea that TCRs continue to signal upon pMHC dissociation until phosphatases dephosphorylate the signalling competent TCR or the TCR itself is internalised.

3.5.1 Model phenotype and experimental support

The kinetic proofreading with sustained signalling model predicts that there is a pMHC dose-dependent optimum as a function of dissociation time (Fig. 3.2d.). There is an optimal dissociation time at low doses due to a balance between kinetic proofreading and serial binding: the greatest activation will be at an intermediate dissociation time that enables a single pMHC to produce multiple TCRs that are in the sustained signalling state. There is no optimal dissociation time at high pMHC doses because there is no need for pMHCs to serially bind TCRs to produce a continuous signal since signalling is not limited. At high pMHC doses it is possible to generate many TCRs in a competent-signalling state, and this is true even for short dissociation times. Although pMHCs with shorter dissociation times are less likely to produce competent-signalling TCRs due to kinetic proofreading, they can maintain many competent-signalling TCRs at high doses since they can bind a sustained signalling TCR and prevent it from returning to its basal state. This can be seen as a breakdown in kinetic proofreading. The sustained signalling model therefore predicts that like the occupancy model, the $E_{\max}$ is independent of the dissociation time.

3.6 Kinetic proofreading with negative feedback model

The kinetic proofreading with negative feedback model is an extension of the kinetic proofreading model that allows for TCRs at intermediate steps and/or the final modification step to influence the rate of modification. Mechanistically, this negative regulation could be mediated by SH2 domain-containing protein tyrosine phosphatase 1 (SHP1; also known as PTPN6) being phosphorylated and recruited to the TCR by active Lck that is associated with the phosphorylated TCR [145]. There are also other phosphatases that could be responsible, such as SHP2 (also known as PTPN11), dual-specificity protein phosphatase 6 and others that are under the control of microRNA 181a (miR-181a) [146]. Negative feedback models have initially been formulated using deterministic

model calculations [102], and later using stochastic model simulations [147, 148]. Recently, a phenotypic version of the model has been formulated that repoduces the features of the previous models with a single negative feedback loop [149]. This phenotypic model has been used for the analysis.

3.6.1 Model phenotype and experimental support

Unlike the other models considered so far, this model predicts that there will be an optimum as a function of pMHC dose. Evidence for an optimal pMHC has been found in a few experiments [103, 127, 136, 137], although with limited data points. This model does not predict an optimum with pMHC dissociation time.

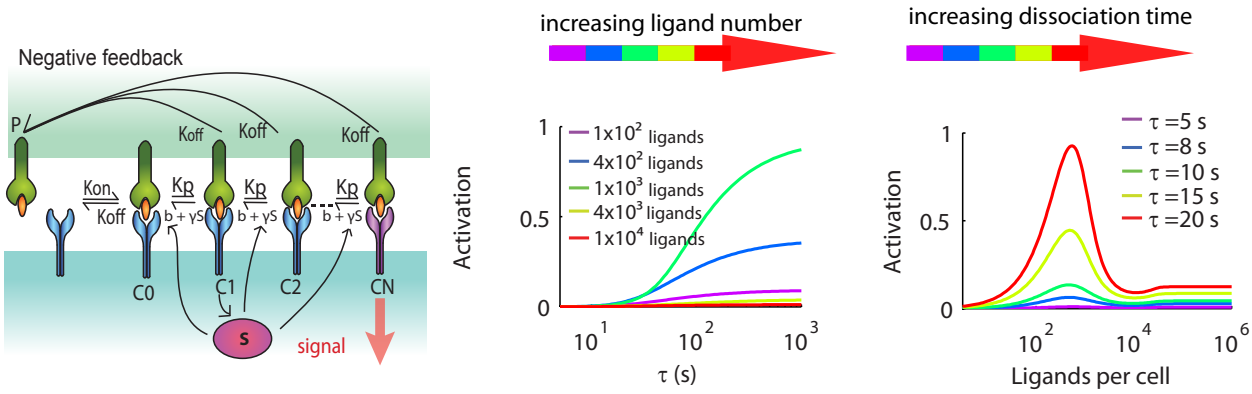

Figure 3.3: Kinetic proofreading with negative feedback model: Left: Schematic of model. **Centre:** Model predictions for T cell activation as a function of ligand dissociation time (τ) at a fixed ligand dose. **Right:** Dose-response predictions for ligands of increasing dissociation time (τ). The plots were simulated using the ode15s solver function in Matlab. The plots were normalised by the $E_{\max}$, so that activation was in the range of [0 1]. Parameters used: number of TCRs $T_T = 3 \times 10^4$, $S_T = 6 \times 10^5$, $k_{\text{on}} = 1 \times 10^{-4} s^{-1}$, $N = 10$, $k_{\text{p}} = 0.252 s^{-1}$, $b = 0.04 s^{-1}$, $\gamma = 4.4 \times 10^{-4}$.

3.7 Summary of analytical results

So far, I have evaluated the model predictions for T cell activation. However, I can also compare the ability of each phenotypic model to perform the task of antigen discrimination. A schematic of idealized antigen discrimination is shown in Fig. 3.4a, which has been adapted from a measure of antigen discrimination used in a study by Francois et al. [103]. In this idealised scenario, a T cell would be sensitive to any number of pMHC complexes above a threshold dissociation time.

The specificity plots show that the occupancy model has little specificity, and the kinetic proofreading with sustained signalling has high sensitivity. The kinetic proofreading and kinetic proofreading with negative fedback model most closely resemble the idealised plot.

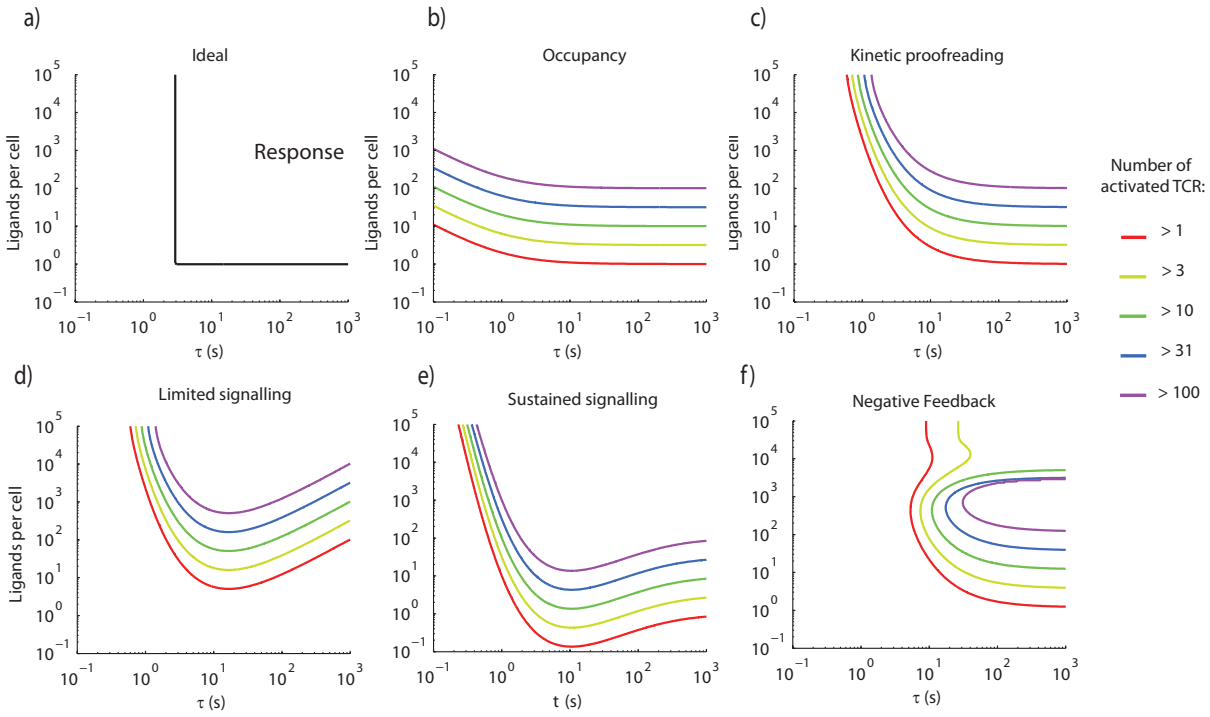

Figure 3.4: Specificity plots for the phenotypic models: a) Idealised plot showing the specificity of TCR recognition, where a T cell can be activated by a ligand with a binding time of $\tau = 3s$ and with sensitivity to detect one ligand. **b) - f)** These plots show the required ligand dissociation time and number needed to activate a certain number of TCRs. The models were simulated and then thresholded at the number of activated TCR specified in the key. The occupancy, kinetic proofreading, limited signalling and sustained signalling models were simulated using the derived analytical results in the Appendix. The negative feedback model was simulated using the ode15s solver function in Matlab. Parameters used for the first four models: number of TCRs $T_T = 1.5708 \times 10^4$, k_{on} = 3.1831 $\times 10^{-5} s^{-1}$, $k_{\text{p}} = 1\ \text{s}^{-1}$, $N = 10$, $\phi = 0.09$ s^{-1}, λ = 0.001 s^{-1}. Parameters used for feedback model: number of TCRs $T_T = 3 \times 10^4$, $S_T = 6 \times 10^5$, $k_{\text{on}} = 1 \times 10^{-4} s^{-1}$, $k_{\text{p}} = 0.252 s^{-1}$, $N = 10$, $b = 0.04 s^{-1}$, $\gamma = 4.4 \times 10^{-4}$.

Box 1: Quantitative predictions of T-cell activation models

In the equations given below, T_T is the total number of TCR, P_T is the total number of pMHC, and both are assumed to remain constant in all models. The E_{max} is proportional to the amount of activation in the limit $P_T \gg T_T$. $C_T = \left(P_T + T_T + K_{\text{D}} - \sqrt{(P_T + T_T + K_{\text{D}})^2 - 4P_T T_T}\right)/2$ and $K_{\text{D}} = k_{\text{off}}/k_{\text{on}}$

The Occupancy model
Activation is proportional to the number of bound pMHC-TCR complexes..

$$\text{Activation} \propto C_T$$
$$EC_{50} = K_{\text{D}} + T_T/2$$
$$E_{\text{max}} = T_T$$

The kinetic proofreading model
Activation is proportional to the fraction of TCRs that have undergone N modification steps with rate k_{p} to reach a signalling-competent state.

$$\text{Activation} \propto \alpha^N C_T$$
$$EC_{50} = K_{\text{D}} + T_T/2$$
$$E_{\text{max}} = \alpha^N T_T$$
$$\alpha = \frac{k_{\text{p}}}{k_{\text{p}} + k_{\text{off}}}$$

Kinetic proofreading with limited signalling
The kinetic proofreading model is modified so that upon a TCR reaching a signalling-competent state, it will signal for a limited time and then become inert with rate ϕ.

$$\text{Activation} \propto \left(\frac{k_{\text{off}}}{k_{\text{off}} + \phi}\right) \alpha^N C_T$$
$$EC_{50} = K_{\text{D}} + T_T/2$$
$$E_{\text{max}} = \frac{k_{\text{off}}}{k_{\text{off}} + \phi}\, \alpha^N T_T$$

Kinetic proofreading with sustained signalling
The kinetic proofreading model is modified so that signalling-competent TCRs will continue to signal following pMHC dissociation before returning to basal state with rate λ.

$$\text{Activation} \propto \left(\frac{k_{\text{on}}(P_T - C_T) + k_{\text{off}} + \lambda}{\lambda + \alpha^N k_{\text{on}}(P_T - C_T)}\right) \alpha^N C_T$$
$$EC_{50} = \frac{\alpha^N C_T(k_{\text{off}} + \lambda - k_{\text{on}} C_T + k_{\text{on}} T_T/2) - T_T \lambda/2}{\alpha^N k_{\text{on}}(T_T/2 - C_T)}$$
$$E_{\text{max}} = T_T$$

3.8 Prediction for co-presentation of pMHCs

A phenotypic model of T cell activation must also be capable of predicting what happens when T cells are stimulated with more than one type of pMHC. In particular, it must be able to explain antagonism, where experimental work has shown that the co-presentation of a second pMHC can inhibit the T cell response to a stimulatory pMHC. Antagonist ligands are usually altered peptide ligands of an agonist peptide and typically have shorter dissociation times [150–152]. It has also been found that self-pMHCs, which have dissociation times shorter than antagonists, are able to enhance the T cell response when co-presented with agonist [153, 154]. As the dissociation time becomes yet shorter, these pMHCs do not elicit a response from the T cell, which are termed null pMHCs. The result of this experimental data is to produce complicated regulation of T cell activation by the presentation of multiple pMHC complexes (Fig. 3.5).

The precise mechanism for how self-pMHC can enhance T cell activation and antagonist pMHCs can decrease T cell activation remains unclear. Under a kinetic proofreading scheme of T cell activation, the implication of pMHCs with short dissociation time is incomplete phosphorylation of the TCR complex if the dissociation time is below a threshold. In experimental agreement with this, antagonist ligands have been shown to activate some, but not all, of the biochemical events necessary for TCR signalling. It has been found that stimulation of the TCR by antagonist ligands results in incomplete patterns of ζ-chain phosphorylation and a failure to activate ZAP-70 [145, 155–157]. It has also been found that antagonist ligands can attract the polarisation of the T cell Golgi away from the adjoining dendritic cells that were presenting agonist ligands [152], indicating that antagonists have a dissociation time long enough for immunological synapse assembly. It is still not known however if antagonism is mediated by the outcompeting of agonists for TCR occupancy or if antagonists produce an inhibitory signal. This question has been investigated with experiments involving T cell hybridomas expressing two independent TCRs to determine if the stimulatory activity of an agonist pMHC that binds one TCR can be reduced by an antagonist pMHC that binds the other. In this system, some investigators did not find evidence for cross-antagonism [158, 159], while others did [96, 97]. It has

been argued that a reason for the discrepant results could be that the expression level and spatial separation of the TCRs mean that a local inhibitory signal from one TCR may not affect the second [160]. Signalling-dependent theories have suggested that proteins could associate with the incompletely phosphorylated ζ-chains through single SH2 domains [155, 160]. These proteins would be displaced during full T cell activation by ZAP-70 which has a stronger binding to fully phosphorylated ITAMs through its tandem SH2 domains. In agreement with this, the cytoplasmic tyrosine-phosphatase SHP-1 has been found to be associated with both TCRs during a dual TCR experiment that showed cross-antagonism [96]. More recent work has shown increased SHP-1 activity in T cells presented with a non-stimulatory agonist pMHC [145].

The effect of co-presentation of a second pMHC ligand (presented at 3,000 ligands per cell) for each phenotypic model is shown in Fig. 3.5. Only the kinetic proofreading with negative feedback model predicts the possibility of antagonism as a result of the initiation of negative feedback, which inhibits the response to the agonist. Antagonism is observed for the kinetic proofreading and the kinetic proofreading with limited signalling models at very high concentrations of the second pMHC complex, but the decreased response in this case is mediated by the antagonist ligand outcompeting the agonist for TCR occupancy (Fig. 3.6). As discussed above, experimental data on antagonism are controversial and in many studies, a very high concentration of the antagonistic pMHC complex is required to observe inhibition. This means that it is difficult to reject a model on the basis of whether or not it exhibits antagonism. Note that none of the current phenotypic models are able to reproduce the qualitative observation of co-presentation shown in Fig. 3.5b.

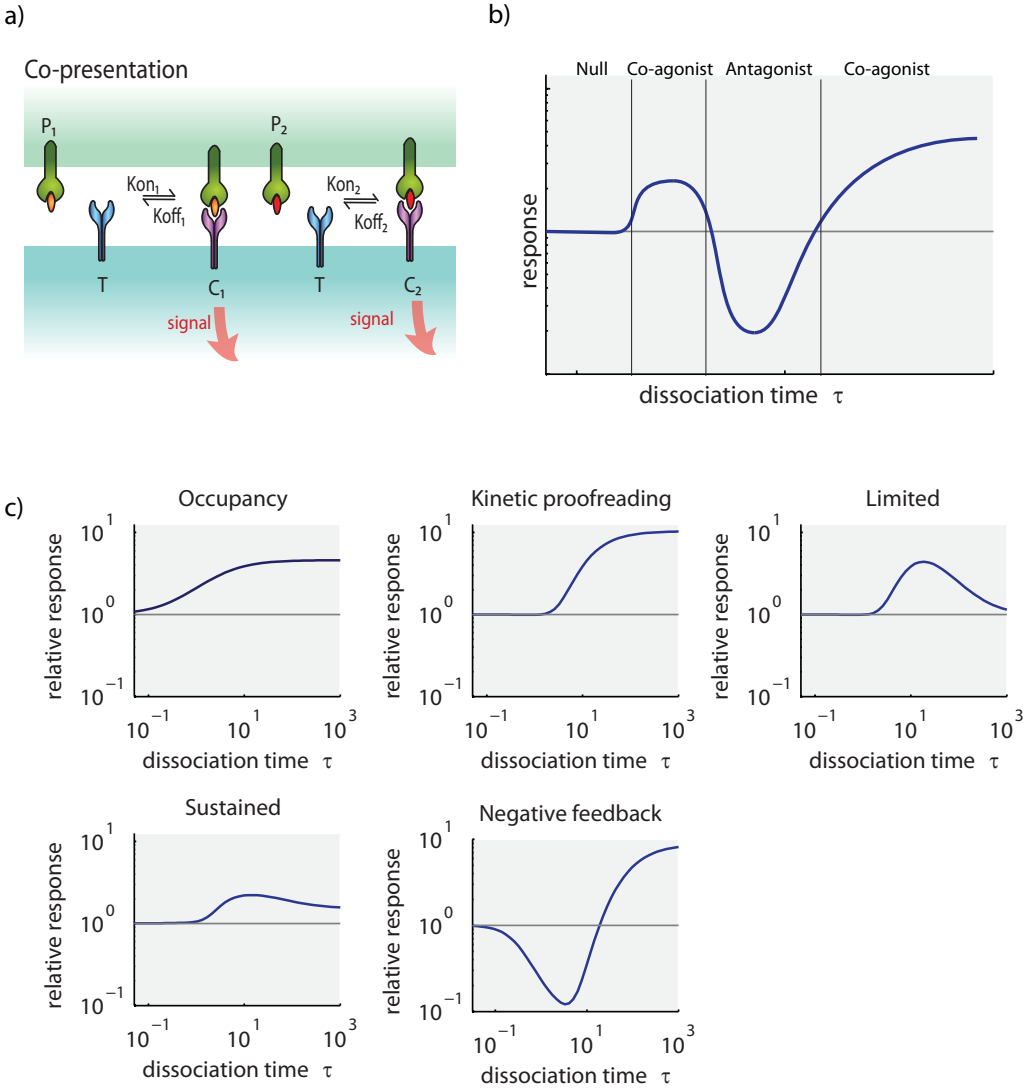

Figure 3.5: Predictions for co-presentation of a second pMHC for the phenotypic models: **a)** A schematic of the binding reactions when two different pMHC complexes are present. **b)** T cell activation is modulated by co-presentation of a second pMHC complex. The presentation of an agonist pMHC is known to elicit T cell responses (horizontal line). The co-presentation of a second pMHC is known to modulate this response (blue line) and this modulation depends on the dissociation time of the second pMHC (x-axis). **c)** These panels show the fold-change in T cell activation when the second pMHC (P2) is presented at 3,000 ligands per cell with the indicated dissociation time (x-axis). The first pMHC (P1) is assumed to have a dissociation time of 10 s and be presented at 1,000 ligands per cell. Parameters used for first four models: number of TCRs$T_T = 1.5708 \times 10^4$, $k_{\text{on}} = 3.1831 \times 10^{-5}$ s^{-1} , $k_{\text{p}} = 1$ s^{-1}, $N = 10$, $\phi = 0.09$ s^{-1}, λ = 0.001 s^{-1}. Parameters used for feedback model: number of TCRs $T_T = 3 \times 10^4$, $S_T = 6 \times 10^5$, $k_{\text{on}} = 1 \times 10^{-4} s^{-1}$, $k_{\text{p}} = 0.252 s^{-1}$, $N = 10$, $b = 0.04 s^{-1}$, $\gamma = 4.4 \times 10^{-4}$.

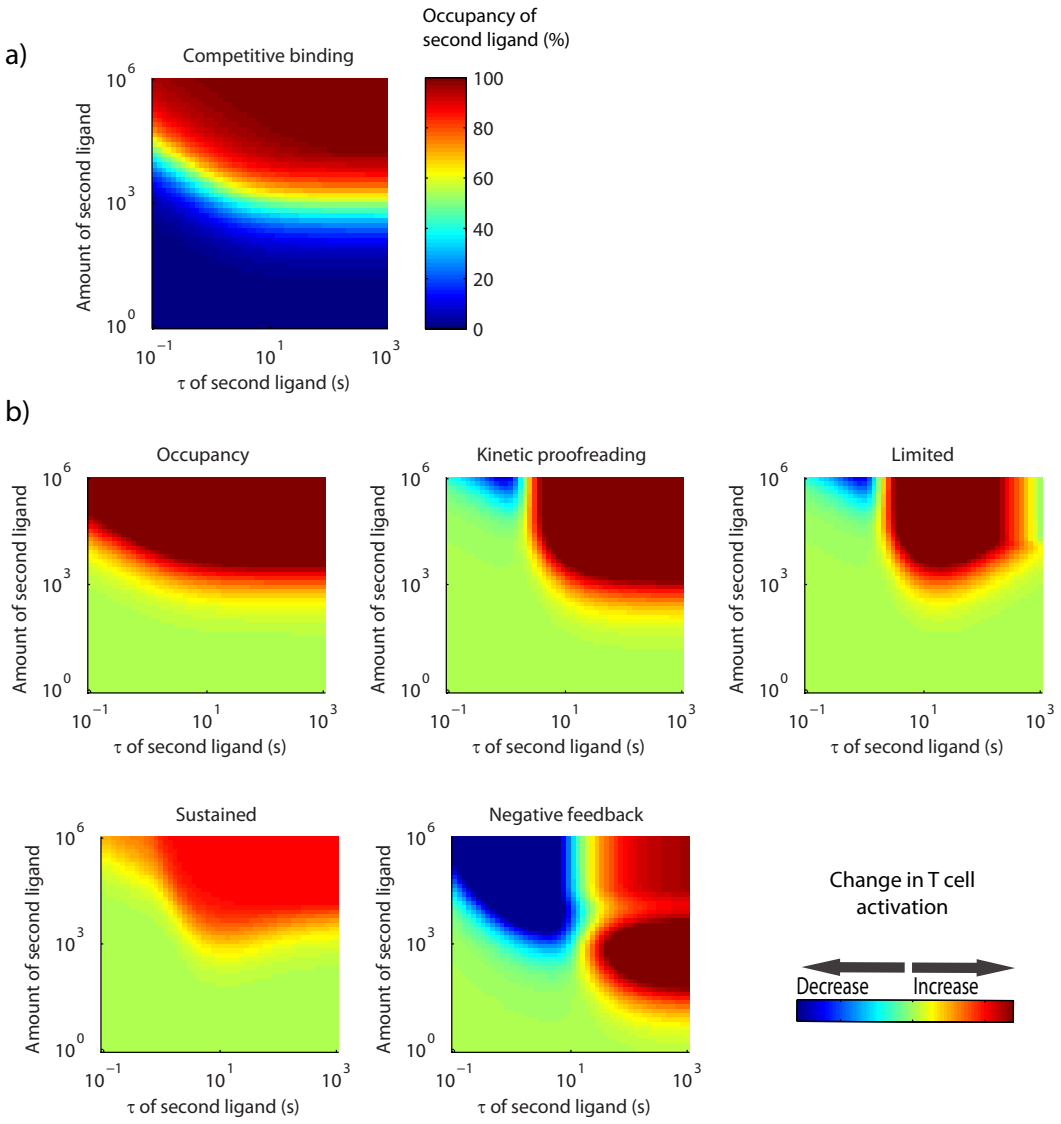

Figure 3.6: Predictions for co-presentation for a second pMHC of varying dissociation time and concentration: a) TCR occupancy of the second pMHC: The first ligand has τ = 10s and is presented at 10^3 ligands. The second ligand has a dissociation time and ligand number denoted by the axes. The plot shows the percentage of occupied TCRs that are engaged by the second ligand. This figure was produced using the analytical result for co-presentation under the occupation model. Parameters used: number of TCRs$T_T = 1.5708 \times 10^4$, k_{on} = 3.1831 $\times 10^{-5} s^{-1}$. **b)** The change in the level of T cell activation when a second pMHC is co-presented compared to the first pMHC alone. The first pMHC has τ = 10s and is presented at 10^3 ligands. The second pMHC has a dissociation time and ligand number denoted by the axes. The occupancy, kinetic proofreading, limited signalling and sustained signalling models were all simulated using the analytical derivations. The negative feedback model was simulated using the ode15s solver function in Matlab. A heat map was applied to matrices that contained the relative change in activation due to co-presentation. The same color bar was used for all plots so that the models could be compared. Parameters used for first four models: number of TCRs $T_T = 1.5708 \times 10^4$, k_{on} = 3.1831 $\times 10^{-5} s^{-1}$, $k_{\text{p}} = 1$ s^{-1}, $N = 10$, $\phi = 0.09$ s^{-1}, λ = 0.001 s^{-1}. Parameters used for feedback model: number of TCRs $T_T = 3 \times 10^4$, $S_T = 6 \times 10^5$, $k_{\text{on}} = 1 \times 10^{-4} s^{-1}$, $k_{\text{p}} = 0.252 s^{-1}$, $N = 10$, $b = 0.04 s^{-1}$, $\gamma = 4.4 \times 10^{-4}$.

3.9 Effects of thresholds and switches

So far, it has been assumed that the fraction of signalling-competent TCRs in each model directly determines the extent of activation in individual T cells. However, TCR signals are processed by complex cellular signalling machinery [1], which ultimately determines the extent of T cell activation (Fig. 3.7a.). Since cellular signalling is known to exhibit thresholds and switches [102, 161–163], the consequences of such signal processing will be examined for the phenotypic models.

There is evidence for digital signalling in T cells, whereby the concentration of phosphorylated extracellular signal regulated kinase (pERK) in individual T cells seems to exist in only two modes namely, either fully dephosphorylated or fully phosphorylated [102, 162]. Mechanisms for producing such all-or-none responses often involve feedback between signalling proteins [162, 164]. The effect of the assumption that cellular signalling is an all-or-none event is to produce a good threshold and a good switch, which changes the predicted dose-respose profiles from the phenotypic models (as shown in Fig. 3.7b.). T cell activation is now predicted to be highly sensitive to the number of ligands, and this produces steep doseresponse curves. Such highly sensitive doseresponse curves have been experimentally observed for various functional T cell responses, such as the production of interleukin-2 (IL-2), tumour necrosis factor and interferon-γ (IFNγ), and certain functional readouts, such as CD69 expression, seem to occur in an all-or-none manner [90, 91, 108, 162].

A key drawback with all-or-none cellular signalling is that it cannot explain the differential activation states of certain functional responses in individual T cells, which is further exemplified by the fact that $E_{\max}$ seems to be independent of the dissociation time (Fig. 3.7b.) This is inconsistent with experimental data showing that the amount of IFN-γ produced by individual T cells directly depends on the pMHC concentration and dissociation time [91, 115] and it has recently been shown that the rate of IL-2 production is proportional to antigen dose [165].

One possible way to reconcile these observations is to assume that the cellular signalling pathway for these functional responses exhibits a threshold but not a switch (Fig.

3.7c.). A simple signalling mechanism to produce a good threshold but a poor switch is multisite phosphorylation [166]. Under this assumption, T cell activation is sensitive to pMHC number while still maintaining differential activation states for individual T cells. Experiments measuring the number of triggered TCRs (a proxy for TCR signalling) as a function of IFN-γ have produced this precise relationship [161].

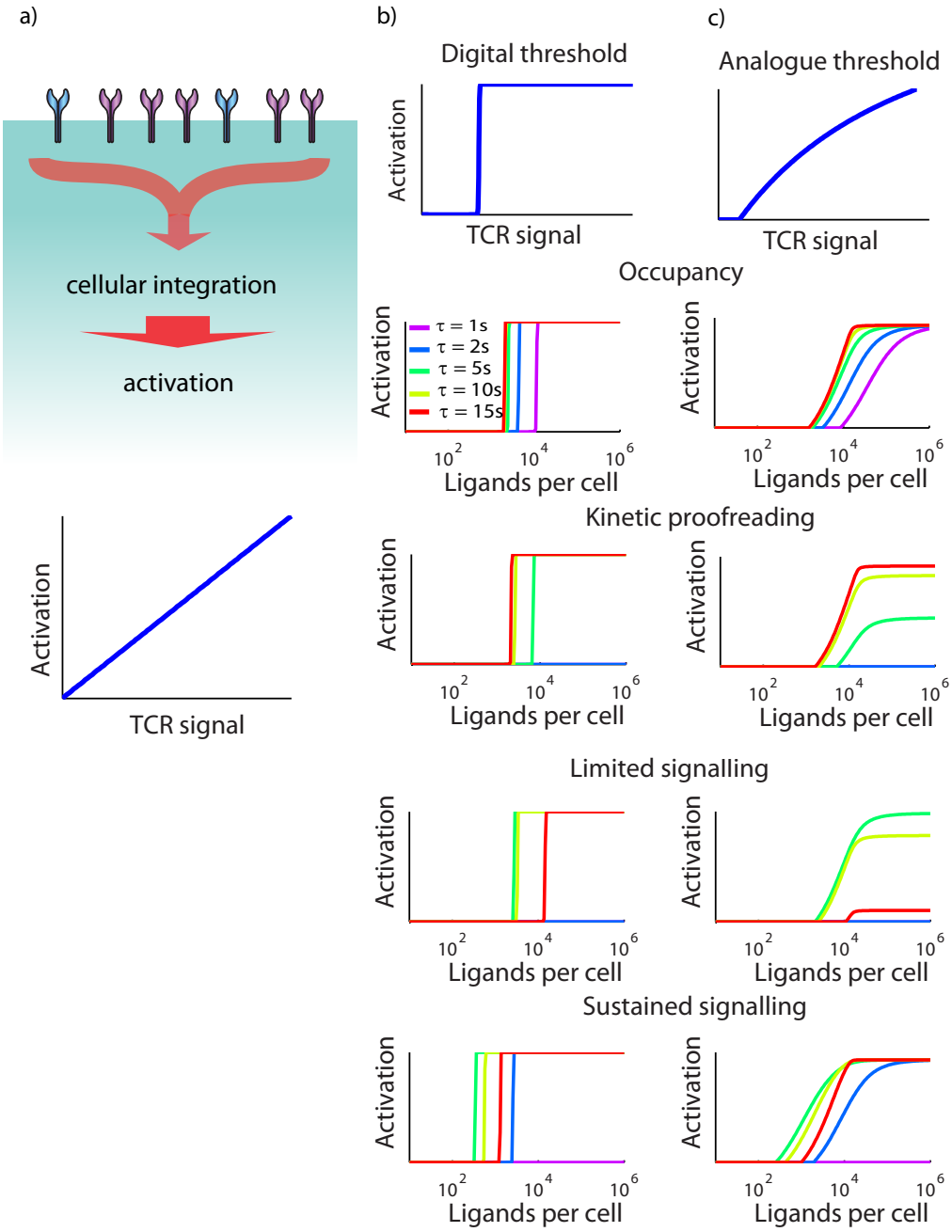

Figure 3.7: Effects of thresholds and switches in cellular signalling on T cell activation: a) The cellular signalling machinery integrates signals from signalling-competent T cell receptors (TCRs) and translates this information into the degree of T cell activation. All models that have been presented so far have assumed that the cellular signalling machinery linearly relates the TCR signal into T cell activation. **b)** Predictions for models when the cellular machinery produces a good threshold and good switch. **c)** Predictions for models when the cellular machinery produces a good threshold and poor switch. The plots were made by calculating the models at the shown dissociation times and then applying a transformation of either b) a threshold and switch or c) a threshold to the TCR signal and the resultant activation plotted as a function of ligand dose. Parameters used: number of TCRs $T_T = 1.5708 \times 10^4$, k_{on} = 3.1831 $\times 10^{-5} s^{-1}$, $k_{\text{p}} = 1\ \text{s}^{-1}$, $N = 10$, $\phi = 0.09\ \text{s}^{-1}$, λ = 0.001 s^{-1}

3.10 Discussion

In this chapter, the models of T cell activation have been reformulated into simple phenotypic models. This has enabled the direct comparison of their predictions for the T cell response for different pMHC doses and binding parameters. In some form or another, there is experimental support for all of the proposed phenotypic models.

Experiments that show a correlation between EC_{50} and K_{D} [87–89, 99] support all of the models apart from kinetic proofreading with negative feedback. Experiments that show a correlation between $E_{\max}$ and dissociation time [90, 91, 94, 134] provide support for kinetic proofreading. The evidence of an optimal dissociation time, which has been found *in vitro* [92–94] and *in vivo* studies [130, 131, 135] supports the kinetic proofreading with sustained signalling model at low pMHC doses and also the kinetic proofreading with limited signalling model at all pMHC doses. Although there is experimental support for an optimal dissociation time that is dose-dependent [95], this is only from one study. In addition, the sustained signalling model predicts that all pMHCs reach the same maximal repsonse at high pMHC doses, which is inconsistent with many large datasets [90, 91, 94, 134]. It can therefore be concluded that the majority of the experimental evidence supports the kinetic proofreading with limited signalling model. Although some datasets show a correlation between $E_{\max}$ and dissociation time, rather than an optimal, this could be because they do not go to sufficiently long dissociation times to see this behaviour. Studies that see an optimal dissociation time generally used pMHC-TCR interactions of superphysiological affinity [92, 94].

In its present formulation, the kinetic proofreading with negative feedback model is unable to reproduce an optimal dissociation time but it does predict an optimal pMHC dose for T cell activation. There is some experimental evidence for an optimal antigen dose [103, 127, 137, 167], but additional work with antigens of varying affinities is needed. None of the models can explain the complex relationship of multiple pMHC presentation, although the kinetic proofreading with negative feedback model does predict antagonism mediated by negative signalling. It is important to note that the published experimental data are incomplete, with experiments typically using only a small panel

of TCRs (or pMHC complexes) with a limited range of affinities, and a single or just a few different doses of antigen or pMHC. This means that further quantitative experiments must be done to further inform the modelling.

This analysis highlights that a large dataset consisting of T cell activation measurements as a function of pMHC dose and affinity can be used to differentiate between the various phenotypic models because each model makes different predictions (Fig. 3.2). In the following chapter, I present the results from precisely this type of experiment. It is found that the experimental data cannot be explained by any of the phenotypic models. In Chapter 5, I develop a novel phenotypic model that can account for the experimental data.

4
Experimental results

4.1 Introduction

TCR recognition of pMHC triggers a signal transduction cascade within the T cell that culminates in T cell activation. A given TCR has a degree of cross-reactivity such that it can bind to a number of different pMHCs. There will be variation in the magnitude of the T cell response across different pMHCs. A pMHC that activates all functions of the T cell is termed an agonist, and agonists can be strong or weak. A partial agonist will activate some of the T cell's functions. A pMHC that inhibits the signal generated from agonist pMHC is an antagonist. If no response is elicited from the T cell when a pMHC is presented, the pMHC is null [168].

How the binding kinetics between the pMHC-TCR determine the activating potential of a pMHC remains controversial. Studies have attempted to explore this relationship through assays that involve stimulating a population of T cells with titrations of pMHC that are either presented on an APC or plate-bound. Despite numerous studies, there is no consensus across published data since different conclusions have been drawn from the various studies. As discussed in the previous chapter, some studies show that the EC_{50} correlates with $K_{\mathrm{D}}(= k_{\mathrm{off}}/k_{\mathrm{on}})$ [87–89, 99], or equivalently the dissociation time $\tau(= 1/k_{\mathrm{off}})$. Other studies show that the $E_{\max}$ correlates with τ [90, 91, 94, 134], while others show that there is an optimal τ that gives the greatest $E_{\max}$ [92–94]. One study has

found the optimal τ to disappear at high pMHC concentrations [95]. Finally, a few studies have found dose-response profiles that are bell-shaped, that is, there is an inhibition in the response at high pMHC doses [103, 127, 136, 137].

A reason for inconsistencies between studies is due to a number of factors, including limitations in the range of pMHC affinities, which prevents a quantitative exploration across the whole spectrum of TCR stimulation. It could be that some studies do not obtain the result of an optimal τ because they do not use high enough affinity pMHCs. There is also the factor of pMHC dose; some studies only stimulate with one or two pMHC doses. Other studies present pMHC on APCs, which means they are unable to use a good control for pMHC immobilisation. Both of these factors mean that the role of pMHC dose cannot be quantitatively explored. Some studies use systems where one pMHC is used to stimulate T cells expressing distinct TCRs. These experiments cannot control for TCR number, since there are usually differences in expression across transductions of different TCRs.

In order to circumvent these issues, an assay was developed to quantitatively examine T cell activation. The system involves T cells transduced to express a high affinity TCR, termed the c58c61 1G4 High Affinity TCR [32]. This TCR binds to its cognate pMHC with pM K_{D}, and an advantage of this is that it allows a panel of pMHC to be generated that have a large range of measurable affinities for the TCR. The panel was generated by introducing point mutations to the cognate pMHC, and the results show that these pMHC have almost a 10^5 range in affinity for the TCR, as measured by surface plasmon resonance. I show in this chapter the results of stimulation assays, where titrations of immobilised pMHC are presented to populations of T cells expressing the 1G4 High Affinity TCR and different measures of activation are taken several hours after stimulation. The results show the dose-response profiles of cytokine secretion for Jurkats (IL-8) and Primary cells (IFN-γ) are bell-shaped. It is also found that at low pMHC doses, an intermediate τ gives the greatest response. Finally, I show that the bell-shaped dose response is not a result of cell-death from high levels of T-cell stimulation.

Knowledge of how pMHC-TCR binding parameters determine T cell activation is useful for the development of immunotherapies that attempt to overcome the typically

weak response of the immune system to tumour-specific antigens. The wildtype 1G4 TCR binds to the peptide with amino acid sequence SLLMWITQC derived from the cancer testis antigen NY-ESO-1 (NY-ESO-1:157-165) when presented on MHC molecule HLA-A2 [169–171]. The NYESO-1 antigen is an ideal target for immunotherapy since it is upregulated in many cancer types, including melanoma, breast cancer, bladder cancer and prostate cancer, while restricted in normal tissues [123]. The NYESO-1:157-165 epitope - or its analogues - in particular has been the focus of development for vaccine-based immunotherapies and diagnosis [170, 172–175]. It has been found that mutating the cystine to valine improves the immunogeneicity of the epitope by improving its binding affinity to HLA-A2 [170–173]. Applications targeting the NYESO-1:157-165 9V peptide include ImmTACs, which couple a soluble high affinity TCR to an anti-CD3 single-chain variable fragment (scFv) [174] that can be adminstered to target T cells to NYESO-1 expressing cancers. Another study has developed affinity matured Fab antibodies against the peptide, which could be used for diagnostic purposes or grafted onto T cells for directed killing [176].

4.2 Production of panel of pMHC with 10^5-fold range in affinity for the 1G4 High Affinity TCR

A panel of pMHC variants that bind to the 1G4 High Affinity TCR were generated by making mutations of the HLA-A2/NYESO-1:157-165 9V pMHC (WT/9V). Mutations were made to either the HLA-A2 heavy chain, the peptide sequence, or both. No mutations were made to anchor residues. The nomenclature for mutations is to note the mutations to the HLA-A2 molecule and the peptide sequence with respect to the WT/9V pMHC. Mutations for the HLA-A2 complex were to alanine, or else a glycine if the residues were alanine to begin with. The HLA-A2 heavy chain and β_2-microglobulin were expressed in E.coli and refolded with the peptides. The α and β chains of the c58c61 High affinity 1G4 TCR were expressed in E.coli and refolded. The protein structures of the 1G4 High Affinity TCR and WT/9V are shown in Fig. 4.1.

The binding kinetics between variants of the WT/9V pMHC and 1G4 high TCR were measured by Biacore. The pMHC subunits were first purified according to Chapter 2

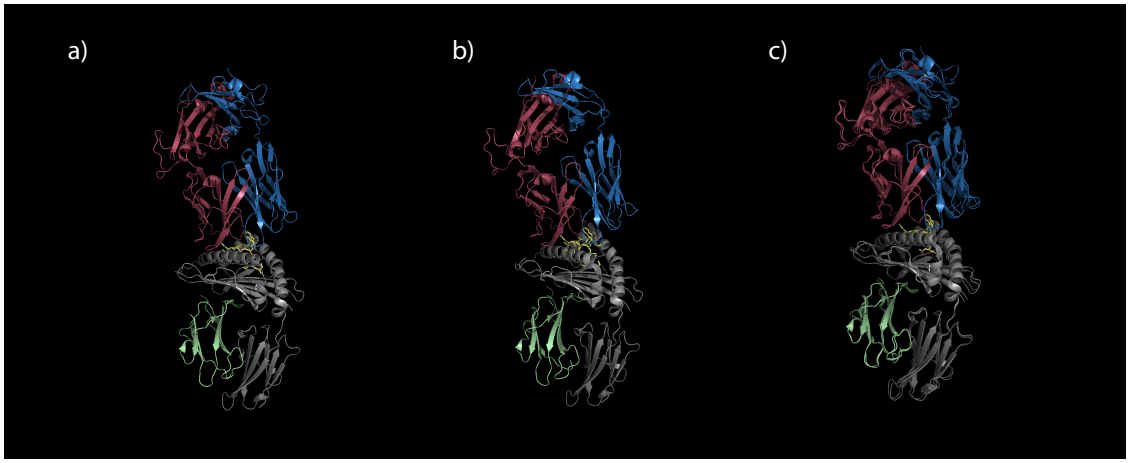

Figure 4.1: Protein structure of WT 1G4 TCR and c58c61 1G4 High Affinity TCR binding to NYESO-1 9V pMHC: a) WT 1G4 TCR (PDB ID: 2BNR) [171], **b)** c58c61 1G4 High Affinity TCR [177] (PDB ID: 2P5E), **c)** Overlap of WT 1G4 TCR and c58c61 1G4 Both TCRs are in complex with HLA-A2 presenting NYESO-1 9V.

Section 2.3. For high affinity ligands, a single concentration of TCR was used (Fig. 4.2 9V and 4A). This is because the dissociation time between the pMHC-TCR was hours, and so performing measurements at multiple doses was not feasible. For intermediate affinity ligands and below, multiple TCR concentrations were used (Fig. 4.2 8K) due to the shorter dissociation time. Using multiple concentrations gives more accuracy in the measured parameters. For both high and intermediate affinity pMHCs, the k_{off} and k_{on} were fitted directly to the surface plasmon resonance (SPR) traces. For lower affinity ligands there was greater noise in the SPR trace due to lower amount of pMHC immobilised on the chip, making it difficult to determine the k_{on} directly. To account for this, the K_{D} was determined by equilibrium binding analysis and the k_{on} was then calculated using the fitted k_{off} (Fig. 4.2 5P). Fitting the K_{D} by equilibrium binding uses less information from the SPR curve compared to fitting the k_{on}, and so could be more prone to error. However, if the SPR curve is noisy, specific binding can provide a better estimate.

The SPR experiments show that the panel of pMHC have affinities spanning 10^5, with the majority of this variation being in the k_{off} of the ligand. A scatter plot of the average k_{on} and k_{off} values is shown in Fig. (4.3) and summarised in Table 4.1.

MHC/peptide	k_{off} (s^{-1})	No.	SEM	k_{on} ($\text{M}s)^{-1}$	No.	SEM	K_{D} (M)	SEM
72, 75/9V	6.03E-05	3	4.02E-06	8.54E+05	3	8.24E+03	7.06E-11	5.38E-12
WT/9V	8.26E-05	7	1.03E-06	1.17E+06	7	2.80E+04	7.07E-11	2.57E-12
151,154/9V	1.42E-04	4	3.68E-06	7.62E+05	4	2.77E+04	1.86E-10	1.16E-11
WT/4A	1.54E-03	3	1.77E-05	1.41E+06	3	1.15E+05	1.09E-09	1.01E-10
WT/5Y	1.67E-03	4	1.18E-04	1.26E+06	4	3.14E+05	1.33E-09	4.26E-10
WT/8S	1.33E-02	4	2.29E-03	1.03E+06	4	2.72E+05	1.29E-08	5.64E-09
WT/6T	7.14E-02	2	1.43E-02	8.64E+05	1	na	8.27E-08	na
WT/8K	8.33E-02	4	6.46E-03	4.10E+05	3	2.98E+04	2.03E-07	3.05E-08
69,154/8S	8.82E-02	2	1.85E-03	5.79E+05	2	6.50E+03	1.52E-07	4.90E-09
WT/5F	1.01E-01	4	7.08E-03	1.09E+06	4	2.03E+05	9.31E-08	2.39E-08
WT/5P	9.80E-01	4	7.76E-02	2.02E+06	2	2.39E+05	4.85E-07	9.59E-08
69,154/5F	1.06E+00	2	1.45E-02	9.73E+05	2	2.25E+04	1.09E-06	4.01E-08
WT/4A8K	1.95E+00	5	5.31E-02	1.10E+06	5	1.34E+05	1.78E-06	2.65E-07
WT/4A5P	3.78E+00	1	na	7.07E+05	1	na	5.34E-06	na
WT/4A5A	5.64E+00	3	5.62E-01	2.52E+05	3	5.47E+04	2.24E-05	7.10E-06
WT/5A	9.20E+00	1	na	6.98E+05	1	na	1.32E-05	na

Table 4.1: Summary of binding kinetics data for mutants of the HLA-A2/NYESO-1 pMHC to the c58c61 1G4 High Affinity TCR: The average measurement, number of measurements taken and the standard error of the mean (SEM). Measurements were taken using surface plasmon resonance and analysed in GraphPad Prism. The MHC mutants were generated by Hong-Sheng Lim. Expression and refolding of the TCR was done by Hong-Sheng Lim and expression and refolding of pMHC variants was done by Hong-Sheng Lim and Melissa Lever. Biacore measurements were taken by Hong-Sheng Lim, Ann Tivey and Melissa Lever.

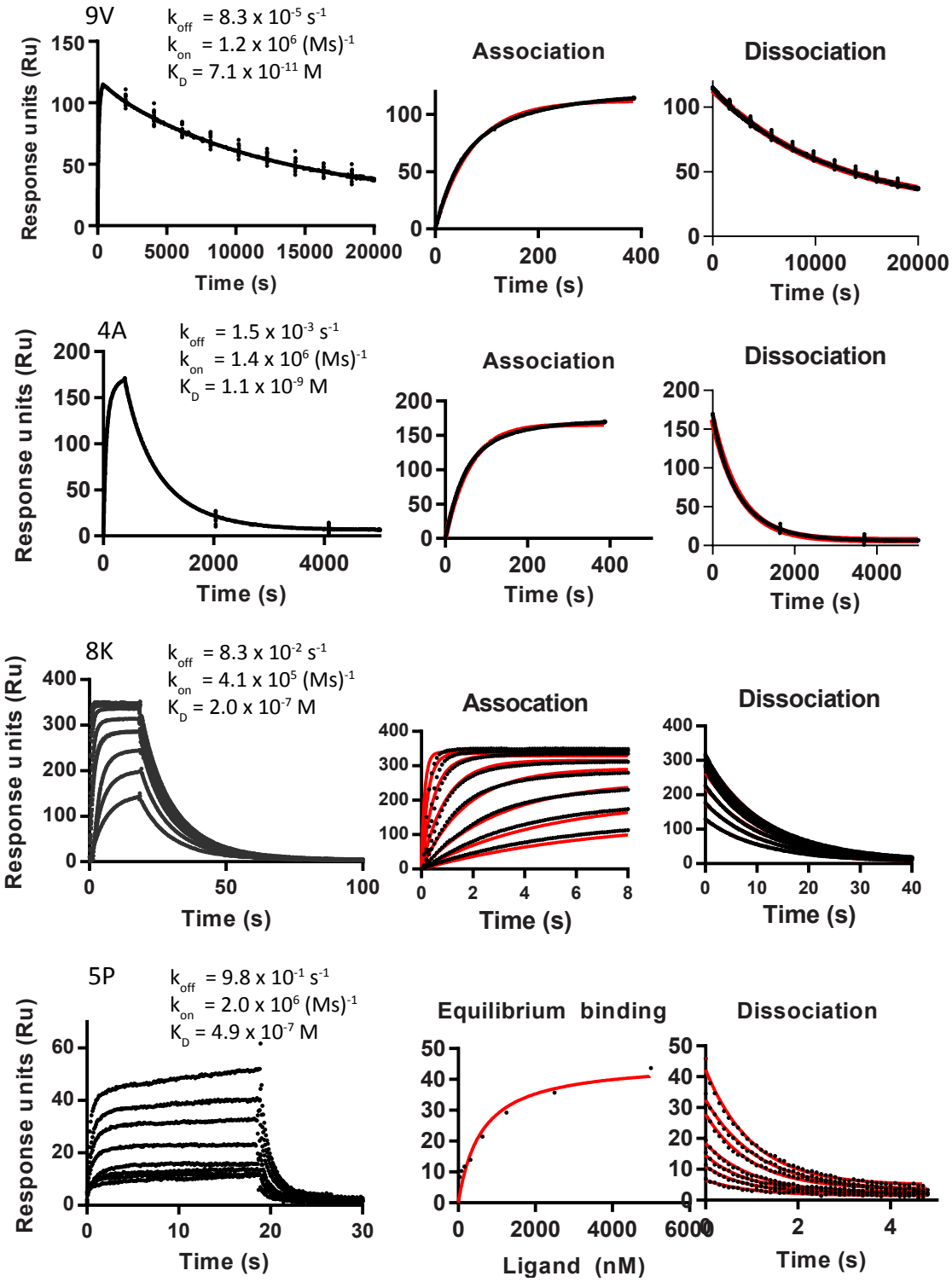

Figure 4.2: Example binding kinetic datasets for mutants of the HLA-A2/NYESO-1 pMHC to the c58c61 1G4 High Affinity TCR: Measurements were taken using surface plasmon resonance and analysed in GraphPad Prism. The MHC mutants were generated by Hong-Sheng Lim. Expression and refolding of the TCR was done by Hong-Sheng Lim and expression and refolding of pMHC variants was done by Hong-Sheng Lim and Melissa Lever. Biacore measurements were taken by Hong-Sheng Lim, Ann Tivey and Melissa Lever.

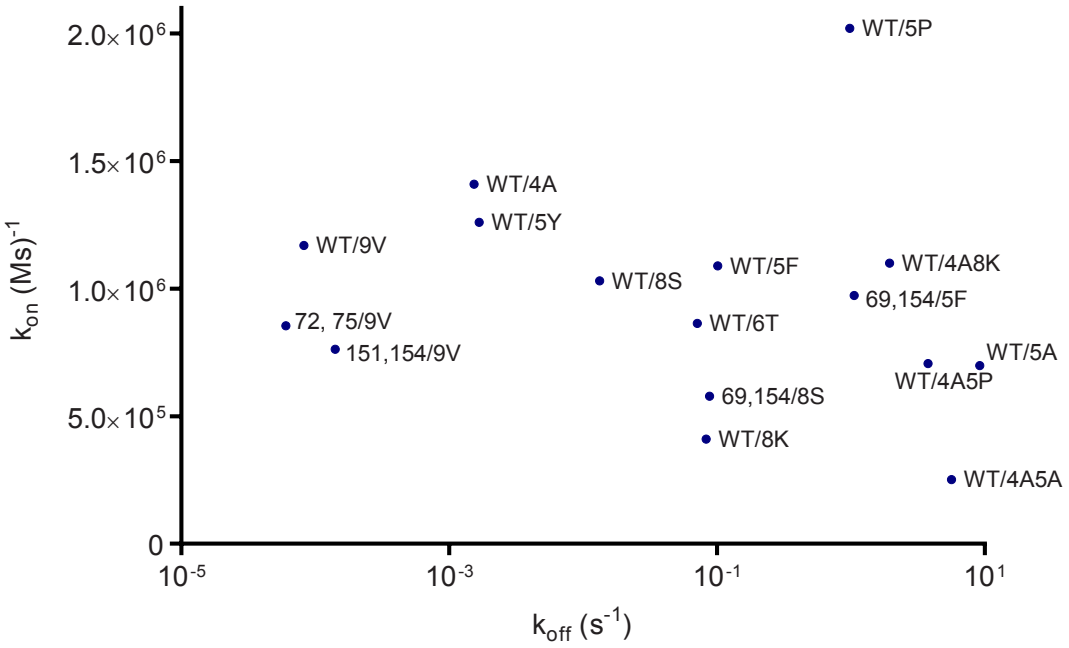

Figure 4.3: Summary of binding kinetics data for mutants of the HLA-A2/NYESO-1 pMHC to the c58c61 1G4 High Affinity TCR: Measurements were taken using surface plasmon resonance and analysed in GraphPad Prism. The MHC mutants were generated by Hong-Sheng Lim. Expression and refolding of the TCR was done by Hong-Sheng Lim and expression and refolding of pMHC variants was done by Hong-Sheng Lim and Melissa Lever. Biacore measurements were taken by Hong-Sheng Lim, Ann Tivey and Melissa Lever.

4.3 Stimulation of primary cells

Primary CD8+ T cells were isolated from HLA-A2 negative donors and transduced with the 1G4 High Affinity TCR (Chapter 2 Section 2.6). Transduction efficiencies were in the range of 50-60% (Fig. 4.4). The entire population of cells were stimulated by titrations of plate-bound pMHC, as described in Chapter 2 Section 2.7.1. Secretion of cytokines Interferon-γ (IFN-γ) (Fig. 4.5) and the Macrophage inflammatory protein-1β (MIP-1β) (Fig. 4.7) were measured after 4 hours of stimulation. 4 hours was chosen as the end time-point for stimulation because it has been found that the rate of IFN-γ secretion is linear at this time and the magnitude of secretion is sufficiently large to distinguish between different pMHCs [91]. MIP-1β production from CD8+ primary cells has been assayed after 4 hours of incubation in a study by van den Berg et al. [128]. The pMHC immobilisation controls are shown in Fig. 4.6.

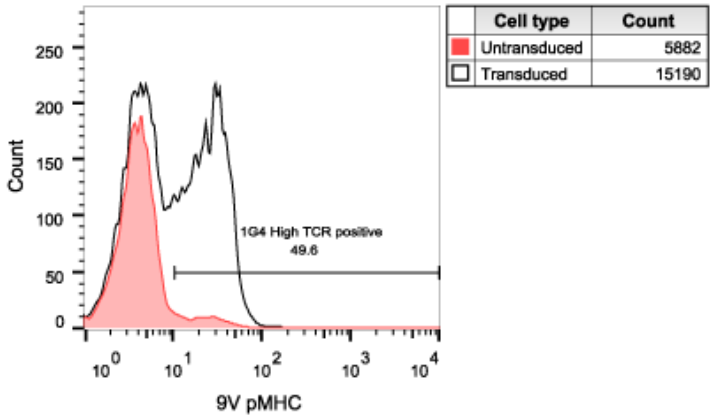

Figure 4.4: Transduction efficiency of c58c61 1G4 High Affinity TCR for Primary cells: transduction efficiency for all experiments was in the range of 50-60%. Transduction was performed by Hong-Sheng Lim and Melissa lever.

IFN-γ is a type II interferon, and is the only one in its class. The interferons were first found to be antiviral agents, but they were later found to have broader roles in regulating the immune system [178]. IFN-γ modulates a variety of cellular programs through transcriptional regulation of relevant genes. It binds to the IFN-γ receptor and signals primarily through the Jak-Stat pathway, which leads to the activation of Stat1 that controls transcription of target genes. The diverse roles of IFN-γ include the upregulation

of antigen presentation through class I and class II, CD4+ T cell differentation into T helper 1 (Th1) cells, cell growth and apoptosis in macrophages, and inhibitory and activatory roles in B cells [178, 179].

MIP-1β is part of the CC chemokine subfamily. Chemokines are chemotactic cytokines that induce recruitment of leukocytes by forming a chemical gradient. MIP-1 proteins bind to CC chemokine receptors that are on the target cell surface. This leads to downstream functions including chemotaxis, degranulation, and phagocytosis [180]. The production of MIP-1β can be induced in most mature hematopoietic cells and it can attract most leuokoctyes. MIP-1β has been found to have a neutralising effect against HIV [181], and is one of the main HIV suppressive factors of CD8+ T cells. The mechanism of suppression is through the binding of MIP-1β to CCR5, which is a major co-receptor for M-tropic HIV-1 strains [182].

There are two significant features of the IFN-γ dataset. One feature is that there is an inhibition in IFN-γ secretion at high doses of presented pMHC, and this is for all pMHCs across datasets apart from the lowest affinity pMHCs (WT/5P and WT/4A5P) in a few datasets (Fig. 4.5c,d). The second feature is that intermediate affinity pMHCs give the greatest activation at low pMHC doses. This feature is found for all datasets apart from Fig. 4.5d, where WT/9V is the most potent. Since this is the only cytokine secretion dataset (including both jurkat and primary cell data) where the highest affinity pMHC is the most potent, it can be considered an outlier. It can be seen that the most potent pMHCs tend to be WT/4A and WT/5Y, which have $K_{\mathrm{D}} \approx n$M and a dissociation time in the region of 10 minutes. Although there is quantitative variation across datasets of the extent of inhibition at high doses and over which pMHCs are most potent, the same qualitative features are conserved across datasets.

The MIP-1β secretion was taken from the same supernatant of the stimulation assays used for Fig. 4.5a-b. In contrast to IFN-γ secretion, it can be seen that the inhibition is less pronounced. It can still be seen however that intermediate affinity pMHCs give the most potent response.

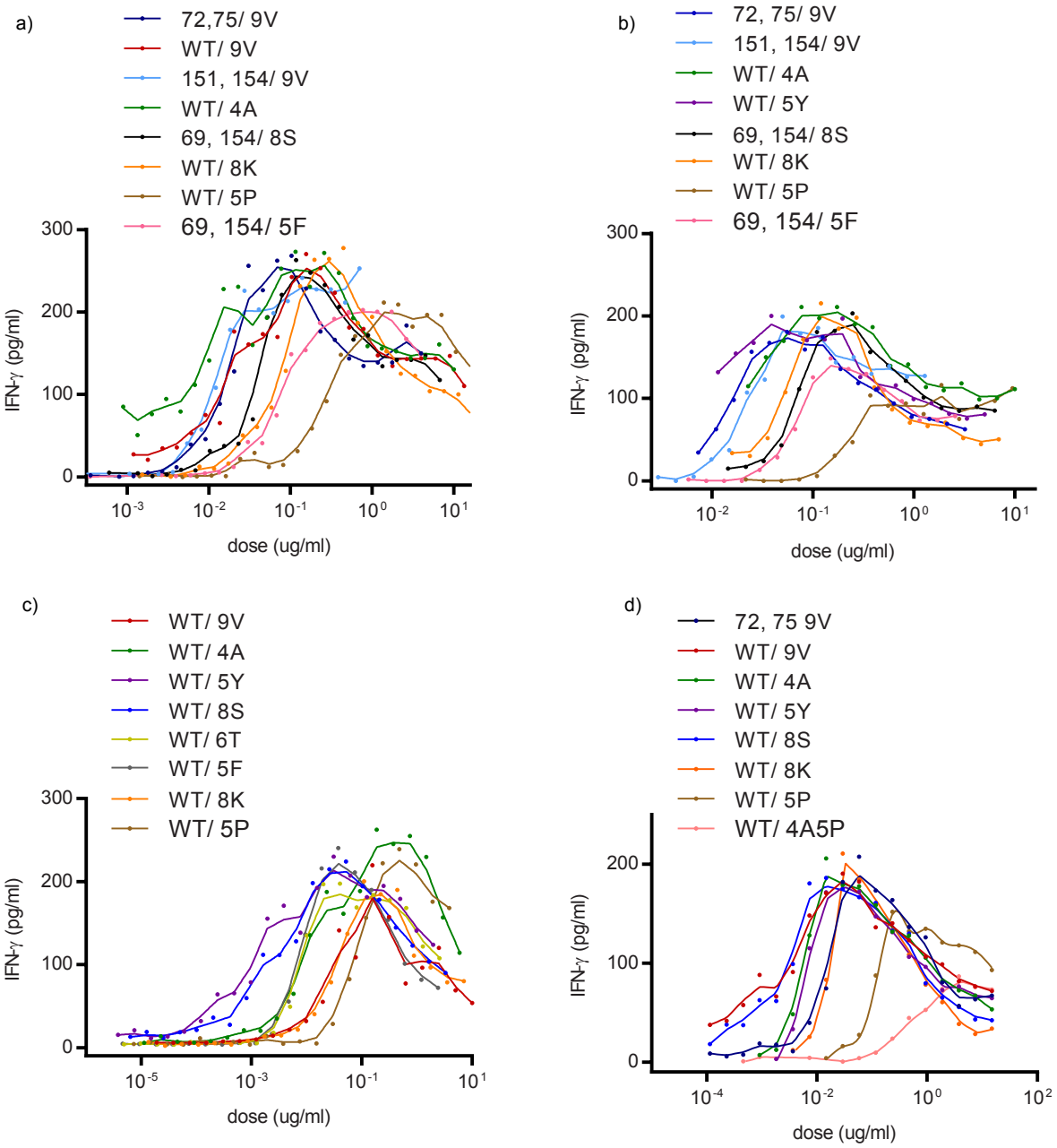

Figure 4.5: Stimulation of primary T cells with high affinity TCR reveals optimal ligand dose and affinity for IFN-γ secretion: IFN-γ secretion from CD8+ primary cells expressing the 1G4 High Affinity TCR stimulated for 4 hours with plate-bound variants of the HLA-A2/NYESO-1 pMHC. A coarse Lowess curve was fitted to the data in Graphpad Prism. Panels a) and b) were performed by Melissa Lever and panels c) and d) were performed by Hong-Sheng Lim.

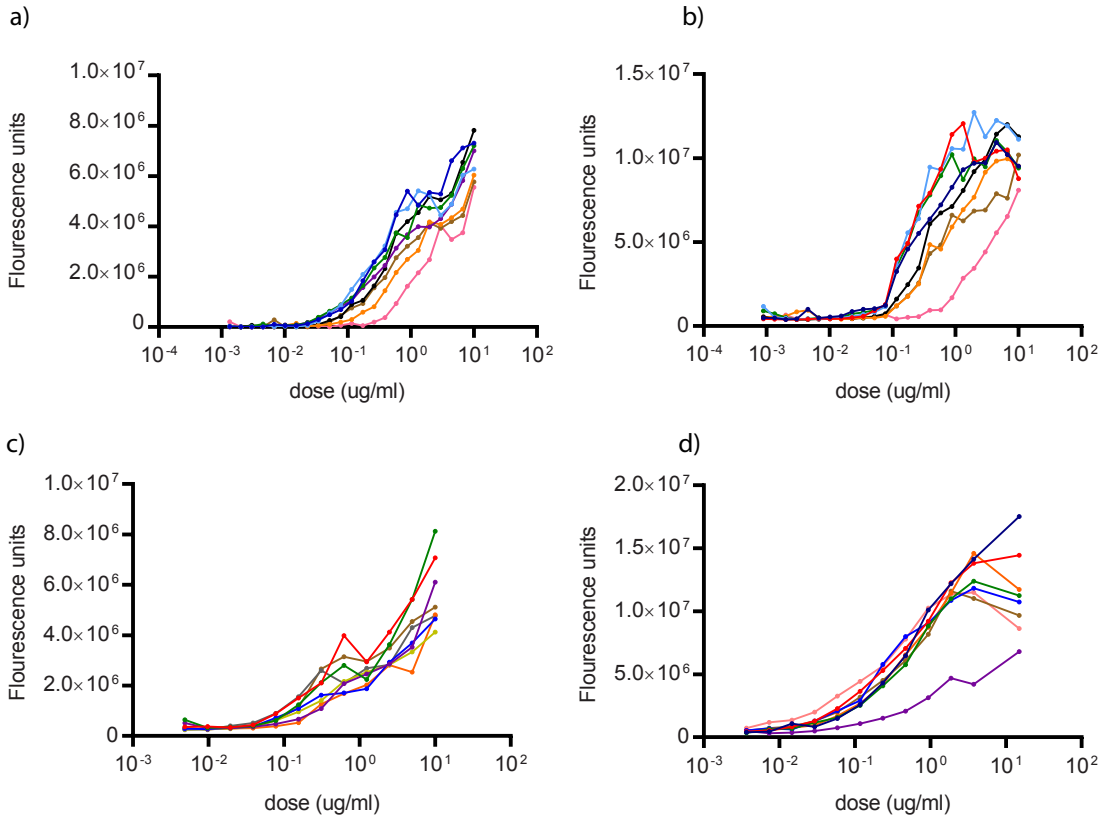

Figure 4.6: Immobilisation controls for IFN-γ experiments: An anti-HLA-A2 antibody and a secondary fluorescent antibody were used to check pMHC immobilisation on streptavidin plates. The dose-response assays were corrected for pMHC immbolisation. The panels correspond to the datasets from Fig. 4.5. Panels a) and b) were performed by Melissa Lever and panels c) and d) were performed by Hong-Sheng Lim

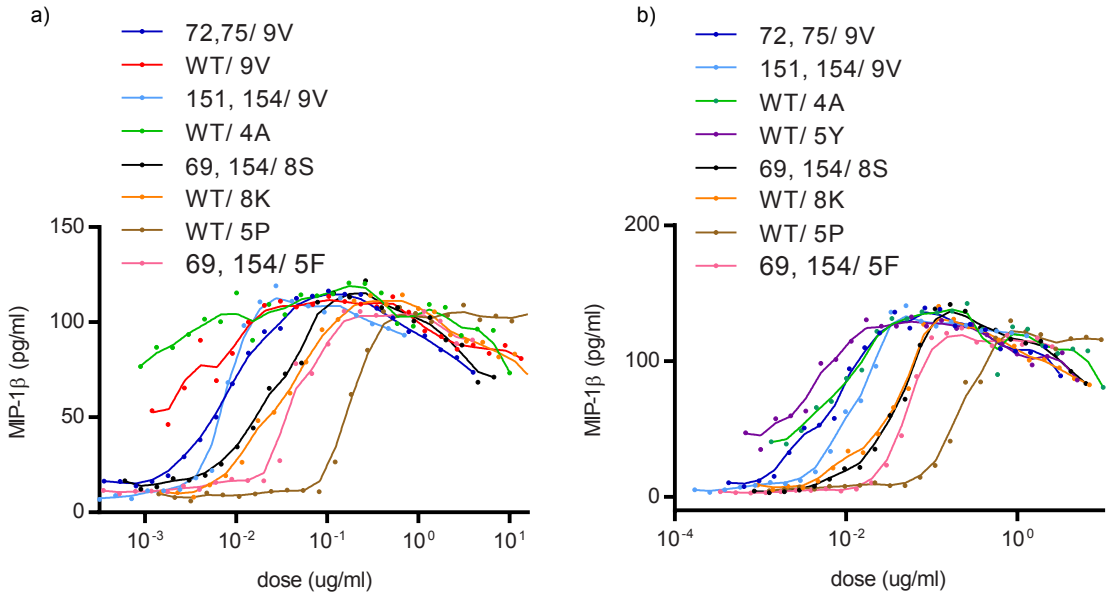

Figure 4.7: The optimum ligand dose is less pronounced for MIP-1β secretion: Secretion of MIP-1β by CD8+ primary cells expressing the 1G4 High Affinity TCR after plate-bound stimulation with variants of the HLA-A2/NYESO-1 pMHC for 4 hours. MIP-1β was measured from the same supernatant that was used to measure IFN-γ secretion (Fig. 4.5a-b). A coarse Lowess curve was fitted to the data in Graphpad Prism. These experiments were performed by Hong-Sheng Lim.

4.4 Stimulation of Jurkat cells

Stimulation assays were also performed on E6.1 CD8α+ Jurkat T cells expressing an NFAT-luciferase reporter. The cells were transduced to express the 1G4 High Affinity TCR (Section 2.6). In these cells, the transcription of firefly luciferase is activated by NFAT. The luciferase monomer can be catalysed into oxyfluoroluciferin with the substrate 5'-fluoroluciferin. This reaction produces a bright luminescence which can be measured as a proxy for NFAT reporter activity.

Jurkats secrete a limited amount of cytokines in comparison to Primary cells [183], but they were found to secrete significant amounts of the IL-8 in response to stimulation. IL-8 is a chemokine and its production is kept low in the absence of external stimulation. Upon stimulation IL-8 production is rapidly induced by the transcription factors NF-κB and AP-1 [184]. It is therefore a suitable readout for cellular activation.

The Jurkat cells were stimulated as described in Section 2.7.1 for 16 hours. NFAT reporter activity (Section 2.7.3) and IL-8 secretion (Section 2.7.4) were measured . IL-8 secretion shows that as for IFN-γ secretion from primary cells, there is an optimal pMHC dose and intermediate affinities are the most potent (Fig. 4.8). There is quantitative variation across the datasets in that the pMHC that is most potent varies, and the extent of inhibition varies. However, the qualitative features are maintained across datasets.

The optimal pMHC dose is also evident at the level of NFAT transcription (Fig. 4.9). It is not clear that intermediate affinities are most potent, although it is difficult to determine since the luminescence assay is noisy in comparison to the cytokine secretion assays.

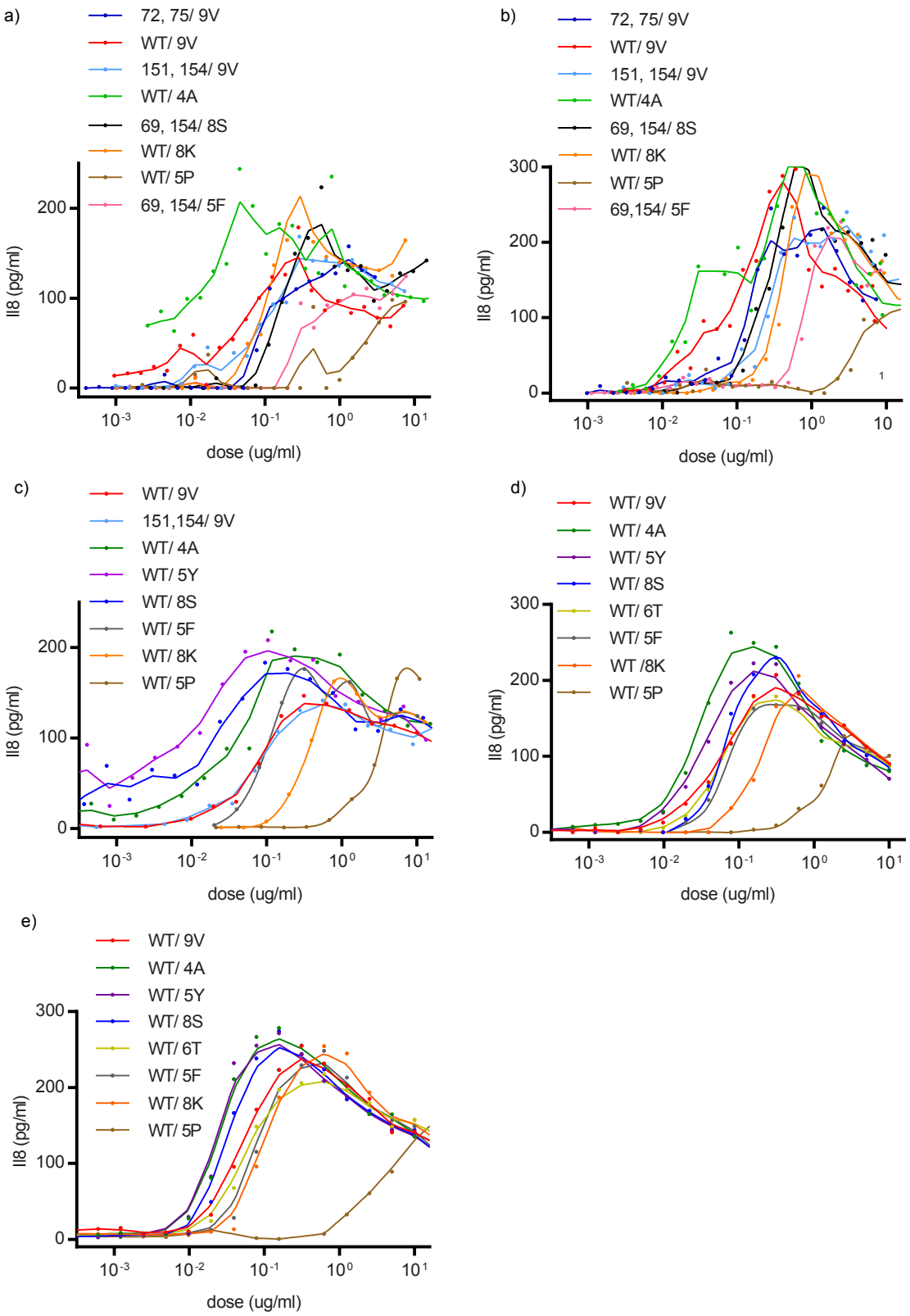

Figure 4.8: The optimum dose and binding time is confirmed with IL-8 secretion from jurkats: Secretion of IL-8 by CD8α+ jurkats expressing an NFAT-luciferase reporter and the 1G4 High Affinity TCR after plate-bound stimulation with variants of the HLA-A2/NYESO-1 pMHC for 16 hours. A coarse Lowess curve was fitted to the data in GraphPad Prism. Panels a) and b) were performed by Hong-Sheng Lim and panels c)-e) were performed by Melissa Lever

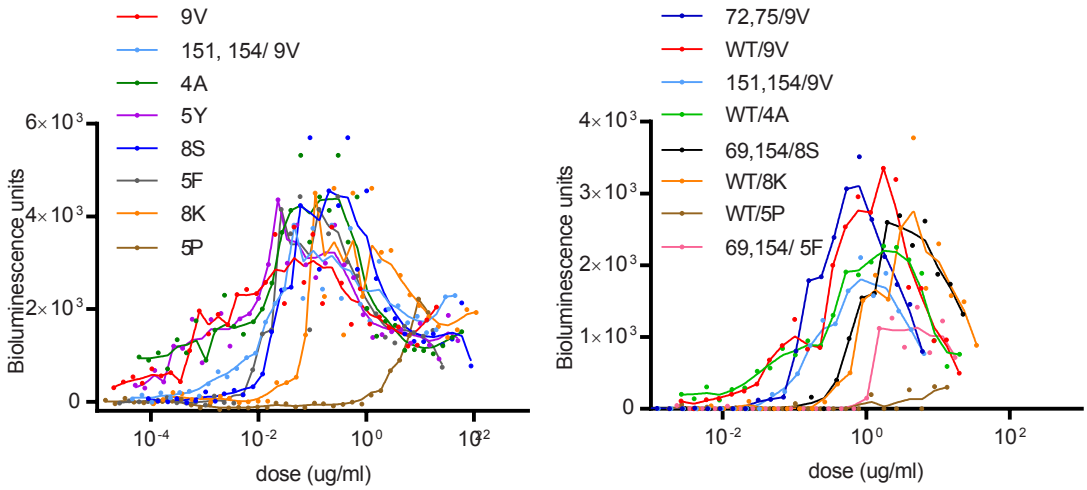

Figure 4.9: The optimum dose is evident at the level of NFAT transcription: NFAT transcription by CD8α+ jurkats expressing an NFAT-luciferase reporter and the 1G4 High Affinity TCR. Bioluminesence was read after plate-bound stimulation with variants of the HLA-A2/NYESO-1 pMHC for 16 hours. A coarse Lowess curve was fitted to the data in GraphPad Prism. Panel a) was performed by Melissa Lever and panel b) was performed by Hong-Sheng Lim

4.5 Controls for cell death

In order to confirm that the inhibition at high doses was not due to cell death from over-stimulation of the cells, an Annexin-V assay was performed on the jurkat cells following 16 hours of stimulation (Section 2.7.5). Annexin-V can be used to detect cells that express phosphatidylserine on their surface, which occurs during apoptosis and necrosis [185]. It has been confirmed through Annexin-V staining that tetramer stimulation of T cells induces cell death after 12 hours of stimulation, and so a similar process could be happening with plate-bound stimulation assays. By comparing Annexin-V staining from pMHCs WT/4A and WT/8K with IL-8 secretion from previous stimulation assays (Fig. 4.10), it can be seen that the pMHC induced increase in apoptosis/necrosis reaches a maximum at the same levels of presented pMHC as IL-8. This argues strongly that the reduction in T cell functional readouts at high pMHC concentration is not a consequence of cell death. Furthermore, the amount of cell death is in the region of 4-12$\%$, while the percentage drop in cytokine secretion is at more than 50%. It can therefore be reasoned that the shape of the dose-response curves is due to a signalling mechanism that is distinct to cell death.

Further evidence to support the notion that the optimal pMHC dose is due to a signalling mechanism within the T cell is that the IFN-γ data shows an optimal within 4 hours of stimulation, and it is unlikely that activation induced cell death could operate on this time scale. Additionally, the MIP-1β data do not show an optimal that is as striking as for the IFN-γ data, even though the ELISA for this cytokine was performed on the same supernatant from the IFN-γ assay; if the peak was due to cell death then it would be expected that IFN-γ and MIP-1β would show a similar shaped optimal, assuming that both cytokines were secreted linearly within 4 hours.

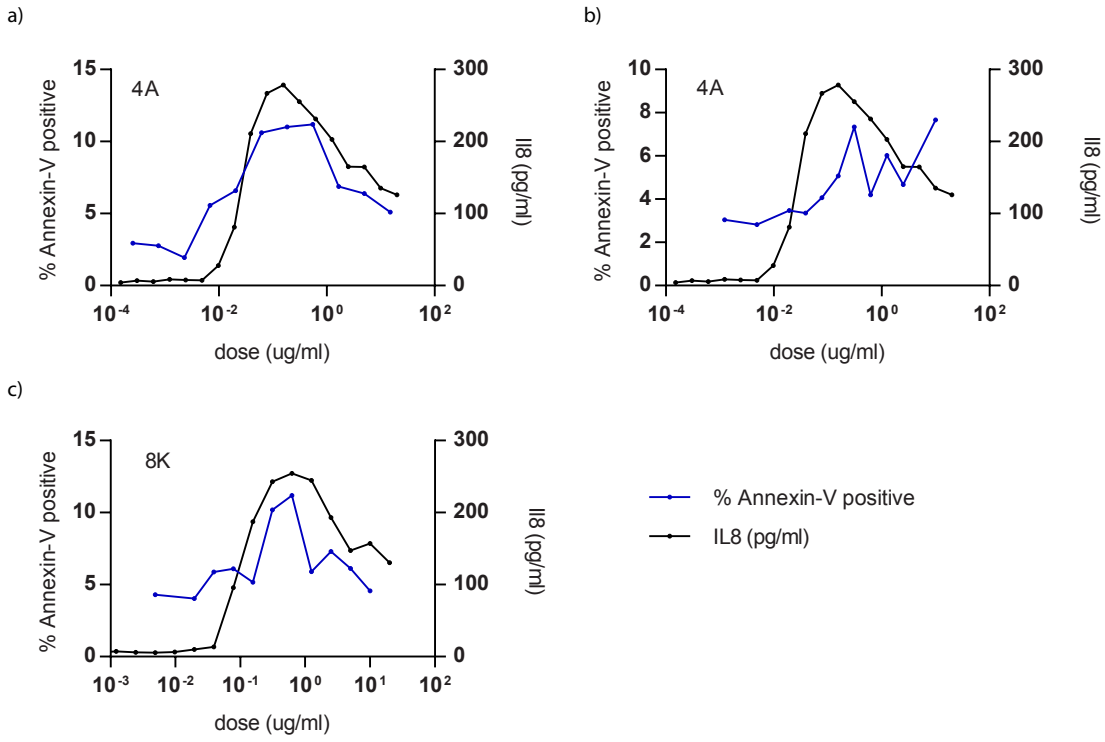

Figure 4.10: Cell death is not responsible for the inhibition at high doses: CD8α+ jurkats expressing the 1G4 High Affinity TCR were stimulated by plate-bound pMHC. Cell viability was measured after 16 hours of stimulation by Annexin-V staining. Values for IL-8 secretion are from a separate stimulation experiment (Fig. 4.8d). Experiments were performed by Melissa Lever.

4.6 Discussion

The phenotype of T cell activation was investigated through a quantitative assay that involved stimulating T cells with titrations of plate bound pMHC that had a broad range of affinity for the TCR that was expressed by the T cells. The TCR used is the 1G4 High Affinity TCR. The readouts of activation included IFN-γ and MIP-1β for primary cells and IL8 and NFAT activity for jurkats. The IFN-γ and IL-8 data show the same qualitative phenotype of an optimal pMHC dose and an intermediate affinity that gives the most potent response. The MIP-1β data also show that an intermediate affinity is most potent, but there is a less dramatic peak in the dose-dependent optimal. The NFAT data do show clear bell-shaped dose-response profiles, but it is unclear if intermediate affinities are most potent because there is a lot of noise in the data.

None of the existing models can explain the entirety of any of the datasets. The kinetic proofreading with limited signalling model can explain how intermediate affinity pMHCs are the most potent. The kinetic proofreading with negative feedback model does show an inhibition at high pMHC doses, however, this model predicts that the maximal height of a curve correlates with pMHC dissociation time. This does not agree with the data, since most datasets show very little variation between the maximal height and dissociation time, and in the cases that there is variation, there is no consistent relationship.

The optimal pMHC dose has been seen in other studies [87, 103, 127, 137, 167], but generally not as dramatically as occurs in this dataset. A reason for this could be that through the combination of using a very high affinity TCR and by presenting immobilised pMHC to maximal capacity on streptavidin plates, the T cells are being stimulated to extents far more strongly than in previous studies. It has been shown that the inhibition is not due to cell death. It is therefore likely that a negative signalling mechanism could be responsible. Various mechanisms of negative regulation of the TCR signal have been suggested that are either proximal to the TCR or further downstream [75]. It could also be possible that the optimal pMHC dose is due to a mechanism at the T cell surface, for example, a sequestering of TCR that comes into effect at high pMHC doses and affinities. However, this is unlikely because the streptavidin molecules

have four biotin binding sites, which means that the pMHC are presented as multimers and so would induce TCR clustering [186].

The other significant feature of the dataset is the optimal pMHC affinity, or dissociation time, which is in the region of 10 minutes. Several studies have found that there is an optimal pMHC affinity [90, 91, 94, 134, 187]. Interestingly, this time-scale corresponds to the down-modulation of TCR from the cell surface following stimulation by pMHC [139, 188, 189].

The readouts of MIP-1β and IFN-γ secretion from primary cells differ, suggesting that the signal transduction cascades for these cytokines are different. The dose-response profiles for these cytokines from a single experiment show the same order of pMHC potency, but they differ in the magnitude of the inhibition. This implies that the mechanism that mediates pMHC potency is upstream of the mechanism that mediates the inhibition at high doses. IFN-γ and MIP-1β could have the same early signal transduction cascade, which then diverges downstream. This could make sense if there is a limited signalling mechanism that enforces intermediate affinities to be the most potent. Since the transcription of genes to produce cytokines is dependent on the integration of multiple signalling pathways, it could be that MIP-1β transcription has less dependence on the pathway that mediates the inhibition at higher pMHC doses than IFN-γ.

If pMHC potency is mediated proximal to the membrane, it is interesting to speculate why NFAT activity does not show the same order of pMHC potency compared to IL-8. However, since the NFAT data are noisy, it is hard to determine the pMHC order in these datasets. If it is the case that the highest affinity pMHCs overlap each other at low pMHC doses, then it could be that there is a threshold in the Ca^{2+} pathway that cause the responses from the most potent pMHCs downstream of the TCR to saturate, as shown for the thresholded figures in Fig. 3.7.

Philosophy...is written in the language of mathematics, and its characters are triangles, circles, and other geometrical figures, without which it is humanly impossible to understand a single word of it; without these, one is wandering around in a dark labyrinth.

— Galileo's *The Assayer*

5 Modelling of experimental data

5.1 Introduction

The quantitative dataset generated by stimulating T cells with pMHC of over 10^5-fold range in affinity has shown several key features, summarised in Fig. 5.1. All pMHCs, excluding a few of the lowest affinity pMHCs, show bell-shaped dose response profiles. The maximum height of these dose-response profiles is assumed to be the same for all pMHCs; although there is some variation within a dataset, there is no consistent relationship between peak height and dissociation time between experiments. The datasets show that a pMHC of intermediate dissociation time gives the strongest activation at low pMHC doses. A phenotypic model must therefore exhibit these features for pMHCs that have an affinity spanning from physiological to superphysiological.

A phenotypic model must also show the characteristics for pMHCs of physiological affinity and below. As shown in Chapter 3, previous datasets in the literature that examine low affinity pMHCs show dose-response profiles that are sigmoidal, and have an $E_{\max}$ that decreases with diminishing dissociation time (Fig. 4a ref. [90], Fig. 2a ref. [91] and Fig. S1 ref. [88]). The required phenotypic features of the model are summarised in Fig. 5.1.

None of the models examined in Chapter 3 can explain all the key features, but there are models that can explain aspects of the data. The kinetic proofreading with negative feedback model can explain the bell-shaped dose response. The kinetic proofreading

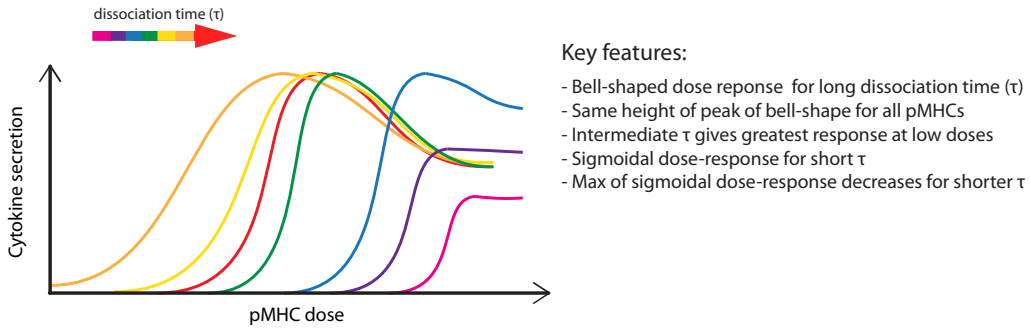

Figure 5.1: Key features of experimental data: A phenotypic model must exhibit features from the quantitative dataset as well as previous results in the literature. The quantitative dataset shows a bell-shaped dose-response for pMHCs with long dissociation time (τ), the same maximal height for all bell-shaped dose-response profiles, and an intermediate dissociation time giving the strongest activation at low doses. Previous experimental data show sigmoidal dose-response profiles for short dissociation times, with the $E_{\max}$ decreasing as the dissociation time shortens.

model can show that pMHCs of low affinity have sigmoidal dose-response profiles with an $E_{\max}$ that decreases with diminishing dissociation times. Finally, the kinetic proofreading with limited signalling and the kinetic proofreading with sustained signalling models both show that intermediate dissociation times give the greatest activation at low pMHC doses.

In this Chapter, I will formulate a phenotypic model of these key features of T cell activation by starting with the simplest possible model. From these initial assumptions, additional assumptions will be added in iterative steps and the model will be simulated. Models that cannot explain the data will be rejected at each iteration until a model is found that can explain the data. The model is related to previous models of T cell activation in the discussion. Mathematical derivations of the models are in the Appendix.

5.2 Incoherent feed forward motif can explain inhibition at high doses

The simplest model of T cell activation is the occupancy model (Fig. 5.2), and this is the starting point for the development of a phenotypic model. The model assumes that T cell activation (A) is proportional to the fraction of bound pMHC-TCR complex ($\hat{C_N}$) at equilibrium. It is unable to explain any of the key features of the quantitative dataset by itself, but by coupling an incoherent feed forward loop (incoherent FFL) downstream

of the engaged TCR, the resulting occupancy with incoherent FFL model exhibits a bell-shaped dose-response for all pMHCs (Fig 5.3).

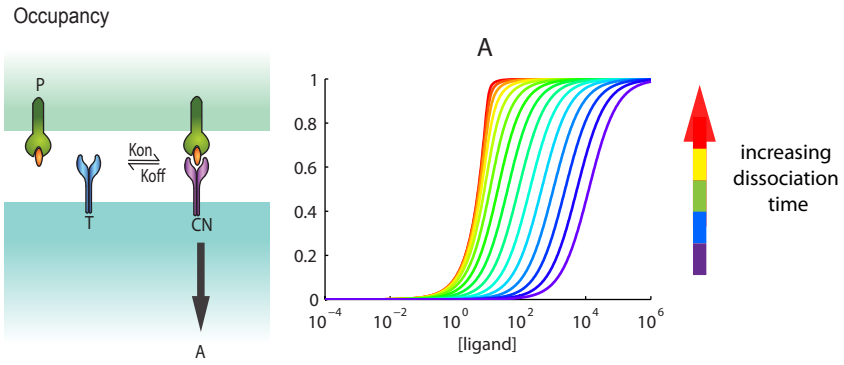

Figure 5.2: Occupation model is the starting point for developing a phenotypic model: The occupancy model is the simplest model of T cell activation and is unable to predict any of the key features of the quantitative dataset or previous data. The model assumes that a concentration of pMHC (P) binds a concentration of TCR (T) to form a concentration of bound complex (C_N). T cell activation (A) is proportional to the fraction of engaged TCR $\hat{C_N}$. It serves as a starting point for a phenotypic model that exhibits these features.

The incoherent feed forward loop [190, 191] is a motif that occurs frequently in biomolecular regulatory networks and can produce biphasic responses in either a time-dependent [192–194] or a dose-dependent manner [192, 195, 196]. The FFL consists of a single input that modulates a single output through two or more intermediate pathways. An incoherent FFL is the instance when the pathways have opposing functional roles of inhibition or activation. The effect of implementing an incoherent FFL into an occupancy model of T cell activation is to produce a bell-shaped dose response that has the same height of maxima for all curves. An advantage of using this motif is that since the negative signalling is downstream of the engaged TCR, and therefore an independent module to the pMHC-TCR engagement, the resulting equations can be solved analytically.

Although the kinetic proofreading with negative feedback model [103] exhibits bell-shaped dose-response profiles, it is not used as a basis for developing a phenotypic model. This is because this model predicts that the maximum height of dose-response profiles decreases with decreasing affinity, and there is no intersection between dose-response profiles for various pMHCs, while the quantitative dataset does show intersecting curves.

The incoherent FFL consists of two molecules, X and Y, which are activated downstream of the fraction of engaged TCRs in a signalling-competent state ($\hat{C_N}$). Once activated, these molecules act on the activation of a downstream molecule A, which X inhibits Y activates. T cell activation is defined as the activation of A. In order for this motif to exhibit a bell-shaped dose-response, constraints must be imposed on the parameters that govern the rate of formation of X, Y and A. The requirement for activation of A at low doses and inhibition at high doses means Y must be activated and reach saturation at lower pMHC doses compared to X. This can be done by making the rate of formation of Y more sensitive to $\hat{C_N}$ than X is to $\hat{C_N}$. Additionally, the rate of inhibition on A must be greater than its activation [191].

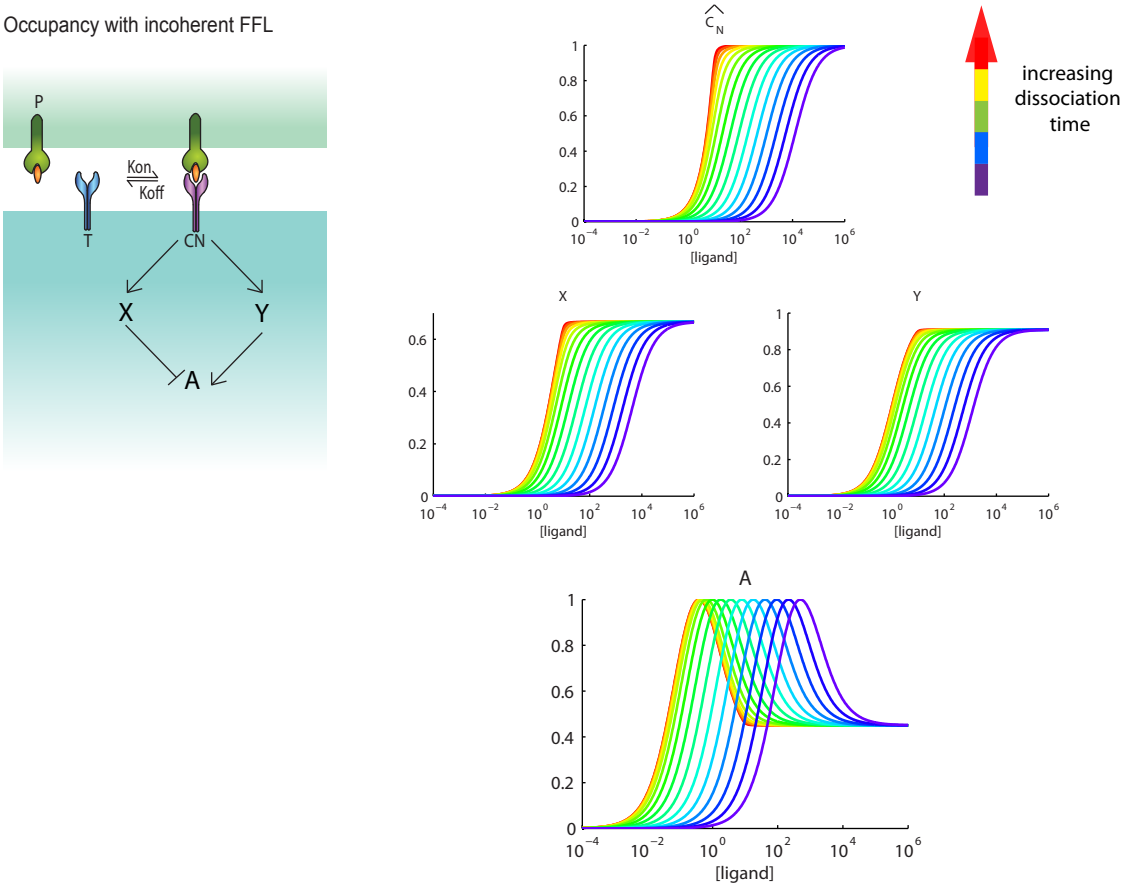

Figure 5.3: Occupancy model coupled to incoherent FFL can explain optimal: Coupling an incoherent FFL downstream of an occupied TCR gives the result that every pMHC produces a bell-shaped dose response if it is presented at sufficient concentrations. The model cannot explain sigmoidal dose-response profiles for low affinity pMHCs or the optimal pMHC affinity at low pMHC doses. Parameters used: $\beta = 0.1, \rho = 0.5, \delta = 50, \gamma = 1.1$, which are described in A.2.

Since the model is a phenotypic model, the molecules X, Y and A do not have to represent a specific molecule. They can instead represent a module of molecules that interact in such a way that they can be approximated by a single molecule. The arrows between molecules are also effective, and can represent multiple signalling processes. Although the incoherent FFL is downstream of the engaged TCR, the model contains no assumption as to where this motif lies in the signal transduction cascade. The motif could be membrane-proximal or cytosolic, depending on whether molecules X,Y and A represent membrane-proximal or cyotsolic interactions.

A consequence of this model is for a pMHC of any affinity to exhibit a bell-shaped dose response. This result does not reflect experimental data for pMHCs of physiological affinities and lower that exhibit dose-response profiles that are not bell-shaped and have an $E_{\max}$ that varies with the pMHC dissociation time [88, 90, 91].

5.3 Incorporating kinetic proofreading can explain decreasing maxima for short dissociation times

A way to accommodate the experimental data for low affinity pMHCs is to include kinetic proofreading into the model. This allows the engaged TCR to discriminate between pMHCs based on their dissociation time, such that a pMHC with a short dissociation time will never transduce a signal, no matter at what dose it is presented. When kinetic proofreading is coupled to an incoherent FFL, the outcome is for pMHCs with short dissociation times to be unable to exhibit a bell-shaped dose response, regardless of the pMHC dose (Fig. 5.4). The reason for this is that kinetic proofreading produces a correlation between the $E_{\max}$ of signalling-competent TCRs ($\hat{C_N}$) and the dissociation time. Since X and Y are dependent on $\hat{C_N}$, the $E_{\max}$ for activation of X and Y will also correlate with the dissociation time. Because Y is more sensitive to $\hat{C_N}$ than X, for pMHCs of sufficiently short dissociation time there will be some activation of Y but no activation of X. The outcome is to produce a dose-response profile that is not bell-shaped.

The phenotype of this model closely resembles the experimental data from a study by Anderson et al [87] that looked at NFAT transcription for T cells stimulated with immobilised TCR over a 10^4 range in affinity. Their experiments show a bell-shaped dose-response for high affinity pMHCs and a dose-response profile that clearly plateaus for the lowest affinity pMHC (Fig. 1a Ref. [99]). There is no evidence for an optimal affinity at low concentrations in this study, which is likely due to the range of affinities used. The highest affinity pMHC used has a K_{D} of 2.3×10^{-9}, which is in the region of where the optimal affinity has been found in the experiments in this thesis.

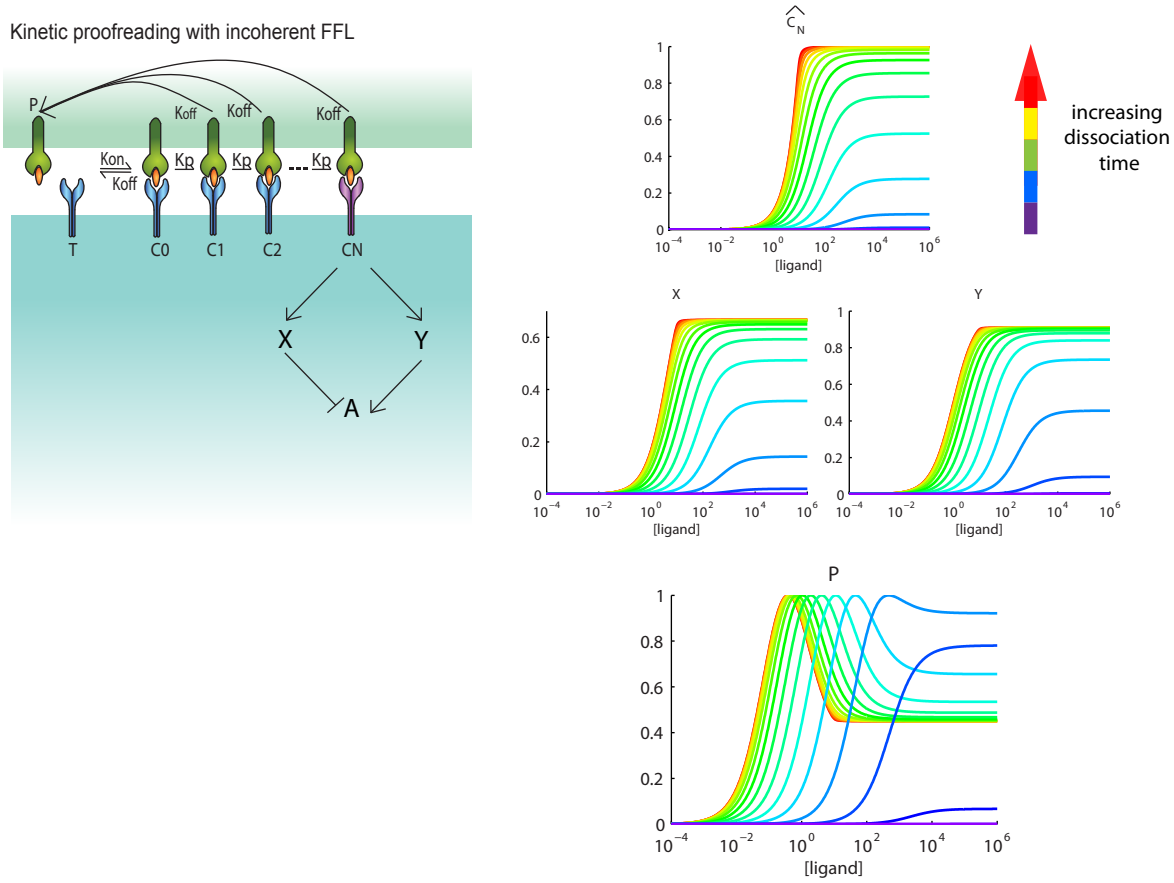

Figure 5.4: Kinetic proofreading coupled to an incoherent FFL can explain different maxima for short dissociation times: Coupling kinetic proofreading to a downstream incoherent FFL allows certain dissociation times to activate molecule Y but not X, to produce sigmoidal dose-response profiles. The $E_{\max}$ of these resultant curves correlate with the dissociation time. This model does not explain the optimal pMHC affinity at low doses. Parameters used: $\beta = 0.1, \rho = 0.5, \delta = 50, \gamma = 1.1, k_{\mathrm{p}} = 2s^{-1}$, which are described in A.2.

5.4 Incorporating limited signalling can explain increased potency of intermediate dissociation times

The final requirement of the phenotypic model is to demonstrate that intermediate affinity pMHCs, rather than the highest affinity pMHC, give the greatest response at low concentrations. This can be done by incorporating limited signalling, which penalises pMHCs with long dissociation times. This is done by limiting the duration for which an engaged TCR can signal (Fig. 5.5) to result in pMHCs of intermediate affinity producing the greatest number of TCRs in the signalling-competent state $\hat{C_N}$. The downstream implications of this in the incoherent FFL are that intermediate affinity pMHCs will give the greatest activation of X and Y and the dose-response profiles of these complexes will begin to rise at lower pMHC doses compared to lower (and higher) affinity pMHCs. Activation of the final complex A will therefore exhibit a dose-response profile that is bell-shaped and the curve will begin to rise at lower concentrations compared to pMHCs of lower (and higher) affinity. For pMHCs of both low (and high) affinity there are fewer TCRs in the signalling-competent state $\hat{C_N}$ and decreased activation of both X and Y. The model predicts that as the pMHC affinity moves away from the optimum, the bell-shaped dose response profile will diminish as there is less activation of X, which is less sensitive to $\hat{C_N}$ than Y. Although the model predicts that both sufficiently low and high affinity pMHCs can produce dose-response profiles that plateau, it is hard with the current assay used to produce pMHC-TCR pairs that are high enough affinity to see this. WT/9V and 72,75/9V are the highest affinity pMHCs used with superphysiological affinities in the pM range and yet they are still able to produce a bell-shaped dose-response. By comparison, it is easier to produce low affinity pMHCs, and previous experimental results show that pMHCs of physiological affinity and below plateau.

A consequence of this model is that if T cell activation is plotted over pMHC dissociation time at low concentrations, intermediate affinity pMHCs produce the greatest amount of activation (Fig. 5.6). This is in agreement with several experimental studies that look at T cell activation as a function of pMHC affinity [92–94, 197]. This gives a validation for the limited signalling aspect of the model, but not it does not provide

evidence for the incoherent FFL, since dose-response assays must be performed to see this effect. The only study out of these that also considered T cell activation through dose-response experiments was that by Irving et al [94]. The assay measured target cell lysis of T2 cells pulsed with pMHC (Fig. 5d ref. [94]) and the results show bell-shaped dose-response profiles for most pMHCs presented and interestingly, the highest affinity pMHC plateus at high pMHC doses.

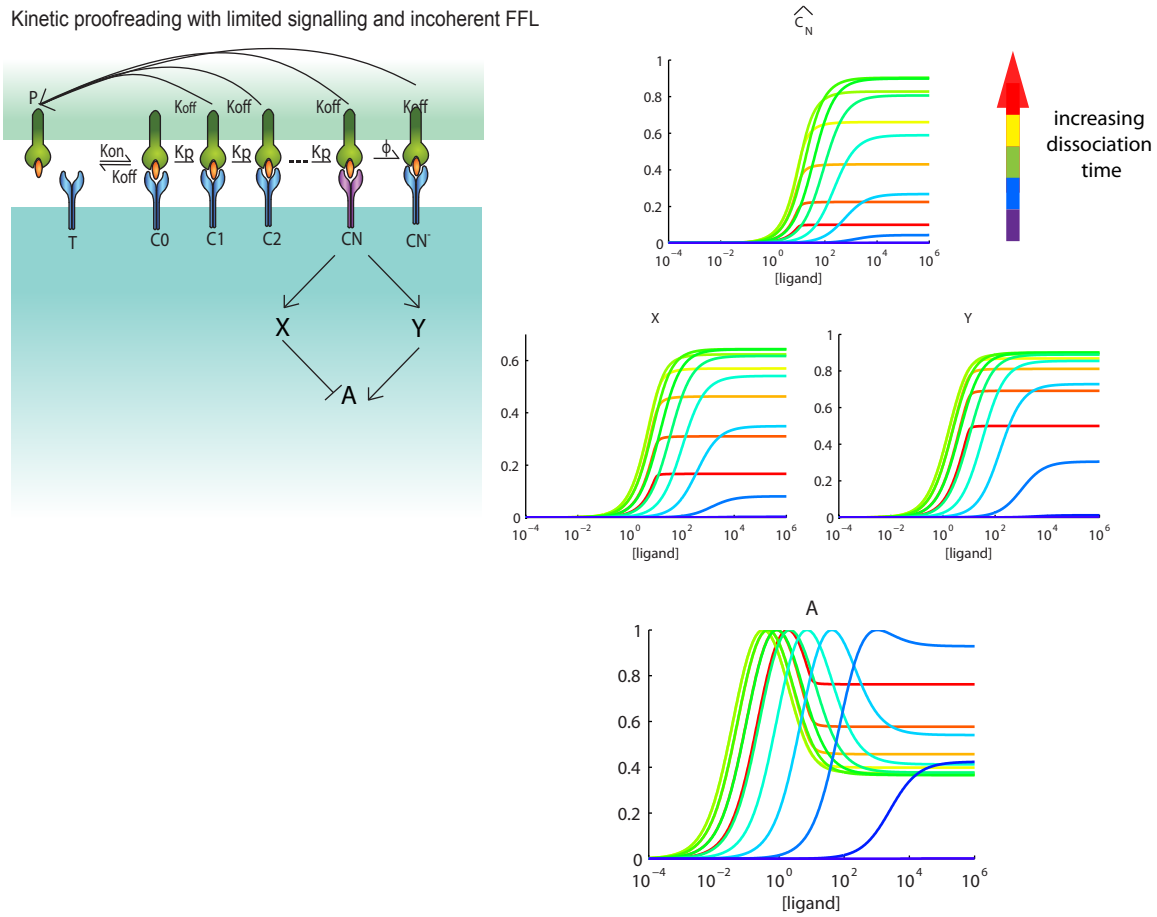

Figure 5.5: Kinetic proofreading with limited signalling coupled to incoherent FFL can explain how intermediate affinity pMHCs give the most potent response. Adding limited signalling results in intermediate affinity pMHCs giving the greatest activation of $\hat{C_N}$ and the most potent activation of downstream molecules X and Y, and this results in intermediate affinity pMHCs giving the greatest activation at low doses. Parameters used: $\beta = 0.1, \rho = 0.5, \delta = 300, \gamma = 1.1, k_{\mathrm{p}} = 4s^{-1}, \phi = 0.0009s^{-1}$, which are described in A.2

5.5 Discussion

The analysis of a quantitative dataset of T cell activation has informed the development of a model that captures the T cell signal transduction cascade from TCR engagement to cytokine secretion. This model is a phenotypic model, which means that it makes the minimal amount of assumptions to generate the phenotype of T cell signalling. The assumptions of the model are that upon a pMHC binding a TCR, a kinetic proofreading scheme is initiated to produce a signalling-competent TCR that will signal for a limited duration. Downstream of the TCR signal is an incoherent FFL, the output of which is proportional to T cell activation. This model is termed the kinetic proofreading with limited signalling model coupled to an incoherent FFL and it exhibits a bell-shaped dose-response for high affinty pMHCs, an optimal pMHC affinity at low doses, and sigmoidal dose-response profiles with decreasing $E_{\max}$ for low affinity pMHCs. The phenotypic model represents the dataset in a qualitative way because despite investigating T cell activation quantitatively, there is variance across datasets of the dose-response profiles and which pMHC affinity is optimal. The phenotypic model can therefore at best represent the data in a qualitative way.

The phenotypic approach to model development can be compared to models that try to explicitly model the signal transduction cascade, such as the model by Altan-Bonnet and Germain [102]. Why is the simpler phenotypic approach also successful at developing a model of T cell activation? One reason is that a phenotypic model approximates complicated signalling steps into modules that make a smaller set of assumptions, such that rate constants in the model can represent multiple biochemical steps. The result is a model with fewer parameters compared to an explicit modelling approach which means that the model has less uncertainty because there are less unknown parameters. The model also provides greater intuition into how model assumptions result in a given phenotype.

5.5.1 Predictions of the phenotypic model

The phenotypic model can be simulated to predict T cell activation as a function of the dissociation time τ for fixed pMHC concentrations (Fig. 5.6), as has been done in Fig. 3.1. The model predicts that for low pMHC concentrations there is an optimal

intermediate dissociation time. The mechanism of this optimal is limited signalling. As the pMHC concentration is increased, it can be seen that the optimal broadens out into two optimal dissociation times. This is due to limited signalling and the incoherent FFL. Since intermediate dissociation times produce the greatest amount of signalling competent TCRs, they will produce the greatest activation of the inhibitor X, and the activation of X increases as the concentration of pMHC is increased. The result of this inhibition at intermediate dissociation times is to produce two optimals, one at very short dissociation times, and a second at superphysiological dissociation times (grey shaded area). It is unlikely that this prediction can be tested experimentally because it is difficult to produce pMHCs with sufficiently long dissociation times. The highest affinity pMHC used in this study had a pM K_{D} and still exhibited a bell-shaped dose-response.

Do these predictions of a concentration dependent optimal which has an intermediate optimal dissociation time at low concentrations and a short optimal dissociation time at high concentrations fit with other experimental studies? A study that looked at IFN-γ secretion from T-cells stimulated with cells pulsed with 1μM pMHC ($\sim 50\mu$g/ml and therefore a high dose) found an optimal dissociation time of 16s [94]. This can be compared with the optimal of $\sim$ 10 minutes found in this study at concentrations of $10^{-2}\mu$g/ml. This is consistent with the predictions of the phenotypic model.

5.5.2 Mechanistic hypotheses for phenotypic model and their utility

Once a phenotypic model has been developed, it can then be asked what molecular mechanisms could give rise to the features of the model, and what their utility could be. Kinetic proofreading postulates that an engaged TCR must undergo successive modifications before producing a signal. It is established that these modifications relate to the activation and recruitment of tyrosine kinases to the TCR-CD3 complex. Although the precise sequence of events governing TCR triggering is unclear, it is known that it is initiated by a mechanism that pushes the kinase/phosphatase balance of the TCR-CD3 complex towards phosphorylation, which is mediated by Src family kinases Lck and Fyn [41]. The TCR-CD3 complex contains ten immunoreceptor tyrosine activation motifs (ITAMs) on its cytoplasmic domains, each of which contain two tyrosine residues. These

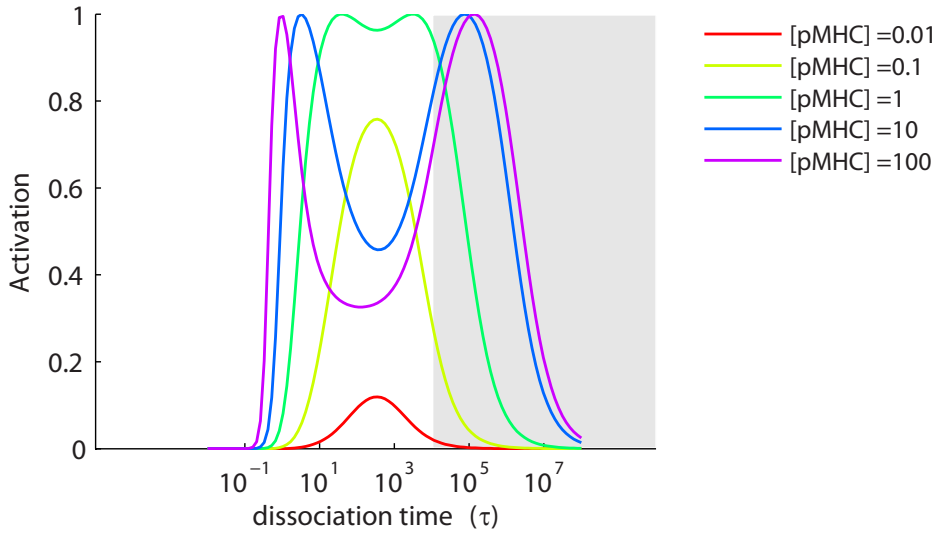

Figure 5.6: Model predictions for the role of dissociation time: The phenotypic model can be simulated to show how activation depends on dissociation time τ for fixed pMHC concentrations. This is shown for dissociation times that are experimentally accessible, and also for dissociation times that go beyond this (grey shaded region). A prediction is for one optimal at low pMHC doses and two optimals at high doses. Parameters used: $\beta = 0.1, \rho = 0.5, \delta = 1000, \gamma = 1, k_{\mathrm{p}} = 4s^{-1}, \phi = 0.0009s^{-1}$, which are described in A.2

act as docking sites for proteins containing tandem SH2 domains, such as ZAP-70 [19]. It is likely that both tyrosine residues on an ITAM must be phosphorylated to recruit ZAP-70, since it has been shown that stimulation with antagonist pMHCs leads to partial ITAM phosphorylation and a failure to activate ZAP-70 [145, 157]. ZAP-70 is then activated by Lck, and the activation of ZAP-70 is sufficient for the transmission of the activation signal to downstream signalling pathways [198]. The time requirement therefore to doubly phosphorylate ITAMs and recruit and activate ZAP-70 generates a delay between TCR engagement and the generation of a signalling-competent TCR-CD3 complex.

The utility of kinetic proofreading is to enable discrimination between pMHCs based on their dissociation time [86, 98]. The kinetic proofreading steps severely attenuate the signal from pMHCs that do not have a dissociation time of sufficient duration to reach the competent-signalling state, and so the difference in signal transduced from pMHCs with small differences in dissociation time is amplified non-linearly. Kinetic proofreading therefore enables a high specificity of pMHC selection based on dissociation

time, but this is at the cost of sensitivity to pMHCs, since the kinetic proofreading steps filter the signal from all pMHCs [86].

The experimental data has shown that there is an optimal dissociation time of around 10 minutes at low pMHC concentrations. The serial triggering model is usually cited as an explanation for producing an optimal dissociation time [92, 94, 139]. This model postulates that the rate of TCR triggering determines the magnitude of activation. This leads to an optimal dissociation time because a pMHC must bind for long enough to trigger a TCR but not for so as to limit serial binding. Since the optimal is at around 10 minutes, the rate of TCR triggering influences the amount of activation only for dissociation times of 10 minutes or longer. The optimal dissociation time is therefore of little relevance to physiological pMHCs, although it does help elucidate the signalling model within the T cell.

Assuming that the TCR/pMHC dissociation times measured in solution are similar to the physiological dissociation at the T cell surface, limited signalling proposes that the TCR becomes inert on a timescale of minutes. A potential mechanism for this process is the down-modulation (reduced surface expression) of TCRs following TCR triggering. Studies have shown that stimulation of TCRs leads to TCR down-modulation that is dependent on both pMHC dose and affinity [139, 189, 199]. Current evidence suggests that there is a high basal rate of TCR internalisation and recycling back to the cell surface, and this is only minimally increased for stimulated T cells [189]. This implies that down-modulation is the result of a reduction of recycling of TCRs back to the cell-surface. This could be mediated by the ubiquitylation of triggered TCRs by Cbl E3 ubiquitin ligases[200, 201], which marks the TCRs for degradation. There is speculation over the utility of TCR down-modulation, but it has suggested that it is vital to implement a mechanism that terminates the signal transduction through the TCR so that it does not signal indefinitely [200]. A further significance of TCR down-modulation could be to protect from autoimmunity by suppressing excessive responses [201].

The final module in the phenotypic model is the incoherent FFL, which occurs downstream of a TCR in a signalling-competent state. It contains an activatory molecule and an inhibitory molecule that influence an output that is proportional to T cell activation. What could be responsible for the negative regulation? There are many negative signalling

controls in the signal transduction cascade which are mediated by inhibitory receptors and phosphatases [75]. Candidates for the negative feedforward module must act at a relevant time-scale such that they are activated a short time period after the initial TCR engagement. This would discount inhibitory receptors, which are upregulated on a time-scale of hours and phosphatases that act constitutively [75]. Inhibitory receptors are also not relevant because their ligands were not used in the experiments. A potential inhibitory molecule is Src-homology 2 domain (SH2)-containing phosphatase-1 (SHP-1), which has been established as a negative regulator of signalling during early events in the signal transduction cascade. It has been proposed to interact with many molecules such as the TCR ζ-chain, including ZAP-70, LCK, and SLP-76 and LAT [202]. A recent study has found that the molecule THEMIS constitutively associates with SHP-1 through the adapter molecule GRB2. The THEMIS:SHP complex can then be recruited to LAT, which allows it to dampen local ITAM phosphorylation and downstream pathways [203]. It is therefore possible that SHP-1 can negatively affect pathways downstream of activated ZAP-70 by acting on LAT, SLP-76 or other molecules.

It has been proposed in a study by Wolchinsky et al. [137] that the activatory signal of LAT is inhibited by SHP-1/2. and the activatory signal of SLP-76 is inhibited by cbl proteins. It is argued that at low pMHC doses, the activation is dominant, while at high pMHC doses the inhibition is fully activated.

The incoherent FFL has mostly been analysed in time-dependent networks and has been shown to lead to accelerated response times to an input compared to simple regulatory circuits [190]. By analogy, a dose-dependent incoherent FFL shows an increase in sensitivity to pMHC, which is mediated by the activatory molecule Y. This increase in sensitivity compensates for the attentuation in signal that is a result of kinetic proofreading. The coupling of kinetic proofreading to an incoherent FFL can therefore explain how T cells exhibit specificity (due to kinetic proofreading) and sensitivity (due to the incoherent FFL), which are two of the hallmark characteristics of T cell activation [86]. A dose-dependent incoherent FFL has also been described as a bandpass filter [191], since it attenuates the TCR signal outside a given range. This is brought about by the inhibitory molecule X, and could be a mechanism to prevent over-reactive T-cell responses to TCR stimulus.

Finally, it must be noted that although this given model can explain the data, there could be many other possible models that are also explanatory. This phenotypic model is however relatively simple compared to other modelling attempts [102], which gives the benefit that it is easier to modify to meet the demands of new experimental data, since the model shows an intuitive relationship between assumption and phenotype. Model development has been restricted to a system that has come to steady state. These assumptions are reasonable since the phenotype of our model is robust over time points ranging from 4 hours to 24 hours. Considering models that have not come to steady state could also explain the phenotype of the data, but they would not reflect the fact that the experimental phenotype persists for many hours.

All my knowledge of the world, even my scientific knowledge, is gained from my own particular point of view, or from some experience of the world without which the symbols of science would be meaningless.

— Maurice Merleau-Ponty's *Phenomenology of Perception*

6 Conclusion

6.1 Summary of thesis

The main theme in this thesis has been to investigate and demonstrate the phenotypic approach to developing a model of T cell activation. To begin, I reviewed the phenotypic models in the literature and formulated them under a consistent framework so that they could be meaningfully compared to each other. I then generated a quantitative dataset of T cell activation in order to explore the phenotype of T cell activation. The experimental system utilised T cells transduced with a therapeutic high affinity T cell receptor and the experiments involved stimulating these T cells with pMHC over a wide range of doses and affinities. Cytokine secretion was measured downstream which allowed me to map the relationship between input (pMHC dose, affinity) and output (cytokine secretion). Two main qualitative features arose from the data, which were an optimal pMHC dose, such that activation decreased at high pMHC doses, and of an intermediate affinity producing the greatest response at low pMHC doses. I found that none of the existing models could explain all features of the dataset, and so began to develop a phenotypic model that could explain the data. By a process of iteratively formulating models and then rejecting those that were not consistent with the phenotype of the data, I arrived at the model termed the kinetic proofreading with limited signalling coupled to an incoherent feed forward loop model. The formalism of the model is a simple coupling of the

signalling-competent TCR in kinetic proofreading to a downstream incoherent feed forward motif, with the additional assumption that an engaged signalling-competent TCR remains active for a limited period of time. This resulting model provides insight to the signal transduction network within the T cell.

In the remainder of the conclusion, I discuss how the phenotypic modelling approach has been successfully applied to other biological systems, and how it compares to other systems biology modelling approaches. I then show the insights that have been gained by applying the phenotypic approach to T cells. Finally, I show applications of the phenotypic model to immunotherapies that harness engineered high affinity TCRs to target tumours.

6.2 Systems biology and phenotypic models

One of the main goals in molecular systems biology has been to understand how the interaction networks between genes and proteins determine the functional aspects of cell physiology [204]. To this end, there have been several different approaches to elucidate the molecular interaction networks within cells. These include the bottom-up and top-down approaches, as well as the phenotypic approach that I have taken in this thesis. The bottom-up approach uses mechanistic information on specific proteins taken from the literature, including their interactions, concentrations and rate parameters, to produce a detailed dynamical network. It is then seen if the set of equations describing this network can give rise to the desired functional phenotype. The top-down approach takes advantage of 'omics' data, which may include metabolome, fluxome, transcriptome and proteome information of a system. Through making perturbations to the experimental system and measuring correlations between molecules, an interaction network can be inferred. However, from top-down measurements alone the rate parameters of connections are unknown, and they must be found through experiment [205, 206]. The less common approach is the phenotypic approach, which is a simpler method that also has predictive power. The phenotypic approach aims to develop a minimal biochemical network that can exhibit the phenotype of experimental data. The model can be informed by interactions from the literature as well as experimental data. However, the model is a simplification of the full interaction network. This means that the 'molecules' and

'connections' in the model are effective, such that they can represent multiple signalling steps. The resulting phenotypic model is therefore much simpler than one designed from bottom-up or top-down approaches.

The phenotypic approach has been successfully employed to explain T cell signalling [103], biochemical adaptation [207], cell decisions [208], oscillations [209], and even the entire immune response [210]. A phenotypic modelling approach can be advantageous when considering a system with many molecules and interactions. This is because a molecular model of such a system will have many rate parameters, many of which are unknown, which means that there are many parameters to be fit. This can lead to overfitting, which occurs when a model with many parameters can be constrained to fit the data, even if the model is not a good representation of the experimental system. With a sufficient number of parameters in a model, it can be constrained to fit any dataset, and is therefore not a useful model [211]. A phenotypic model by comparison has fewer assumptions and less parameters to be fit, which means one can have more confidence in the model. A phenotypic model therefore has greater predictive power, which means the assumptions of the model can be tested.

An example of phenotypic modelling is a model of the cell division cycle by Novák and Tyson published in 1993 [212], which models the dynamics of cell cycle control proteins. Their model contained 11 ODEs and did not include all of the biochemical details known at the time [213]. This model could predict the activity of maturation-promoting factor (MPF) in response to cyclin concentration, and it predicted that the MPF response was bistable. On this basis, several predictions were made that were later confirmed by experiment [213]. What was then shown in their 1993 paper was that this model could be reduced to only 2 ODEs and a few rate parameters, and that the phenotype of this reduced model was still able to exhibit many of the characteristics of the cell cycle in frog eggs and fission yeast cells [213]. This shows how a minimal model, although simplified, can still be an accurate predictor of the experimental outcome.

Another example of phenotypic modelling is the minimal model that can exhibit ultrasensitivity, which was initially developed by Goldbeter and Koshland [214]. Ultrasensitivty is defined as an amplification in the response to a stimulus change that is more

sensitive than a Hill function with a Hill coefficient of 1. The model was based on the finding that multi-step signalling cascades, where the activated form of one protein activates another protein downstream, and so on, exhibited ultrasensitivity [214]. This generic model was later used to develop a phenotypic model of the MAPK cascade. The model predicted an ultrasensitivity in the response, and this was confirmed by experiments on the MAPK cascade in *Xenopus* oocyte extracts [215]. Since phenotypic models are abstracted versions of the underlying signalling mechanisms, the generalised model architecture can be easily applied to other biochemical systems. It is thought that despite the complexity of biological networks, there is a small set of possible architectures that can give rise to the phenotypes in nature [190, 216]. Minimal models can therefore be used to interpret complex interaction networks generated by high throughput 'top-down' techniques.

However, it can be the case that for some situations, a detailed model is necessary, for there is no point in a parsimonious model if it cannot explain the data [213]. An example is a mechanistic model of bacterial chemotaxis by Barkai and Leibler that predicted that many aspects of bacterial chemotaxis, such as adapatation to changes in the chemical environment, are robust to changes the rate parameters of the network. This was later confirmed in an experimental system by Alon that involved changing the concentration of components in the chemotaxis network in E.coli [217]. By comparison, a phenotypic model by Segel et al. predicted that adapation was highly sensitive to the rate parameters. Another example is a model by Hoffman et al. of the IκB-NF-κB signalling module [218]. The authors first considered a simple two-component system with negative feedback. Although this simple model could exhibit some of the experimental behaviour, it was insufficient to explain all of it. This model was used to inform the development of a mechanistic model that could explain the data. This example does show, however, how a phenotypic model can be used to inform the development a more complex model.

Another instance when a mechanistic model is advantageous is when information on the effect of perturbation to a specific gene or protein is needed. For example, it has been shown that a detailed model of exit in mitosis in budding yeast could predict the phenotype of mutants that were later validated by experiment [219]. A mechanistic model may also be needed if one wants to know the role of a specific drug, since it affects a specific

protein. However, it can also be argued that a phenotypic model could include mechanistic details of the important gene/protein in question, while using effective molecules and interactions for the rest of the network.

There are therefore advantages and disadvantages to both the mechanistic and phenotypic approaches to model development. If the aim is to develop a model that can exhibit and predict every aspect of a system, then a mechanistic model is necessary. However, as more interactions in the network are discovered over time through experimental advances, the mechanistic approach will get increasingly more complicated and uncertain if the rate parameters are not known. If the aim is to develop a predictive model that accurately describes the qualities of the underlying network without fleshing out all the details, then in many cases a simple phenotypic model is an effective way to do this.

6.3 Insights from the phenotypic model of T cell activation

The role of pMHC:TCR dissociation time with regards to T cell activation has long been debated. Different studies have variously concluded that T cell activation increases monotonically with dissociation time [88, 90, 91, 134], that there is an optimal dissociation time [92–94], and that there is a concentration dependent optimal that is only evident at low pMHC concentrations [95]. I investigated the phenotype of T cell activation by stimulating T cells with pMHCs with dissociation times that vary over a 10^5-range and at concentrations varying over a 10^5 range to quantitatively probe T cell stimulation. The results of these experiments clarify the relationship between dissociation time and activation. The data show that at low pMHC concentrations there is an optimal dissociation time, and this time corresponds to roughly 10 minutes, as measured in solution by Biacore. At intermediate pMHC doses there is no clear optimal dissociation time. However at very high pMHC concentrations, the phenotypic model predicts that there is again an optimal dissociation time, which is of a short timescale. A second optimal is also predicted at superphysiological dissociation times which may not be experimentally observable.

The optimal short dissociation time at high pMHC doses is due to the decrease in response to intermediate dissociation time pMHCs, which means that in dose-response

assays the lowest affinity pMHCs can intersect and rise above the curves of higher affinity pMHCs. This result was not confirmed experimentally in this thesis, since only a few datasets showed that the lowest affinity pMHCs were optimal at high pMHC concentrations. Further experiments done by other students in the lab (Nicola Trendel and Hong-Sheng Lim) have confirmed this result using a panel of pMHCs that go to even lower affinities than used in this study. There is therefore a concentration-dependent optimal dissociation time that is evident at low and high pMHC concentrations. Comparing the results from these experiments to previous studies in the literature suggests that the discrepancy in previous studies could be due to limitations in the range of dissociation times and concentrations that were used. For example, the studies that conclude that there is no optimal dissociation time are likely to have been using pMHCs with a range of dissociation times that were to short to detect an optimal dissociation time at low pMHC doses. Chervin et al. [90] use dissociation times up to 100s, which is lower than the 10 minute optimal found in this study, and Holler and Kranz [88] use pMHCs with K_{D} down to $5n$M, while the optimal pMHC identified in this study has a K_{D} close to $1.5n$M.

The architecture of the phenotypic model reveals that there are two distinct mechanisms for the optimal dissociation times operating at low and high pMHC dose. Limited signalling is responsible for the optimal at low pMHC concentrations. This is where a TCR in a signalling-competent state signals for a period of time before becoming inert. Assuming that the TCR/pMHC dissociation times that were measured in solution are similar to the physiological dissociation at the T cell surface, the process by which this happens is around 10 minutes. It follows that only mechanisms that have a timescale of this magnitude are plausible. A common explanation suggested for this optimal is the serial triggering model [92, 94, 139], where the rate of TCR triggering determines the magnitude of activation. However, a serial triggering model would predict a short dissociation time to be optimal, since this would correspond to a pMHC of physiological dissociation time that can serially bind TCRs [139]. However, the data shows that the rate of TCR triggering becomes a detriment to activation when the dissociation time is greater than around 10 minutes. A more plausible mechanism is the internalisation

and down-modulation of TCR following pMHC engagement, which has been shown to occur on time-scales of tens of minutes [189, 201].

The model architecture that drives the optimal for short dissociation times at high pMHC concentrations is the incoherent FFL coupled to kinetic proofreading. A result of this motif is for dissociation times that were optimal at low pMHC concentrations to give a lower response compared to short dissociation times because they are greater activators of the inhibitor in the incoherent FFL. This effect is increased due to limited signalling. An untested prediction of the phenotypic model is that the optimals work on different time scales: the optimal dissociation time at low pMHC concentrations will take at least 10 minutes to come into effect, whereas the optimal short dissociation time at high pMHC concentrations acts within seconds. This could explain how a study by Hebeisen et. al found that a K_{D} of 1-5μM, which corresponds to a short dissociation time, produced the maximal phosphorylation of ERK within 1 minute of T cell stimulation with high concentration of multimer pMHCs [220].

The identities of the main proteins responsible for the incoherent FFL are at this point unknown, but the inhibitory molecule could be SHP-1, the activatory molecule ZAP-70 and the downstream complex LAT. The signalling network can be invstigated by perturbing the experimental system and seeing how the resulting phenotype is changed. The role of SHP-1 could be investigated by knocking it down and seeing if this restores the dose-response profiles of all pMHCs to sigmoidal. Kinetic proofreading could be investigated by adding the inhibitor PP2, which inhibits Src-family kinases.

The phenotypic model demonstrates that despite the complex signal transduction cascade within the T cell, surprisingly, these signalling steps can be approximated by the activation of a few effective molecules. This raises the question of why the cascade needs to be so complicated. One reason could be that the T cell does not simply have to respond to a concentration of a single type of pMHC, but rather has to compute complex environmental information including the combined presentation of different pMHCs, cytokine environment, and co-stimulatory/inhibitory ligand interactions. The complexity of the model would have to be increase to explain these effects. In addition, only a few possible readouts of T cell activation have been considered in this study. It is likely that

other measures of activation would have qualitatively different dose-response profiles and so a more complicated model would be required to accommodate this.

6.4 Applications of phenotypic model to immunotherapies

The predictions of the phenotypic model can be used to guide therapies that harness T cells to target cancer. The natural T cell repertoire has difficulty detecting tumours due to their high expression of self antigen, because TCRs have a low binding affinity for self antigen due to thymic negative selection [221]. T cells that are able to bind tumour associated peptide antigens do so with low affinity compared to viral antigens [221]. Immunotherapies are therefore being developed that involve engineering TCRs to have a high affinity to tumour antigen, which are then introduced into the patient in soluble form [222] or expressed in T cells and adoptively transferred [223]. The 1G4 High affinity TCR used in this study was engineered for the soluble application in the form of immune-mobilising monoclonal TCRs against cancer (ImmTACs). These are soluble high affinity TCRs that are fused to fused to an anti-CD3 scFv, which enables them to bind to and activate T cells. The mechanism of the therapy is initiated when immTacs bind specifically to the cognate pMHC on the tumour. This directs a polyclonal T cell population to the tumour via the anti-CD3 scFv, which leads to the formation of an immunological synapse and tumour cell killing [222].

Although the 1G4 High affinity TCR was designed for ImmTAC use, the way it has been implemented in this study has been in the manner of gene-engineered T cells for adoptive transfer. These T cells can contain either physiological MHC-restricted TCRs or non MHC-restricted chimeric antigen receptors (CARs). CAR-T cells have shown remarkable success in treatment of leukemia and lymphoma, and are now being utilised to other cancers [224]. CARs comprise an antibody-like extracellular antigen binding motif that binds to a cell-surface antigen. This is linked to an intracellular signalling domain that includes CD3ζ (first generation CARs) and potentially one or more costimulatory signalling endodomains such as CD28 (second and third generation CARs) [225]. There has been speculation as to what affinity of CAR optimises CAR-T

cell signalling [224]. It is likely that there is an optimal window for CAR affinity. One study reports no increase in sensitivity with increased affinity [226], while others report a dramatic decrease in sensitivity [227, 228].

The phenotypic model can be used to inform what affinity CAR would give the greatest response for a given concentration of tumour antigen. It has been found that tumour antigens are expressed on low levels on the cell surface [224], and so the phenotypic model predicts that in these conditions an intermediate affinity in nM range would give the greatest efficacy. One potential difference between signal transduction through CARs and TCRs is the number of ITAMs that must be phosphorylated to produce a signalling-competent complex. CARs contain three ITAMs and may form dimers, which can be compared to ten ITAMs on the TCR complex. It is not clear that the ten ITAMs on a TCR must be phosphorylated in order for it to be signalling-competent [19], however if it is true that a CAR is activated with fewer kinetic proofreading steps than a TCR, this would have implications for the functional response. If the equivalent pMHC dose was given to a CAR and T cell system, the response from the CAR system would be more potent if less kinetic proofreading steps were needed.

The predictions of the phenotypic model are limited to the effect of pMHC affinity and concentration on activation, as well as receptor number, and so the model is most applicable to first generation CARs. Further work would address the role of co-stimulatory domains and co-receptors on model predictions, which can be applied to second and third generation CARs. For this work, the phenotypic model can be used as a scaffold for a more complete model of the signal transduction cascade.

6.5 PI3K signalling pathways

An alternative pathway for the metabolism of phosphoinositides is mediated by phosphoinositide-3 kinases (PI3Ks), which are lipid kinases that act by phosphorylating membrane phosphatidylinositol (PtdIns) and its by-products on the 3'-OH position of the inositol ring. The resultant products are PtdIns-3-phosphate, PtdIns-4,5-biphosphate (PIP_2) and PtdIns-3,4,5-triphosphate (PIP_3). Mammalian PI3Ks comprise a p110 subunit, which is catalytic, and a p85 subunit through which it associates with the plasma membrane. The p85 subunit contains an SH2 domain that binds to phosphorylated adaptor molecules, such as LAT, as well as 3'-phosphoinositides that it has generated. Molecules can bind to PIP_2 and PIP_3 through their PH domains, which are globular domains of $\tilde{1}20$ amino acids that bind phospholipids with high affinity and specificity [61, 62]. This includes the serine/threonine kinases Akt, also known as Protein kinase B, and phosphoinositide-dependent protein kinase 1 (PDK1). Akt is fully activated when it is phosphorylated by PDK1 and mTOR complex 2 (mTORC2). This allows Akt to translocate from the membrane to the cytosol and nucleus where it can regulate signalling pathways that control cell proliferation, metabolism and differentiation[63] .

PI3K is activated following TCR-pMHC engagement, although the mechanism is unclear. and its activation precedes the calcium flux through the T cell [64, 65]. It has been found after a T cell comes into contact with an APC, PIP_3 accumulates at the contact zone before an IS has formed[65], and it is also found throughout the plasma membrane [64, 65]. The production of PIP_3 is sustained for 6-9 hours [65]. Inhibition of PI3K has been found to only mildly affect IS formation and IL-2 production, indicating that it operates on a distinct pathway to these processes [65].

The PI3K pathway has been found to influence the expression of the transcription factor Foxp3, which designates T cells to become regulatory T cell (Tregs) [66]. These are T cells that act to dampen the immune response . foxo1 [67]

6.6 Features of TCR triggering

6.6.1 ZAP-70 independent T cell activation

6.6.2 TCR triggering induces cytoskeletal remodelling and other structural changes

T cells rapidly scan the lymph node for antigen presented by other cells. On encountering antigen, migration is decelerated [68] which is allows the T cell to form a conjugate with the APC and an immunological synapse to sustain signalling. This 'stop signal'[69] is initiated by TCR triggering and is brought about by reorganization of the cytoskeleton [68]. Actin polymerisatoin takes place at the t cell apc interface to generate a lamellapodial sheet, which is an actin projection, over the surface of the APC. This is mediated actin nucleating factors, one of which is the actin related protein 2/3 Arp2/3complex. Once activated, Arp2/3 stimulates the growth of branched actin arrays [3]. The nucleation activity of Arp 2/3 is enhanced by nucleation promoting factors such as Wiskott-Aldrich syndrome protein (WASp) and WASp family-verprolin homologous protein 2 WAVE2. This activation happens at the LAT/SLP-76 signalsome. It is here that Nck recruits WASp. The guanine nucleotide exchange factor VAV activates the Rho family GTPases, including Cdc42 and Rac1. WASp is activated by the GTPase Cdc42, WAVE2 regulated by Rac1 [70].

TCR triggering results in an increase in cell adhesion, mediated by integrins, this is an example of inside-out signaling , where signalling mechanisms originate inside the cell and are transmitted to the extracellular domain of the receptor [71] A primary integrin is LFA-1. its upregulation is dependent on the Vav, PlCgamma and LAT/SLP76 signalsome [3] The PLCγ pathway results in LFA-1 upregulation by GTPase Ras proximity 1 Rap1. Rap1 belongs to Ras superfamiliy of GTPase. It is active in the GTP-bound state and inactive when GDP-bound. Conversion to the active state is mediated by guanine nucleotide exchange factors that enable the release of GDP for GTP. The hydrolosis of bound GTP is accalerated by guanine nucleotide exchange factors (GEFs) [73]. DAG is produced from the PLCγ mediated hydrolysis of PIP2. DAG recruits serine-threonine kinases such as PKCs (protein kinase C). phosphorylation of guanine nucleotide exchange protein RapGEF2 by PKC-theta triggers activation of Rap1 that activates integrin LFA-1,

[72] PKCs phosphorylate beta-chain of LFA-1 which alters the interaction of LFA-1 with cytoskeletal proteins [72]

TCR triggering also results in the polarisation of the microtubule prganising centrer (MTOC), mictubule skeleton and golgi apparatis to the IS. This is to enable the secretion of cytokines and cytotoxic granules to the APC, which travel along microtubules and are directed towards target cell. This process has found to be dependent on Lck, Fyn, Zap, Lat, SLp76, Vav1, Cdc42 and calcium flux [74]

6.6.3 TCR triggering induces reduction in expression of genes and surface molecules

FOXO1 supports the survival of T cells by inducing the expression of the IL-7Ra chain and influences T-cell trafficking by promoting the expression of CD62L, CCR7 and S1P1 via the induction of the transcription factor KLF2 [63] [67]

[72]

6.6.4 TCR triggering of naive cells drives metabolic repogramming and effector differentiation

The activation of naive T cells results in clonal expansion of antigen specific T cells and differentiation into effector cells. Effector cells utilise aerobic glycolysis for energy, while naive, memory and Treg rely on oxidative phosphorylation [77]. The metabolic demands of effector cells are high in order to support the production of effector functions, growth and proliferation [78]. The supply of glucose to the cell is therefore increased to meet this demand by upregulating surface expression of glucose transporter GLUT1 [77].

Transcription factors have been identified that control the reprogramming of metabolism during effector T cell differentiation. It has been found that the transcription factor Myc is necessary for the increase in expression of glucose and glutamine transporters following TCR engagement. It also upregulates transferrin receptor, which is necessary for iron transport into the cell. Its expression is digital, and the percentage of positive cells increases with the affinity of the pMHC-TCR interaction, as well as the dose. The amount of IL-2 present changes Myc expression in an analogue fashion [78]. Transcription factor IRF4 has been found to regulate the expression of molecules required

for aerobic glycolysis. Its expression is determined by the affinity of the pMHC-TCR interaction, as well as the dose [79].

Effector T cells must increase their uptake of amino acids in order to support protein synthesis and other cellular processes. The uptake of leucine in particular is important because leucine availability regulates the serine-theronine kinase complex mTORC1 [80], which has a role in the regulation of activation and differentiation [229]. The uptake of leucine, which is a large neutral amino acid (lNAA) is mediated by System L amino-acid transporters that transport LNAAs across the plasma membrane. This process is controlled by triggering through the TCR, as well as the prescence of IL-2 . Uptake of leucine is necessary for mTORC1 activity as well as the functioning of metabolic machinery for naive cells to become effector cells. The transport activity of System L amino acid transporters is dependent on calcineurin mediated signalling pathways [80].

These studies highlight the role of cell metabolism to support and modulate T cell activation, proliferation and differentiation. The dependency of expression of transcription factors Myc and IRF4 on the strength of TCR stimulation drives the clonal expansion of high affinity effector cells during an immune response [81].

6.7 Thresholds of activation

Different cells/markers have different thresholds. A general model of T cell activation is therefore difficult because the stimulation requirements differ according to the subtype to which a T cell belongs, CD4, CD8, Treg and state of differentiation, whether they are thymocytes or naive/effector memory. The experiments in this thesis consider stimulation through the tcr, but a general model would also need to account for the type of cell which is presenting the antigen, and the cytokine environment [230]

sensitivity to self CD8, and most likely CD4 are dependent on binding to selfMHC in order to survive in the periphery [112] The reactivity of a T cell to self have been shown to express more CD5 molecules [109] [110][111] this corresponds to higher transcription of Nr4a1 that encodes for Nur77, improved readiness for activation and functional differentiation[112] t cells that are more reactive to self may- there is evidence to indicare that cd5hi be more sensitivit to foreign pMHC, greater expansion in response to foreign antigen

6.7.1 Thresholds for different markers of activation

[113] early events of TCR-antigen engagement happen before IS formation. Lck and Zap70 are activated at the periphery of the IS within 15 minutes, after which their activation decreases. But 2 hours of sustained signalling is needed for single cell division of CD4+ naive cells [114] calcium signal, PI3K activity, persists for 10h, is dependent on continuous TCR signalling, as does IL2 secretion and cell proliferation. tcr expression is reduced 'Antigenic ligands not only drive synapse formation but are also equally important for its maintenance. The need for some TCR signaling at all times demonstrates the rapid reversibility of the cellular mechanisms required to preserve an ordered cell-cell interface. [116] Naive Ctls need only 2 hours of sitmulation for several rounds of division and for acquiring cytoxic effector functions. tcr is downregulated [231] cd8 24hr stim in vitro is sufficient for cells to differentiate into effector and memory without further antigenic stimulation

6.7.2 Thresholds for different T cell subsets

conventional view, memory secrete cytokines and perofrm effector functions at lower pMHC doses than naive [232] memory have earlier cytokine secretion that naive at 10uM dose in vitro, but proliferation found to be indentical in vitro and in vivo[117] [118] difference between in vivo in vitro results: in vivo, memory proliferate more - polyclonal antigen presentation - different epitopes and amounts [119] cell prolif: memory cd8s require a higher antigen threshold than naive. when low doses of peptide are presented, naive enter the cell cycle whyile memory do not activate effectors of cell cycle progression or zap70 lower levels of surface TCR and higher levels of non-receptor tyrosine phosphatases, lower upregulation of MYc 10pM pulsed APCs - in vitro

Treg cell selection is supported by having a sensitivty to self-pMHC class II that is intermediate between positive selection and clonal deletion, they therefore tend to have a greater sensitivity to self-pMHC than non-Treg T cells [112]

6.7.3 Implications for the modelling

6.8 Digital nature of T cell activation

Appendices

A Appendix

A.1 Mathematical derivations from Chapter 3

A.1.1 Occupancy model derivation

In this model a pMHC (P) can reversibly bind a TCR (T) to form a pMHC-TCR complex (C). The kinetics are governed by the equation:

$$\frac{dC}{dt} = k_{\text{on}}PT - k_{\text{off}}C. \tag{A.1}$$

At equilibrium, $\frac{dC}{dt} = 0$ and

$$PT = K_{\text{D}}C, \tag{A.2}$$

where $K_{\text{D}} = k_{\text{off}}/k_{\text{on}}$.

The total amount of peptide P_T and total amount of TCR T_T are conserved quantities given by the following conservation equations:

$$P_T = P + C \tag{A.3}$$

$$T_T = T + C. \tag{A.4}$$

Inserting the conservation equations into (A.2) gives,

$$C = \left(P_T + T_T + K_{\text{D}} - \sqrt{((P_T + T_T + K_{\text{D}})^2 - 4P_T T_T)}\right)/2. \tag{A.5}$$

Calculating the $E_{\max}$ and EC_{50}

The variables can be non-dimensionalised to give:

$$\hat{P} = \frac{P}{P_T}, \;\; \hat{T} = \frac{T}{T_T}, \;\; \hat{C} = \frac{C}{T_T}.$$

The conservation equations and (A.2) then become:

$$\hat{P}\hat{T} = \frac{K_{\mathrm{D}}}{P_T}\hat{C} \tag{A.6}$$

$$\hat{P} + \frac{T_T}{P_T}\hat{C} = 1 \tag{A.7}$$

$$\hat{T} + \hat{C} = 1. \tag{A.8}$$

The $E_{\max}$ can then be found by finding $\hat{C}$ in the limit of P_T tending to infinity. At this limit, we have,

$$\lim_{P_T \to \infty} \;\; \frac{K_{\mathrm{D}}}{P_T} = 0, \;\; \frac{T_T}{P_T} = 0.$$

Using the conservation equations it can be seen at this limit that,

$$\hat{P} = 1, \;\; \hat{T} = 0 \text{ and } \hat{C} = 1,$$

and so,

$$E_{\max} = T_T. \tag{A.9}$$

In order to find the EC_{50} we can use the result that when,

$$P_T = EC_{50}, \;\; \hat{C} = E_{\max}/2 = 1/2.$$

By substituting this result into the conservation equations we obtain the EC_{50}:

$$EC_{50} = K_{\mathrm{D}} + T_T/2. \tag{A.10}$$

A.1.2 Kinetic proofreading model derivation

In this model a pMHC (P) can reversibly bind to a TCR (T) to form a pMHC-TCR complex (C_0). Upon binding, a series of biochemical modifications take place to the TCR (C_i) that eventually result with a TCR in a signalling-competent state (C_N). The parameters consist of the biomolecular binding rate (k_{on}), the unbinding rate (k_{off}), and the modification rate (k_{p}). The unbinding of a pMHC from a TCR will immediately reverse the modifications to the TCR. T cell activation is proportional to the amount of bound TCR in the C_N state. The system can be described by the following set of ODEs:

$$\frac{dP}{dt} = -k_{\text{on}}PT + k_{\text{off}}\sum_{i=0}^{N} C_i \tag{A.11}$$

$$\frac{dT}{dt} = -k_{\text{on}}PT + k_{\text{off}}\sum_{i=0}^{N} C_i \tag{A.12}$$

$$\frac{dC_0}{dt} = k_{\text{on}}PT - (k_{\text{off}} + k_{\text{p}})C_0 \tag{A.13}$$

$$\frac{dC_i}{dt} = k_{\text{p}}C_{i-1} - (k_{\text{p}} + k_{\text{off}})C_i \qquad 1 \leq i < N-1 \tag{A.14}$$

$$\frac{dC_N}{dt} = k_{\text{p}}C_{N-1} - k_{\text{off}}C_N. \tag{A.15}$$

We have the conservation equations:

$$P_T = P + C_T \tag{A.16}$$

$$T_T = T + C_T \tag{A.17}$$

where $C_T = \sum_{i=0}^{N} C_i$.

At equilibrium, the time derivative in the differential equations (A.11) - (A.15) can be set to 0. Inserting conservation equations (A.16) and (A.17) into (A.11) results in:

$$C_T = \left(P_T + T_T + K_{\text{D}} - \sqrt{(P_T + T_T + K_{\text{D}})^2 - 4P_T T_T}\right)/2. \tag{A.18}$$

The next step is to relate C_N to C_T so that the magnitude of T cell activation can be expressed as a function of the input parameters.

Using,

$$\alpha = \frac{k_{\text{p}}}{k_{\text{p}} + k_{\text{off}}},$$
$$1 - \alpha = \frac{k_{\text{off}}}{k_{\text{p}} + k_{\text{off}}},$$

then at equilibrium, equation (A.15) becomes,

$$\begin{aligned} C_N &= \frac{k_{\text{p}}}{k_{\text{off}}} C_{N-1} \\ &= \frac{k_{\text{p}}}{k_{\text{off}}} \alpha^{N-1} C_0 \\ &= \Big(\frac{k_{\text{off}} + k_{\text{p}}}{k_{\text{off}}}\Big) \alpha^N C_0 \\ &= \frac{\alpha^N}{1-\alpha} C_0. \end{aligned} \tag{A.19}$$

C_T can then be related to C_N,

$$\begin{aligned} C_T &= \sum_{i=0}^{N-1} C_i + C_N \\ &= \sum_{i=0}^{N-1} \alpha^i C_0 + C_N \\ &= \Big(\frac{1-\alpha^N}{1-\alpha}\Big) C_0 + C_N \qquad \textit{(using geometric sum)} \\ &= \Big(\frac{1-\alpha^N}{1-\alpha}\Big)\Big(\frac{1-\alpha}{\alpha^N}\Big) C_N + C_N \\ &= \Big(\frac{1-\alpha^N+\alpha^N}{\alpha^N}\Big) C_N \end{aligned} \tag{A.20}$$

$$C_T = \frac{1}{\alpha^N} C_N. \tag{A.21}$$

$$\begin{aligned} \text{Therefore, T cell activation} &= C_N \\ &= \alpha^N C_T. \end{aligned} \tag{A.22}$$

Calculating the $E_{\max}$ and EC_{50}

The variables can be non-dimensionaled using $\hat{P} = P/P_T$, $\hat{T} = T/T_T$ and $\hat{C_T} = C_T/T_T$. As with the occupancy model, the non-dimensionalised conservation equations are,

$$1 = \hat{P} + \frac{T_T}{P_T}\hat{C_T} \tag{A.23}$$

$$1 = \hat{T} + \hat{C_T}. \tag{A.24}$$

The non-dimensionalised version of (A.11) is,

$$-k_{\text{on}} P_T \hat{P}\hat{T} + k_{\text{off}}\hat{C_T} = 0, \tag{A.25}$$

which, using (A.24) becomes

$$-k_{\text{on}} P_T \hat{P}\big(1 - \hat{C_T}\big) + k_{\text{off}}\hat{C_T} = 0,$$

$$\text{yielding,} \qquad \hat{C_T} = \frac{k_{\text{on}} P_T \hat{P}}{k_{\text{off}} + k_{\text{on}} P_T \hat{P}},$$

$$\text{that is,} \qquad \hat{C_T} = \frac{P_T \hat{P}}{K_{\text{D}} + P_T \hat{P}}. \tag{A.26}$$

Calculating the $E_{\max}$

When $P_T \to \infty$, we can see from equation (A.26) that,

$$\begin{aligned} \hat{C_T} &= \lim_{P_T \to \infty} \frac{P_T \hat{P}}{P_T \hat{P}} \\ &= 1. \end{aligned}$$

From (A.24) it follows that $\hat{T}$ = 0. Hence,

$$\begin{aligned} E_{\max} &= \alpha^N C_T \\ &= \alpha^N T_T \qquad \text{(from A.17).} \end{aligned}$$

Calculating the EC_{50}

At half the maximal response,

$$\text{T cell activation} = E_{\max}/2 = \alpha^N T_T/2. \tag{A.27}$$

Using the result from A.22 that T cell activation $= \alpha^N C_T$, we have,

$$\alpha^N C_T = \alpha^N T_T/2$$

$$C_T = T_T/2.$$

The non-dimensionalised variables become,

$$\begin{aligned}\hat{C_T} &= 1/2 \\ \hat{T} &= 1/2 \qquad \text{(from A.24)} \\ \hat{P} &= 1 - \frac{T_T}{2P_T} \qquad \text{(from A.23).}\end{aligned}$$

Substituting these non-dimensionalied variables into the second equation in (A.25) we have,

$$\begin{aligned}-k_{\text{on}}P_T\big(1 - \frac{T_T}{2P_T}\big)/2 + k_{\text{off}}/2 &= 0 \\ P_T &= K_{\text{D}} + T_T/2,\end{aligned}$$

and so,

$$EC_{50} = K_{\text{D}} + T_T/2. \tag{A.28}$$

A.1.3 Limited signalling model derivation

The kinetic proofreading with limited signalling is an extension of the kinetic proofreading model that posits that once a TCR has reached the competent signalling state C_N, the bound TCR transitions to a non-signalling state C_N^- with rate ϕ. The equations that govern the system are:

$$\frac{dP}{dt} = -k_{\text{on}}PT + k_{\text{off}}C_T \tag{A.29}$$
$$\frac{dT}{dt} = -k_{\text{on}}PT + k_{\text{off}}C_T \tag{A.30}$$
$$\frac{dC_0}{dt} = k_{\text{on}}PT - (k_{\text{off}} + k_{\text{p}})C_0 \tag{A.31}$$
$$\frac{dC_i}{dt} = k_{\text{p}}C_{i-1} - (k_{\text{p}} + k_{\text{off}})C_i \qquad 1 \leq i < N-1 \tag{A.32}$$
$$\frac{dC_N}{dt} = k_{\text{p}}C_{N-1} - (k_{\text{off}} + \phi)C_N \tag{A.33}$$
$$\frac{dC_N^-}{dt} = \phi C_N - k_{\text{off}}C_N^-, \tag{A.34}$$

where $C_T = \sum_{i=0}^{N} C_i + C_N^-$, and,

$$\text{T cell activation} = C_N.$$

Setting the time derivatives in the above equations to 0 at equilibrium, it can be seen that,

$$\begin{aligned} C_T &= \sum_{i=0}^{N-1} C_i + C_N + C_N^- \\ &= \frac{1-\alpha^N}{1-\alpha} C_0 + C_N + \frac{\phi}{k_{\text{off}}} C_N. \end{aligned} \tag{A.35}$$

By combining (A.30) with (A.31) it can be seen that:

$$\begin{aligned} C_T &= \frac{k_{\text{p}} + k_{\text{off}}}{k_{\text{off}}} C_0 \\ &= \frac{1}{1-\alpha} C_0, \end{aligned}$$

and so (A.35) becomes:

$$C_T = (1-\alpha^N) C_T + \frac{\phi + k_{\text{off}}}{k_{\text{off}}} C_N,$$

and so,

$$C_N = \frac{k_{\text{off}}}{k_{\text{off}} + \phi} \alpha^N C_T. \tag{A.36}$$

Calculating the $E_{\max}$ and EC_{50}

Calculating the $E_{\max}$

As in the kinetic proofreading model, it can be shown that as $P_T \to \infty$, $C_T \to T_T$. The $E_{\max}$ is therefore:

$$E_{\max} = \frac{k_{\text{off}}}{k_{\text{off}} + \phi} \alpha^N T_T. \tag{A.37}$$

Calculating the EC_{50}

At half the maximal response,

$$\text{T cell activation} = E_{\max}/2 = \frac{k_{\text{off}}}{k_{\text{off}}+\phi}\alpha^N T_T/2. \tag{A.38}$$

Using the result from A.36 that T cell activation $= \frac{k_{\text{off}}}{k_{\text{off}}+\phi}\alpha^N C_T$, we have,

$$\begin{aligned}\frac{k_{\text{off}}}{k_{\text{off}}+\phi}\alpha^N C_T &= \frac{k_{\text{off}}}{k_{\text{off}}+\phi}\alpha^N T_T/2,\\ C_T &= T_T/2.\end{aligned}$$

As before with the kinetic proofreading model, we have the conservation equations,

$$\begin{aligned}P_T &= P + C_T,\\ T_T &= T + C_T,\end{aligned}$$

that can be non-dimensionalised to give,

$$1 = \hat{P} + \frac{T_T}{P_T}\hat{C_T}, \tag{A.39}$$

$$1 = \hat{T} + \hat{C_T}. \tag{A.40}$$

The non-dimensionalised variables $\hat{P} = \frac{P}{P_T}$, $\hat{T} = \frac{T}{T_T}$,and $\hat{C_T} = \frac{C}{T_T}$ become,

$$\begin{aligned}\hat{C_T} &= 1/2\\ \hat{T} &= 1/2 \qquad \text{(from A.40)}\\ \hat{P} &= 1 - \frac{T_T}{2P_T}. \qquad \text{(from A.39).}\end{aligned}$$

The non-dimensionalised version of (A.29) is,

$$-k_{\text{on}}P_T\hat{P}\hat{T} + k_{\text{off}}\hat{C_T} = 0 \tag{A.41}$$

which, using (A.40) becomes

$$-k_{\text{on}}P_T\hat{P}\big(1-\hat{C_T}\big) + k_{\text{off}}\hat{C_T} = 0. \tag{A.42}$$

Substituting these non-dimensionalied variables into the second equation in (A.41) we have,

$$-k_{\text{on}}P_T\big(1-\frac{T_T}{2P_T}\big)/2+k_{\text{off}}/2=0$$
$$P_T=K_{\text{D}}+T_T/2,$$

and so,

$$EC_{50}=K_{\text{D}}+T_T/2. \tag{A.43}$$

A.1.4 Kinetic proofreading with sustained signalling model derivation

The kinetic proofreading model can be modified so that TCRs in the signalling-competent state C_N can continue to signal after pMHC unbinding for some period of time (T^*) before they revert back to the basal state (T) with rate λ.

The ODEs that describe the system are:

$$\frac{dP}{dt}=-k_{\text{on}}PT+k_{\text{off}}\sum_{i=0}^{N}C_i-k_{\text{on}}PT^* \tag{A.44}$$
$$\frac{dT}{dt}=-k_{\text{on}}PT+k_{\text{off}}\sum_{i=0}^{N-1}C_i+\lambda T^* \tag{A.45}$$
$$\frac{dT^*}{dt}=k_{\text{off}}C_N-k_{\text{on}}PT^*-\lambda T^* \tag{A.46}$$
$$\frac{dC_0}{dt}=k_{\text{on}}PT-(k_{\text{off}}+k_{\text{p}})C_0 \tag{A.47}$$
$$\frac{dC_i}{dt}=k_{\text{p}}C_{i-1}-(k_{\text{p}}+k_{\text{off}})C_i \quad 1\leq i<N-1 \tag{A.48}$$
$$\frac{dC_N}{dt}=k_{\text{p}}C_{N-1}-k_{\text{off}}C_N+k_{\text{on}}PT^*. \tag{A.49}$$

The conservation equations are:

$$P_T=P+C_T, \tag{A.50}$$
$$T_T=T+T^*+C_T. \tag{A.51}$$

The non-dimensionalised variables are: $\hat{P}=P/P_T,\ \hat{T}=T/T_T,\ \hat{T^*}=T^*/T_T,\ \hat{C_i}=C_i/T_T$.

Conservation equations:

$$1 = \hat{P} + \frac{T_T}{P_T}\hat{C_T} \tag{A.52}$$

$$1 = \hat{T} + \hat{T^*} + \hat{C_T}. \tag{A.53}$$

$$\text{T cell activation} = C_N + T^*. \tag{A.54}$$

At steady state, we can use (A.46) to express the magnitude of T cell activation as a function of C_N,

$$T^* = \frac{k_{\text{off}} C_N}{k_{\text{on}} P + \lambda},$$

giving,

$$\begin{aligned}\text{T cell activation} &= C_N + T^* \\ &= \big(\frac{k_{\text{on}} P + \lambda + k_{\text{off}}}{k_{\text{on}} P + \lambda}\big) C_N \\ &= \big(\frac{k_{\text{on}}(P_T - C_T) + \lambda + k_{\text{off}}}{k_{\text{on}}(P_T - C_T) + \lambda}\big) C_N.\end{aligned}$$

The parameter C_N must then be related to C_T so that T cell activation can be determined in terms of the variables T_T, P_T, and K_{D}. This can be done by substituting, at steady state, (A.47) into (A.45) to give,

$$-(k_{\text{off}} + k_{\text{p}})C_0 + k_{\text{off}} \sum_{i=0}^{N-1} C_i + \lambda T^* = 0. \tag{A.55}$$

Using the result that was shown for the kinetic proofreading model A.20, we have,

$$C_T - C_N = \sum_{i=0}^{N-1} C_i = \big(\frac{1-\alpha^N}{1-\alpha}\big) C_0.$$

Equation (A.56) can then be expressed as:

$$-(k_{\text{off}} + k_{\text{p}})C_0 + k_{\text{off}}\big(\frac{1-\alpha^N}{1-\alpha}\big) C_0 + \lambda \frac{k_{\text{off}} C_N}{k_{\text{on}} P + \lambda} = 0. \tag{A.56}$$

This eventually gives,

$$C_N = \left(\frac{k_{\text{on}}P + \lambda}{\lambda + k_{\text{on}}P\alpha^N}\right)\alpha^N C_T. \tag{A.57}$$

T cell activation can now be determined as a function of C_T

$$\begin{aligned}\text{T cell activation} &= \left(\frac{k_{\text{on}}P + k_{\text{off}} + \lambda}{\lambda + \alpha^N k_{\text{on}}P}\right)\alpha^N C_T \\ &= \left(\frac{k_{\text{on}}(P_T - C_T) + k_{\text{off}} + \lambda}{\lambda + \alpha^N k_{\text{on}}(P_T - C_T)}\right)\alpha^N C_T,\end{aligned} \tag{A.58}$$

where $C_T = \left(P_T + T_T + K_{\text{D}} - \sqrt{(P_T + T_T + K_{\text{D}})^2 - 4P_T T_T}\right)/2$.

Calculating the $E_{\max}$

From (A.58), the parameters can be non-dimensionalised to give:

$$\text{T cell activation} = \left(\frac{k_{\text{on}}P_T\hat{P} + k_{\text{off}} + \lambda}{\lambda + \alpha^N k_{\text{on}}P_T\hat{P}}\right)\alpha^N T_T\hat{C_T}$$

$$= \left(\frac{k_{\text{on}}P_T\hat{P} + k_{\text{off}} + \lambda}{\lambda + \alpha^N k_{\text{on}}P_T\hat{P}}\right)\alpha^N P_T(1-\hat{P}) \qquad \textit{using conservation equation (A.52).}$$

When $P_T \rightarrow \infty$:

$$\text{T cell activation} = \left(\frac{k_{\text{on}}P_T\hat{P} + k_{\text{off}} + \lambda}{\lambda + \alpha^N k_{\text{on}}P_T\hat{P}}\right)\alpha^N P_T(1-\hat{P})$$

$$= \left(\frac{k_{\text{on}}P_T\hat{P} + k_{\text{off}} + \lambda}{\lambda + \alpha^N k_{\text{on}}P_T\hat{P}}\right)\alpha^N P_T(1 - \frac{-(K_{\text{D}} - P_T + T_T) + \sqrt{\left(K_{\text{D}} - P_T + T_T\right)^2 + 4P_TK_{\text{D}}}}{2P_T})$$

$$= \left(\frac{k_{\text{on}}P_T\hat{P} + k_{\text{off}} + \lambda}{\lambda + \alpha^N k_{\text{on}}P_T\hat{P}}\right)\alpha^N(\frac{(K_{\text{D}} + P_T + T_T) - \sqrt{\left(K_{\text{D}} - P_T + T_T\right)^2 + 4P_TK_{\text{D}}}}{2})$$

$$= \left(\frac{k_{\text{on}}P_T\hat{P} + k_{\text{off}} + \lambda}{\lambda + \alpha^N k_{\text{on}}P_T\hat{P}}\right)\alpha^N(\frac{(K_{\text{D}} + P_T + T_T) - P_T\sqrt{\frac{K_{\text{D}}^2}{P_T^2} + 2\frac{K_{\text{D}}}{P_T} + 1 + 2\frac{T_TK_{\text{D}}}{P_T^2} - 2\frac{T_T}{P_T} + \frac{T_T^2}{P_T^2}}}{2})$$

$$= \lim_{P_T\to\infty}\left(\frac{k_{\text{on}}P_T\hat{P}}{\alpha^N k_{\text{on}}P_T\hat{P}}\right)\alpha^N(\frac{(K_{\text{D}} + P_T + T_T) - P_T\sqrt{1 + 2\left(\frac{K_{\text{D}}}{P_T} - \frac{T_T}{P_T}\right)}}{2})$$

$$= \lim_{P_T\to\infty}\left(\frac{k_{\text{on}}P_T\hat{P}}{\alpha^N k_{\text{on}}P_T\hat{P}}\right)\alpha^N(\frac{(K_{\text{D}} + P_T + T_T) - P_T\left(1 + \left(\frac{K_{\text{D}}}{P_T} - \frac{T_T}{P_T}\right)\right)}{2})$$

$$= \lim_{P_T\to\infty} T_T$$

and so $E_{\max} = T_T$.

EC_{50}

At half the maximal response, T cell activation $= T_T/2$ and so,

$$T_T/2 = \left(\frac{k_{\text{on}}(P_T - C_T) + k_{\text{off}} + \lambda}{\lambda + \alpha^N k_{\text{on}}(P_T - C_T)}\right)\alpha^N C_T$$

where $C_T = \left(P_T + T_T + K_{\text{D}} - \sqrt{(P_T + T_T + K_{\text{D}})^2 - 4P_TT_T}\right)/2$.

This can be arranged to give:

$$P_T = \frac{\alpha^N C_T(k_{\text{off}} + \lambda - k_{\text{on}}C_T + k_{\text{on}}T_T/2) - T_T\lambda/2}{\alpha^N k_{\text{on}}(T_T/2 - C_T)} \tag{A.59}$$

The value for P_T must be solved neumerically since C_T is a function of P_T. The resultant value for P_T is the EC_{50} because this is the total amount of presented pMHC needed to give half the maximal response.

A.1.5 Mathematical derivation for co-presentation

The affinity model

If two types of pMHC, P_1 and P_2 are presented to TCR (T) to form bound complex C and D respectively, we have the following set of ODEs,

$$\frac{dC}{dt} = k_{\text{on}_1} P_1 T - k_{\text{off}_1} C \tag{A.60}$$

$$\frac{dD}{dt} = k_{\text{on}_2} P_2 T - k_{\text{off}_2} D. \tag{A.61}$$

The time derivatives can be set to 0 at equilibrium. We have,

$$\text{T cell activation} = C + D.$$

We have the following conservation equations:

$$P_{1_T} = P_1 + C \tag{A.62}$$

$$P_{2_T} = P_2 + D \tag{A.63}$$

$$T_T = T + C + D \tag{A.64}$$

At equilibrium, setting (A.60) and (A.61) to 0 we have,

$$P_1 T = \mathrm{K}_{D_1} C \tag{A.65}$$

$$P_2 T = \mathrm{K}_{D_2} D. \tag{A.66}$$

Using (A.65) and (A.66), we arrive at the expressions,

$$\mathrm{K}_{D_1}\mathrm{K}_{D_2}(C + D) = (\mathrm{K}_{D_1} P_2 + \mathrm{K}_{D_2} P_1) T \tag{A.67}$$

hence,
$$\mathrm{K}_{D_1}\mathrm{K}_{D_2}(C + D) = (\mathrm{K}_{D_1} P_2 + \mathrm{K}_{D_2} P_1)(T_T - (C + D)). \tag{A.68}$$

Using (A.65), (A.66) and (A.62) it can be seen that,

$$P_i = \Big(\frac{\mathrm{K}_{D_i}}{\mathrm{K}_{D_i} + T_T - (C + D)}\Big) P_{i_T}, \tag{A.69}$$

$$\tag{A.70}$$

This can be substituted into (A.68) to eventually give,

$$(\mathrm{K}_{D_1} + T_T - (C + D))(\mathrm{K}_{D_2} + T_T - (C + D))(C + D)$$
$$= (\mathrm{K}_{D_1} + T_T - (C + D))(T_T - (C + D)) P_{2_T} + (\mathrm{K}_{D_2} + T_T - (C + D))(T_T - (C + D)) P_{1_T}.$$

This can be multiplied out to give,

$$\begin{aligned}&(C+D)^3-\big(P_{1_T}+P_{2_T}+2T_T+\mathrm{K}_{D_1}+\mathrm{K}_{D_2}\big)(C+D)^2\\&+\big((\mathrm{K}_{D_1}+T_T)(\mathrm{K}_{D_2}+T_T)+P_{2_T}(2T_T+\mathrm{K}_{D_1})+P_{1_T}(2T_T+\mathrm{K}_{D_2})\big)(C+D)\\&+P_{2_T}(\mathrm{K}_{D_1}T_T+T_T^2)+P_{1_T}(\mathrm{K}_{D_2}T_T+T_T^2)=0.\end{aligned}\tag{A.71}$$

The amount of $C+D$ must then be solved numerically.

Kinetic proofreading

In this model two types of pMHC, P_1 and P_2 are presented to TCR (T) to form bound complex C_0 and D_0 respectively. Upon binding, a series of biochemical modifications take place to the TCR (C_i, D_i) that eventually result with a TCR in a signalling-competent state (C_N, D_N).The parameters consist of the biomolecular binding rates ($k_{\mathrm{on}_1}, k_{\mathrm{on}_2}$), the unbinding rates ($k_{\mathrm{off}_1}, k_{\mathrm{off}_2}$), and the modification rate (k_{p}). The unbinding of a pMHC from a TCR will immediately reverse the modifications to the TCR. T cell activation is proportional to the amount of bound TCR in the C_N+D_N state. The system can be described by the following set of ODEs:

$$\frac{dP_1}{dt}=-k_{\mathrm{on}_1}P_1T+k_{\mathrm{off}_1}C_T \tag{A.72}$$
$$\frac{dC_0}{dt}=k_{\mathrm{on}_1}P_1T-(k_{\mathrm{off}_1}+k_{\mathrm{p}})C_0 \tag{A.73}$$
$$\frac{dC_i}{dt}=k_{\mathrm{p}}C_{i-1}-(k_{\mathrm{p}}+k_{\mathrm{off}_1})C_i \quad 1\le i<N-1 \tag{A.74}$$
$$\frac{dC_N}{dt}=k_{\mathrm{p}}C_{N-1}-k_{\mathrm{off}_1}C_N, \tag{A.75}$$
$$\frac{dP_2}{dt}=-k_{\mathrm{on}_2}P_2T+k_{\mathrm{off}_2}D_T \tag{A.76}$$
$$\frac{dD_0}{dt}=k_{\mathrm{on}_2}P_2T-(k_{\mathrm{off}_2}+k_{\mathrm{p}})D_0 \tag{A.77}$$
$$\frac{dD_i}{dt}=k_{\mathrm{p}}D_{i-1}-(k_{\mathrm{p}}+k_{\mathrm{off}_2})D_i \quad 1\le i<N-1 \tag{A.78}$$
$$\frac{dD_N}{dt}=k_{\mathrm{p}}D_{N-1}-k_{\mathrm{off}_2}D_N \tag{A.79}$$
$$\frac{dT}{dt}=-k_{\mathrm{on}_2}P_2T-k_{\mathrm{on}_1}P_1T+k_{\mathrm{off}_1}C_T+k_{\mathrm{off}_2}D_T \tag{A.80}$$

where $C_T=\sum_{i=0}^{N}C_i$ and $D_T=\sum_{i=0}^{N}D_i$.

$$\text{T cell activation}=C_N+D_N.$$

The conservation equations are,

$$P_{1_T} = P_1 + C_T, \tag{A.81}$$

$$P_{2_T} = P_2 + D_T, \tag{A.82}$$

$$T_T = T + C_T + D_T. \tag{A.83}$$

At equilibrium we have the equations,

$$P_{1_T} = \mathrm{K}_{D_1} C_T, \tag{A.84}$$

$$P_{2_T} = \mathrm{K}_{D_2} D_T. \tag{A.85}$$

The total amount of TCR in bound state $C_T + D_T$ can be found using the result derived for the affinity model (A.71).

Now that $C_T + D_T$ has been found, it can then been seen using (A.84), (A.85) and (A.83) that the individual values of C_T and D_T can be found,

$$C_T = \frac{P_{1_T}(T_T - (C_T + D_T))}{\mathrm{K}_{D_1} + T_T - (C_T + D_T)}, \tag{A.86}$$

$$D_T = \frac{P_{2_T}(T_T - (C_T + D_T))}{\mathrm{K}_{D_2} + T_T - (C_T + D_T)}. \tag{A.87}$$

The kinetic proofreading model for the presentation of a single type of pMHC yielded the following relationship between C_T and C_N (A.21),

$$C_N = \alpha^N C_T,$$

and similarly for the presentation of two types of pMHC we have the expressions,

$$C_N = \alpha_1^N C_T, \tag{A.88}$$

$$D_N = \alpha_2^N D_T, \tag{A.89}$$

where $\alpha_i = \frac{k_\mathrm{p}}{k_\mathrm{p} + k_{\mathrm{off}_i}}$.

$$\text{T cell activation} = \alpha_1^N C_T + \alpha_2^N D_T. \tag{A.90}$$

Kinetic proofreading with limited signalling

The kinetic proofreading with limited signalling is an extension of the kinetic proofreading model that posits that once a TCR has reached the competent signalling state C_N or D_N (depending on whether bound by P_1 or P_2 respectively), the bound TCR transitions to a non-signalling state C_N^- or D_N^- with rate ϕ. The equations that govern the system are,

$$\frac{dP_1}{dt} = -k_{\text{on}_1} P_1 T + k_{\text{off}_1} C_T \tag{A.91}$$
$$\frac{dC_0}{dt} = k_{\text{on}_1} P_1 T - (k_{\text{off}_1} + k_{\text{p}}) C_0 \tag{A.92}$$
$$\frac{dC_i}{dt} = k_{\text{p}} C_{i-1} - (k_{\text{p}} + k_{\text{off}_1}) C_i \quad 1 \leq i < N-1 \tag{A.93}$$
$$\frac{dC_N}{dt} = k_{\text{p}} C_{N-1} - (k_{\text{off}_1} + \phi) C_N \tag{A.94}$$
$$\frac{dC_N^-}{dt} = \phi C_N - k_{\text{off}_1} C_N^- \tag{A.95}$$
$$\frac{dP_2}{dt} = -k_{\text{on}_2} P_2 T + k_{\text{off}_2} D_T \tag{A.96}$$
$$\frac{dD_0}{dt} = k_{\text{on}_2} P_2 T - (k_{\text{off}_2} + k_{\text{p}}) D_0 \tag{A.97}$$
$$\frac{dD_i}{dt} = k_{\text{p}} D_{i-1} - (k_{\text{p}} + k_{\text{off}_2}) D_i \quad 1 \leq i < N-1 \tag{A.98}$$
$$\frac{dD_N}{dt} = k_{\text{p}} D_{N-1} - k_{\text{off}_2} D_N \tag{A.99}$$
$$\frac{dD_N^-}{dt} = \phi D_N - k_{\text{off}_2} D_N^- \tag{A.100}$$
$$\frac{dT}{dt} = -k_{\text{on}_2} P_2 T - k_{\text{on}_1} P_1 T + k_{\text{off}_1} C_T + k_{\text{off}_2} D_T, \tag{A.101}$$

where $C_T = \sum_{i=0}^{N} C_i + C_N^-$, $D_T = \sum_{i=0}^{N} D_i + D_N^-$ and,

$$\text{T cell activation} = C_N + D_N.$$

As for the kinetic proofreading model, the values for C_T and D_T can be found ((A.86) and (A.87)). At equilibrium, the kinetic proofreading with limited signalling model for a single type of pMHC yielded the following relationship between C_T and C_N ((A.57)),

$$C_N = \frac{k_{\text{off}}}{k_{\text{off}} + \phi} \alpha^N C_T,$$

and similarly for the two pMHC model we have,

$$C_N = \frac{k_{\text{off}_1}}{k_{\text{off}_1} + \phi} \alpha_1^N C_T, \tag{A.102}$$

$$D_N = \frac{k_{\text{off}_2}}{k_{\text{off}_2} + \phi} \alpha_2^N D_T, \tag{A.103}$$

where $\alpha_i = \frac{k_{\text{p}}}{k_{\text{p}} + k_{\text{off}_i}}$.

Kinetic proofreading with sustained signalling

The kinetic proofreading model can be modified so that TCRs in the signalling-competent state C_N and D_N (depending on whether bound by P_1 or P_2 respectively) can continue to signal after pMHC unbinding for some period of time (T^*) before they revert back to the basal state (T) with rate λ. The system can be described by the following set of ODEs:

$$\frac{dP_1}{dt} = -k_{\text{on}_1} P_1 T + k_{\text{off}_1} C_T - k_{\text{on}_1} P_1 T^* \tag{A.104}$$

$$\frac{dC_0}{dt} = k_{\text{on}_1} P_1 T - (k_{\text{off}_1} + k_{\text{p}}) C_0 \tag{A.105}$$

$$\frac{dC_i}{dt} = k_{\text{p}} C_{i-1} - (k_{\text{p}} + k_{\text{off}_1}) C_i \quad 1 \leq i < N-1 \tag{A.106}$$

$$\frac{dC_N}{dt} = k_{\text{p}} C_{N-1} - k_{\text{off}_1} C_N + k_{\text{on}_1} P_1 T^* \tag{A.107}$$

$$\frac{dP_2}{dt} = -k_{\text{on}_2} P_2 T + k_{\text{off}_2} D_T - k_{\text{on}_2} P_2 T^* \tag{A.108}$$

$$\frac{dD_0}{dt} = k_{\text{on}_2} P_2 T - (k_{\text{off}_2} + k_{\text{p}}) D_0 \tag{A.109}$$

$$\frac{dD_i}{dt} = k_{\text{p}} D_{i-1} - (k_{\text{p}} + k_{\text{off}_2}) D_i \quad 1 \leq i < N-1 \tag{A.110}$$

$$\frac{dD_N}{dt} = k_{\text{p}} D_{N-1} - k_{\text{off}_2} D_N + k_{\text{on}_2} P_2 T^* \tag{A.111}$$

$$\frac{dT}{dt} = -(k_{\text{on}_2} P_2 + k_{\text{on}_1} P_1) + k_{\text{off}_1} C_T + k_{\text{off}_2} D_T + \lambda T^* \tag{A.112}$$

$$\frac{dT^*}{dt} = k_{\text{off}_2} D_N + k_{\text{off}_1} C_N - (k_{\text{on}_1} P_1 + k_{\text{on}_2} P_2) T^* - \lambda T^*. \tag{A.113}$$

The conservation equations are,

$$P_{1_T} = P_1 + C_T, \tag{A.114}$$

$$P_{2_T} = P_2 + D_T, \tag{A.115}$$

$$T_T = T + T^* + C_T + D_T. \tag{A.116}$$

$$\text{T cell activation} = C_N + D_N + T^*.$$

At equilibrium, the ODEs can be set to 0. From (A.114), (A.115) and (A.113) it can be seen that,

$$T^* = \frac{k_{\text{off}_1} C_N + k_{\text{off}_2} D_N}{k_{\text{on}_1}(P_{1_T} - C_T) + k_{\text{on}_2}(P_{2_T} - D_T) + \lambda}. \tag{A.117}$$

In order to find C_N and D_N, it can be seen using (A.104), (A.108) and (A.116) that,

$$C_T = \frac{P_{1_T}(T_T - (C_T + D_T))}{\mathbf{K}_{D_1} + T_T - (C_T + D_T)}, \tag{A.118}$$

$$D_T = \frac{P_{2_T}(T_T - (C_T + D_T))}{\mathbf{K}_{D_2} + T_T - (C_T + D_T)}. \tag{A.119}$$

At equilibrium, the kinetic proofreading with sustained signalling model for a single type of pMHC yielded the following relationship between C_T and C_N ((A.57)),

$$C_N = \big(\frac{k_{\text{on}}(P_{1_T} - C_T + \lambda}{\lambda + k_{\text{on}} P_{1_T} - C_T \alpha^N}\big)\alpha^N C_T,$$

and similarly for the two presentation model we have,

$$C_N = \big(\frac{k_{\text{on}_1}(P_{1_T} - C_T + \lambda}{\lambda + k_{\text{on}_1} P_{1_T} - C_T \alpha_1^N}\big)\alpha_1^N C_T, \tag{A.120}$$

$$D_N = \big(\frac{k_{\text{on}_2}(P_{2_T} - D_T + \lambda}{\lambda + k_{\text{on}_2} P_{2_T} - D_T \alpha_1^N}\big)\alpha_1^N D_T, \tag{A.121}$$

where $\alpha_i = \frac{k_{\text{p}}}{k_{\text{p}} + k_{\text{off}_i}}$.

A.2 Mathematical derivations from Chapter 5

A.2.1 Mathematical derivation for incoherent feed forward loop

The incoherent FFL consists of 3 molecules, x, y and a, which have an inactive (x^*, y^*, a^*) and active (x, y, z) form. x and y are activated downstream of a TCR in a signalling-competent state. x inhibits a and y activates a. The molecules obey the following conservation equations:

$$x + x^* = x_T, \tag{A.122}$$

$$y + y^* = y_T, \tag{A.123}$$

$$a + a^* = a_T. \tag{A.124}$$

The system is governed by the following equations:

$$\frac{dx}{dt} = k_{\mathrm{NX}} C_N x^* - \nu_X x, \tag{A.125}$$

$$= k_{\mathrm{NX}} C_N (1 - x) - \nu_X x. \tag{A.126}$$

$$\frac{dy}{dt} = k_{\mathrm{NY}} C_N y^* - \nu_Y y, \tag{A.127}$$

$$= k_{\mathrm{NY}} C_N (1 - y) - \nu_Y y. \tag{A.128}$$

$$\frac{da}{dt} = k_{\mathrm{YA}} y a^* - (\nu_A + k_{\mathrm{XA}} x) a, \tag{A.129}$$

$$= k_{\mathrm{YA}} y (1 - a) - (\nu_A + k_{\mathrm{XA}} x) a. \tag{A.130}$$

These variables can be non-dimensionalised, where $\hat{C_N} = C_N/T_T, X = x/x_T, X^* = x^*/x_T, Y = y/y_T, Y^* = y^*/y_T, A = a/a_T, A^* = a^*/a_T$. The conservation equations now become,

$$X + X^* = 1, \tag{A.131}$$

$$Y + Y^* = 1, \tag{A.132}$$

$$A + A^* = 1. \tag{A.133}$$

and the system of ODEs become,

$$\frac{dX}{dt} = \hat{k_{\text{NX}}}\hat{C_N}X^* - \nu_X X, \tag{A.134}$$

$$= k_{\text{NX}}\hat{C_N}(1-X) - \nu_X X. \tag{A.135}$$

$$\frac{dY}{dt} = \hat{k_{\text{NY}}}\hat{C_N}Y^* - \nu_Y Y, \tag{A.136}$$

$$= k_{\text{NY}}\hat{C_N}(1-Y) - \nu_Y Y. \tag{A.137}$$

$$\frac{dA}{dt} = k_{\text{YA}}YA^* - (\nu_A + k_{\text{XA}}X)A, \tag{A.138}$$

$$= k_{\text{YA}}Y(1-A) - (\nu_A + k_{\text{XA}}X)A, \tag{A.139}$$

where $\hat{k_{\text{NX}}} = k_{\text{NX}}T_T$, and $\hat{k_{\text{YX}}} = k_{\text{YX}}T_T$. A cartoon of the model is in Fig. A.1.

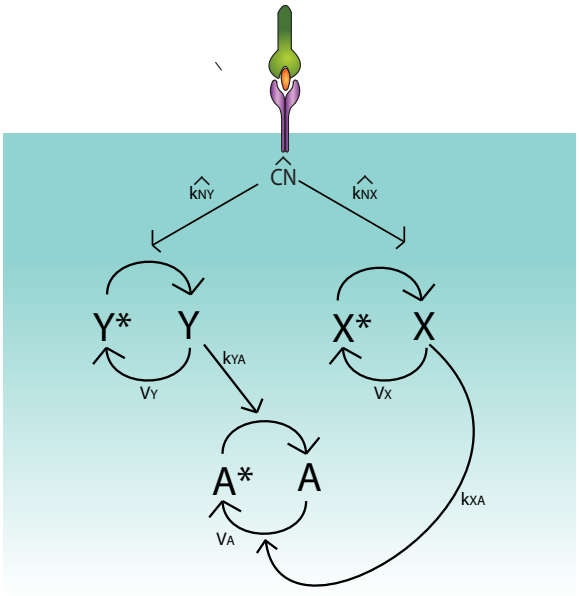

Figure A.1: Cartoon of the incoherent FFL: For all models, the incoherent FFL is downstream of a TCR in a signalling-competent state $\hat{C_N}$. Molecules X and Y are activated by $\hat{C_N}$ and X inhibits A while Y activates A.

At equilibrium:

$$X = \frac{\hat{C_N}}{\hat{C_N} + \frac{\nu_X}{\hat{k_{\text{NX}}}}}, \tag{A.140}$$

$$Y = \frac{\hat{C_N}}{\hat{C_N} + \frac{\nu_Y}{\hat{k_{\text{NY}}}}}, \tag{A.141}$$

$$A = \frac{Y}{Y + \frac{k_{\text{XA}}}{k_{\text{YA}}}X + \frac{\nu_A}{k_{\text{YA}}}}. \tag{A.142}$$

The incoherent FFL can now be characterised by 4 parameters:
$\frac{\nu_X}{k_{\text{NX}}} = \rho, \frac{\nu_Y}{k_{\text{NY}}} = \beta, \frac{k_{\text{XA}}}{k_{\text{YA}}} = \delta, \frac{\nu_A}{k_{\text{YA}}} = \gamma$, to give,

$$X = \frac{\hat{C_N}}{\hat{C_N} + \rho}, Y = \frac{\hat{C_N}}{\hat{C_N} + \beta}, A = \frac{X}{X + \delta Y + \gamma}. \tag{A.143}$$

T cell activation is proportional to A. A can be expressed as a function of $\hat{C_N}$:

$$A = \frac{Y}{Y + \delta X + \gamma}, \tag{A.144}$$

$$= \frac{\frac{\hat{C_N}}{\hat{C_N}+\beta}}{\frac{\hat{C_N}}{\hat{C_N}+\beta} + \delta\frac{\hat{C_N}}{\hat{C_N}+\rho} + \gamma}. \tag{A.145}$$

A.2.2 Coupling models of TCR activation to the incoherent FFL

The expression for $\hat{C_N}$ depends on whether the incoherent FFL is coupled to the occupancy model, the kinetic proofreading model or the kinetic proofreading with limited signalling model.

Occupancy model coupled to incoherent FFL

As shown in Chapter 2, when a concentration of pMHC (P_T) with dissociation constant K_{D} binds to a concentration of TCRs (T_T), the concentration of TCRs in the signalling-competent state $\hat{C_N}$ is equal to the concentration of occupied TCRs (C), where

$$\hat{C_N} = C/T_T, \tag{A.146}$$

$$C = \left(P_T + T_T + K_{\mathrm{D}} - \sqrt{((P_T + T_T + K_{\mathrm{D}})^2 - 4P_T T_T)}\right)/2. \tag{A.147}$$

Kinetic proofreading coupled to incoherent FFL

When kinetic proofreading is implemented, an occupied TCR undergoes N kinetic proofreading steps with rate k_{p} to reach a signalling-competent state $\hat{C_N}$..

$$\hat{C_N} = \alpha^N \hat{C_T}, \tag{A.148}$$

where $\alpha = \frac{k_{\mathrm{p}}}{k_{\mathrm{p}}+k_{\mathrm{off}}}$.

Kinetic proofreading with limited signalling coupled to incoherent FFL

When the signal from a TCR is limited, a TCR in a signalling-competent state transitions to an intert state with rate ϕ. The expression for $\hat{C_N}$ becomes:

$$\hat{C_N} = \frac{k_{\mathrm{off}}}{k_{\mathrm{off}} + \phi}\alpha^N \hat{C_T}. \tag{A.149}$$

Bibliography

[1] J. E. Smith-Garvin, G. A. Koretzky, and M. S. Jordan. “T cell activation.” In: *Annual Review of Immunology* 27 (Jan. 2009), pp. 591–619.

[2] L. Klein et al. “Positive and negative selection of the T cell repertoire: what thymocytes see (and don’t see)”. In: *Nature Reviews Immunology* 14.6 (2014), pp. 377–391.

[3] M. Huse. “The T-cell-receptor signaling network ”. In: *Journal of Cell Science* 2009 (2009), pp. 1269–1273.

[4] K. M. Murphy. *Janeway’s immunobiology*. Garland Science, 2011.

[5] A. Corthay. “How do regulatory T cells work?” In: *Scandinavian Journal of Immunology* 70 (2009), pp. 326–336.

[6] R. A. Seder and R. Ahmed. “Similarities and differences in CD4+ and CD8+ effector and memory T cell generation.” In: *Nature immunology* 4.9 (Sept. 2003), pp. 835–42.

[7] L. Chen and D. B. Flies. “Molecular mechanisms of T cell co-stimulation and co-inhibition”. In: *Nature Reviews Immunology* 13.4 (Mar. 2013), pp. 227–242.

[8] J. Lin and A. Weiss. “T cell receptor signalling”. In: *Journal of cell science* 114.2 (2001), pp. 243–244.

[9] R. J. Brownlie and R. Zamoyska. “T cell receptor signalling networks: branched, diversified and bounded”. In: *Nature Reviews Immunology* 13.4 (Mar. 2013), pp. 257–269.

[10] N. Labrecque et al. “How much TCR does a T cell need?” In: *Immunity* 15 (2001), pp. 71–82.

[11] B. A. Schodin, T. J. Tsomides, and D. M. Kranz. “Correlation between the number of T cell receptors required for T cell activation and TCR-ligand affinity”. In: *Immunity* 5 (1996), pp. 137–146.

[12] N. Anikeeva et al. “Evidence that the density of self peptide-MHC ligands regulates T-cell receptor signaling.” In: *PloS one* 7.8 (Jan. 2012), e41466.

[13] D. J. Irvine et al. “Direct observation of ligand recognition by T cells.” In: *Nature* 419.October (2002), pp. 845–849.

[14] K. C. Garcia et al. “An alphabeta T cell receptor structure at 2.5 A and its orientation in the TCR-MHC complex.” In: *Science (New York, N.Y.)* 274.October (1996), pp. 209–219.

[15] D. N. Garboczi et al. “Structure of the complex between human T-cell receptor, viral peptide and HLA-A2.” In: *Nature* 384 (1996), pp. 134–141.

[16] P. A. van der Merwe and S. J. Davis. “Molecular interactions mediating T cell antigen recognition.” In: *Annual Review of Immunology* 21 (Jan. 2003), pp. 659–84.

[17] B. Berkhout, B. Alarcon, and C. Terhorst. “Transfection of genes encoding the T cell receptor-associated CD3 complex into COS cells results in assembly of the macromolecular structure”. In: *Journal of Biological Chemistry* 263.10 (1988), pp. 8528–8536.

[18] A. M. Weissman et al. “Molecular cloning of the zeta chain of the T cell antigen receptor.” In: *Science (New York, N.Y.)* 239 (1988), pp. 1018–1021.

[19] C. S. Guy and D. A. A. Vignali. “Organization of proximal signal initiation at the TCR:CD3 complex”. In: *Immunological Reviews* 232 (2009), pp. 7–21.

[20] N. S. van Oers et al. “The 21- and 23-kD forms of TCR zeta are generated by specific ITAM phosphorylations.” In: *Nature immunology* 1.4 (Oct. 2000), pp. 322–8.

[21] N. Isakov et al. “ZAP-70 binding specificity to T cell receptor tyrosine-based activation motifs: the tandem SH2 domains of ZAP-70 bind distinct tyrosine-based activation motifs with varying affinity.” In: *The Journal of experimental medicine* 181.1 (1995), pp. 375–380.

[22] J. Bu, A. Shaw, and A. Chan. “Analysis of the interaction of ZAP-70 and syk protein-tyrosine kinases with the T-cell antigen receptor by plasmon resonance”. In: *Proceedings of the National Academy of Sciences* 92.11 (1995), p. 5106.

[23] G. Zenner et al. “Differential and multiple binding of signal transducing molecules to the ITAMs of the TCR-zeta chain.” In: *Journal of cellular biochemistry* 63.1 (Oct. 1996), pp. 94–103.

[24] E. A. Ottinger, M. C. Botfield, and S. E. Shoelson. “Tandem SH2 domains confer high specificity in tyrosine kinase signaling.” In: *The Journal of biological chemistry* 273.2 (Jan. 1998), pp. 729–35.

[25] H. Mukhopadhyay et al. “Systems Model of T Cell Receptor Proximal Signaling Reveals Emergent Ultrasensitivity”. In: *PLoS Computational Biology* 9.3 (2013).

[26] E. W. Shores et al. “Role of the multiple T cell receptor (TCR)-zeta chain signaling motifs in selection of the T cell repertoire.” In: *The Journal of experimental medicine* 185.5 (1997), pp. 893–900.

[27] L. A. Pitcher et al. “Selective expression of the 21-kilodalton tyrosine-phosphorylated form of TCR zeta promotes the emergence of T cells with autoreactive potential.” In: *Journal of immunology (Baltimore, Md. : 1950)* 174 (2005), pp. 6071–6079.

[28] J. Neefjes et al. “Towards a systems understanding of MHC class I and MHC class II antigen presentation”. In: *Nat Rev Immunol* 11.12 (2011), pp. 823–36.

[29] R. N. Germain. “MHC-dependent antigen processing and peptide presentation: Providing ligands for T lymphocyte activation”. In: *Cell* 76 (1994), pp. 287–299.

[30] B. Laugel et al. “Design of soluble recombinant T cell receptors for antigen targeting and T cell inhibition”. In: *Journal of Biological Chemistry* 280.3 (2005), pp. 1882–1892.

[31] G. Å. Løset et al. “Phage display engineered T cell receptors as tools for the study of tumor peptide–MHC interactions”. In: *Frontiers in oncology* 4 (2014).

[32] Y. Li et al. “Directed evolution of human T-cell receptors with picomolar affinities by phage display.” In: *Nature biotechnology* 23.3 (2005), pp. 349–354.

[33] Q.-J. Li et al. “CD4 enhances T cell sensitivity to antigen by coordinating Lck accumulation at the immunological synapse.” In: *Nature immunology* 5.8 (Aug. 2004), pp. 791–9.

[34] J. R. Wyer et al. “T Cell Receptor and Coreceptor CD8 Bind Peptide-MHC Independently and with Distinct Kinetics”. In: *Immunity* 10 (1999), pp. 219–225.

[35] S. J. Davis and P. A. van der Merwe. “Lck and the nature of the T cell receptor trigger”. In: *Trends in immunology* 32.1 (2011), pp. 1–5.

[36] K. Nika et al. “Constitutively active Lck kinase in T cells drives antigen receptor signal transduction.” In: *Immunity* 32.6 (June 2010), pp. 766–77.

[37] A. Stirnweiss et al. “T cell activation results in conformational changes in the Src family kinase Lck to induce its activation”. In: *Science signaling* 6.263 (2013), ra13–ra13.

[38] G. J. Freeman et al. “B7, a new member of the Ig superfamily with unique expression on activated and neoplastic B cells.” In: *Journal of immunology (Baltimore, Md. : 1950)* 143 (1989), pp. 2714–2722.

[39] M. Azuma et al. “B70 antigen is a second ligand for CTLA-4 and CD28.” In: *Nature* 366 (1993), pp. 76–79.

[40] G. J. Freeman et al. “Murine B7-2, an alternative CTLA4 counter-receptor that costimulates T cell proliferation and interleukin 2 production.” In: *The Journal of experimental medicine* 178.December (1993), pp. 2185–2192.

[41] P. A. van der Merwe and O. Dushek. “Mechanisms for T cell receptor triggering.” In: *Nature Reviews. Immunology* 11.1 (Jan. 2011), pp. 47–55.

[42] A. K. Chakraborty and A. Weiss. “Insights into the initiation of TCR signaling”. In: *Nature Immunology* 15.9 (2014), pp. 798–807.

[43] L. Balagopalan et al. “The LAT story: a tale of cooperativity, coordination, and choreography.” In: *Cold Spring Harbor perspectives in biology* 2.8 (Aug. 2010), a005512.

[44] B. B. Au-Yeung et al. “A genetically selective inhibitor demonstrates a function for the kinase Zap70 in regulatory T cells independent of its catalytic activity.” In: *Nature immunology* 11.12 (2010), pp. 1085–1092. arXiv: NIHMS150003.

[45] M. J. Miller et al. “T cell repertoire scanning is promoted by dynamic dendritic cell behavior and random T cell motility in the lymph node.” In: *Proceedings of the National Academy of Sciences of the United States of America* 101.4 (Jan. 2004), pp. 998–1003.

[46] M. L. Dustin. “T-cell activation through immunological synapses and kinapses”. In: *Immunological Reviews* 221 (2008), pp. 77–89.

[47] A. Kupfer and G. Dennert. “Reorientation of the microtubule-organizing center and the Golgi apparatus in cloned cytotoxic lymphocytes triggered by binding to lysable target cells.” In: *Journal of immunology (Baltimore, Md. : 1950)* 133.5 (1984), pp. 2762–2766.

[48] J. B. Huppa and M. M. Davis. “T-cell-antigen recognition and the immunological synapse.” In: *Nature Reviews. Immunology* 3.12 (Dec. 2003), pp. 973–83.

[49] C. R. Monks et al. “Three-dimensional segregation of supramolecular activation clusters in T cells.” In: *Nature* 395.1986 (1998), pp. 82–86.

[50] J. Xie et al. “Photocrosslinkable pMHC monomers stain T cells specifically and cause ligand-bound TCRs to be ’preferentially’ transported to the cSMAC.” In: *Nature immunology* June (June 2012), pp. 1–8.

[51] M. Oh-hora. “Calcium signaling in the development and function of T-lineage cells”. In: 231 (2009), pp. 210–224.

[52] F. Macian. “NFAT proteins: key regulators of T-cell development and function.” In: *Nature Reviews. Immunology* 5.6 (June 2005), pp. 472–84.

[53] J. Lin and A. Weiss. “T cell receptor signalling”. In: *Cell Science* 114 (2001), pp. 243–244.

[54] D. K. Morrison. “MAP kinase pathways”. In: *Cold Spring Harbor perspectives in biology* 4.11 (2012), a011254.

[55] A. Kannan et al. “Signal transduction via the T cell antigen receptor in naive and effector/memory T cells.” In: *The International Journal of Biochemistry and Cell Biology* 44.12 (Dec. 2012), pp. 2129–34.

[56] S. Paul and B. C. Schaefer. “A new look at T cell receptor signaling to nuclear factor-κB”. In: *Trends in Immunology* 34.6 (2013), pp. 269–281.

[57] S. Vallabhapurapu and M. Karin. “Regulation and Function of NF- κ B Transcription Factors in the Immune System”. In: (2009).

[58] A. Sica et al. “Interaction of NF-kappaB and NFAT with the interferon-gamma promoter.” In: *The Journal of biological chemistry* 272.48 (1997), pp. 30412–30420.

[59] E. Serfling et al. “NFATc1/αA: The other Face of NFAT Factors in Lymphocytes”. In: *Cell Communication and Signaling* 10.1 (2012), p. 16.

[60] L. Jin et al. “An asymmetric NFAT1 dimer on a pseudo-palindromic kappa B-like DNA site.” In: *Nature structural biology* 10.10 (2003), pp. 807–811.

[61] P. S. Costello, M. Gallagher, and D. A. Cantrell. “Sustained and dynamic inositol lipid metabolism inside and outside the immunological synapse.” In: *Nature immunology* 3.11 (2002), pp. 1082–1089.

[62] J. Harriague and G. Bismuth. “Imaging antigen-induced PI3K activation in T cells.” In: *Nature immunology* 3.11 (2002), pp. 1090–6.

[63] D. Vermijlen, M. Y. Braun, and A. Marchant. “Do PI3-kinase mutations drive T cells insane?” In: *Cellular & molecular immunology* (2014), pp. 1–3.

[64] J. Harriague and G. Bismuth. “Imaging antigen-induced PI3K activation in T cells.” In: *Nature immunology* 3.11 (2002), pp. 1090–6.

[65] P. S. Costello, M. Gallagher, and D. A. Cantrell. “Sustained and dynamic inositol lipid metabolism inside and outside the immunological synapse.” In: *Nature immunology* 3.11 (2002), pp. 1082–1089.

[66] S. Sauer et al. “T cell receptor signaling controls Foxp3 expression via PI3K, Akt, and mTOR.” In: *Proceedings of the National Academy of Sciences of the United States of America* 105.22 (2008), pp. 7797–7802.

[67] S. Fabre et al. “Stable activation of phosphatidylinositol 3-kinase in the T cell immunological synapse stimulates Akt signaling to FoxO1 nuclear exclusion and cell growth control.” In: *Journal of immunology (Baltimore, Md. : 1950)* 174 (2005), pp. 4161–4171.

[68] S. Kumari et al. “T cell antigen receptor activation and actin cytoskeleton remodeling”. In: *Biochimica et Biophysica Acta (BBA) - Biomembranes* 1838.2 (2014), pp. 546–556.

[69] M. L. Dustin et al. “Antigen receptor engagement delivers a stop signal to migrating T lymphocytes.” In: *Proceedings of the National Academy of Sciences of the United States of America* 94.April (1997), pp. 3909–13.

[70] B. Reicher and M. Barda-Saad. “Multiple pathways leading from the T-cell antigen receptor to the actin cytoskeleton network.” In: *FEBS letters* 584.24 (2010), pp. 4858–64.

[71] J. Faull et al. “Signaling Through”. In: *Journal of the American Society of Nephrology* (), pp. 1091–1097.

[72] M. N. Navarro and D. A. Cantrell. “Serine-threonine kinases in TCR signaling”. In: *Nature Immunology* 15.9 (2014), pp. 808–814.

[73] K. Katagiri and T. Kinashi. “Rap1 and integrin inside-out signaling”. In: *Integrin and Cell Adhesion Molecules*. Springer, 2012, pp. 279–296.

[74] D. D. Billadeau, J. C. Nolz, and T. S. Gomez. “Regulation of T-cell activation by the cytoskeleton”. In: *Nature Reviews Immunology* 7.February (2007), pp. 131–143.

[75] O. Acuto, V. Di Bartolo, and F. Michel. “Tailoring T-cell receptor signals by proximal negative feedback mechanisms.” In: *Nature Reviews. Immunology* 8.9 (Sept. 2008), pp. 699–712.

[76] J. J. Knox et al. “Characterization of T-bet and Eomes in peripheral human immune cells”. In: *Frontiers in Immunology* 5.May (2014), pp. 1–13.

[77] C. S. Palmer et al. “Glucose Metabolism Regulates T Cell Activation, Differentiation, and Functions”. In: *Frontiers in Immunology* 6.January (2015), p. 1.

[78] G. C. Preston et al. “Single cell tuning of Myc expression by antigen receptor signal strength and interleukin - 2 in T lymphocytes”. In: *The EMBO journal* 34.15 (2015), pp. 2008–2024.

[79] K. Man et al. “The transcription factor IRF4 is essential for TCR affinityfffdfffdfffdmediated metabolic programming and clonal expansion of T cells”. In: *Nature Immunology* 14.11 (2013), pp. 1155–1165.

[80] L. V. Sinclair et al. “Control of amino-acid transport by antigen receptors coordinates the metabolic reprogramming essential for T cell differentiation”. In: *Nature Immunology* 14.5 (2013), pp. 500–508.

[81] K. Man and A. Kallies. “Synchronizing transcriptional control of T cell metabolism and function”. In: *Nature Reviews Immunology* 15.9 (2015), pp. 574–584.

[82] D. Finlay and D. Cantrell. “Phosphoinositide 3-kinase and the mammalian target of rapamycin pathways control T cell migration”. In: *Annals of the New York Academy of Sciences* 1183 (2010), pp. 149–157.

[83] M. Matloubian et al. “Lymphocyte egress from thymus and peripheral lymphoid organs is dependent on S1P receptor 1.” In: *Nature* 427 (2004), pp. 355–60.

[84] B. D. Evavold and P. M. Allen. “Separation of IL-4 production from Th cell proliferation by an altered T cell receptor ligand.” In: *Science (New York, N.Y.)* 252.5010 (May 1991), pp. 1308–10.

[85] Y. Sykulev et al. “Evidence that a single peptide-MHC complex on a target cell can elicit a cytolytic T cell response.” In: *Immunity* 4.6 (June 1996), pp. 565–71.

[86] O. Feinerman. "Quantitative challenges in understanding ligand discrimination by $\alpha\beta$ T cells". In: *Molecular Immunology* 45.3 (2008), pp. 619–631.

[87] P. S. Andersen et al. "Role of the T cell receptor ligand affinity in T cell activation by bacterial superantigens." In: *The Journal of biological chemistry* 276.36 (Sept. 2001), pp. 33452–7.

[88] P. D. Holler and D. M. Kranz. "Quantitative analysis of the contribution of TCR/pepMHC affinity and CD8 to T cell activation." In: *Immunity* 18.2 (Feb. 2003), pp. 255–64.

[89] S. Tian et al. "CD8+ T cell activation is governed by TCR-peptide/MHC affinity, not dissociation rate". In: *The Journal of Immunology* 179.5 (2007), p. 2952.

[90] A. S. Chervin et al. "The impact of TCR-binding properties and antigen presentation format on T cell responsiveness." In: *Journal of immunology (Baltimore, Md. : 1950)* 183.2 (July 2009), pp. 1166–78.

[91] O. Dushek et al. "Antigen potency and maximal efficacy reveal a mechanism of efficient T cell activation." In: *Science signaling* 4.176 (2011), ra39.

[92] A. M. Kalergis et al. "Efficient T cell activation requires an optimal dwell-time of interaction between the TCR and the pMHC complex." In: *Nature immunology* 2.3 (Mar. 2001), pp. 229–34.

[93] D. Coombs et al. "Activated TCRs remain marked for internalization after dissociation from pMHC." In: *Nature immunology* 3.10 (Oct. 2002), pp. 926–31.

[94] M. Irving et al. "Interplay between T cell receptor binding kinetics and the level of cognate peptide presented by major histocompatibility complexes governs CD8+ T cell responsiveness." In: *The Journal of biological chemistry* 287.27 (June 2012), pp. 23068–78.

[95] P. A. González et al. "T cell receptor binding kinetics required for T cell activation depend on the density of cognate ligand on the antigen-presenting cell." In: *Proceedings of the National Academy of Sciences of the United States of America* 102.13 (Mar. 2005), pp. 4824–9.

[96] B. N. Dittel et al. "Cross-antagonism of a T cell clone expressing two distinct T cell receptors." In: *Immunity* 11.3 (Sept. 1999), pp. 289–98.

[97] J. M. Robertson and B. D. Evavold. "Cutting edge: dueling TCRs: peptide antagonism of CD4+ T cells with dual antigen specificities." In: *Journal of immunology (Baltimore, Md. : 1950)* 163.4 (Aug. 1999), pp. 1750–4.

[98] T. W. McKeithan. "Kinetic proofreading in T-cell receptor signal transduction." In: *Proceedings of the National Academy of Sciences of the United States of America* 92.11 (May 1995), pp. 5042–6.

[99] P. S. Andersen et al. "A response calculus for immobilized T cell receptor ligands." In: *The Journal of biological chemistry* 276.52 (Dec. 2001), pp. 49125–32.

[100] C. Chan, A. J. George, and J. Stark. "Cooperative enhancement of specificity in a lattice of T cell receptors." In: *Proceedings of the National Academy of Sciences of the United States of America* 98.10 (May 2001), pp. 5758–63.

[101] H. A. Van Den Berg, N. J. Burroughs, and D. A. Rand. "Quantifying the strength of ligand antagonism in TCR triggering." In: *Bulletin of mathematical biology* 64.4 (July 2002), pp. 781–808.

[102] G. Altan-Bonnet and R. N. Germain. “Modeling T cell antigen discrimination based on feedback control of digital ERK responses.” In: *PLoS biology* 3.11 (Nov. 2005), e356.

[103] P. Francois et al. “PNAS Plus: Phenotypic model for early T-cell activation displaying sensitivity, specificity, and antagonism”. In: *Proceedings of the National Academy of Sciences* (Feb. 2013).

[104] F. Wertek and C. Xu. “Digital response in T cells: to be or not to be.” In: *Cell research* 24.3 (2014), pp. 265–6.

[105] J. Das et al. “Digital Signaling and Hysteresis Characterize Ras Activation in Lymphoid Cells”. In: *Cell* 136.2 (2009), pp. 337–351. arXiv: NIHMS150003.

[106] M. Podtschaske et al. “Digital NFATc2 Activation per Cell Transforms Graded T Cell Receptor Activation into an All-or-None IL-2 Expression”. In: *PLoS ONE* 2.9 (2007), e935.

[107] M. N. Navarro et al. “Protein kinase D2 is a digital amplifier of T cell receptor-stimulated diacylglycerol signaling in naïve CD8fffd?fffd T cells.” In: *Science signaling* 7.348 (2014), ra99.

[108] J. Huang et al. “A Single peptide-major histocompatibility complex ligand triggers digital cytokine secretion in CD4+ T Cells”. In: *Immunity* 39.5 (2013), pp. 846–857.

[109] R. B. Fulton et al. “The TCR’s sensitivity to self peptide-MHC dictates the ability of naive CD8(+) T cells to respond to foreign antigens.” In: *Nature immunology* 16.1 (2015), pp. 107–17.

[110] J. Mandl et al. “T Cell-Positive Selection Uses Self-Ligand Binding Strength to Optimize Repertoire Recognition of Foreign Antigens”. In: *Immunity* 38 (2013), pp. 263–274.

[111] S. P. Persaud et al. “Intrinsic CD4+ T cell sensitivity and response to a pathogen are set and sustained by avidity for thymic and peripheral complexes of self peptide and MHC.” In: *Nature Immunology* 15.3 (2014), pp. 266–74. arXiv: NIHMS150003.

[112] K. A. Hogquist and S. C. Jameson. “The self-obsession of T cells: how TCR signaling thresholds affect fate decisions’ and effector function.” In: *Nature immunology* 15.9 (2014), pp. 815–23.

[113] K. H. Lee et al. “T cell receptor signaling precedes immunological synapse formation”. In: *Science* 295.February (2002), pp. 1539–1542.

[114] J. B. Huppa et al. “Continuous T cell receptor signaling required for synapse maintenance and full effector potential.” In: *Nature immunology* 4.8 (2003), pp. 749–55.

[115] R. Itoh, Y; Germain. “Single cell analysis reveals regulated hierarchical T cell antigen receptor signaling thresholds and intraclonal heterogeneity”. In: *The Journal of experimental medicine* 186.5 (1997).

[116] M. J. van Stipdonk, E. E. Lemmens, and S. P. Schoenberger. “Naïve CTLs require a single brief period of antigenic stimulation for clonal expansion and differentiation.” In: *Nature immunology* 2.5 (2001), pp. 423–429.

[117] C. Zimmermann, A. Pr, and C. Blaser. “Kinetics of the response of naive and memory CD8 T cells to antigen : similarities and differences”. In: *Eur J Immunol* 29 (1999), pp. 284–290.

[118] H. Veiga-Fernandes et al. “Response of naïve and memory CD8+ T cells to antigen stimulation in vivo.” In: *Nature immunology* 1.1 (2000), pp. 47–53.

[119] E. R. Mehlhop-Williams and M. J. Bevan. “Memory CD8+ T cells exhibit increased antigen threshold requirements for recall proliferation.” In: *The Journal of experimental medicine* 211.2 (2014), pp. 345–56.

[120] S. Okasha. “Emergence, hierarchy and top-down causation in evolutionary biology”. In: *Interface Focus* 2.August 2011 (2012), pp. 49–54.

[121] D. T. Campbell. “11.’Downward Causation’in Hierarchically Organised Biological Systems”. In: *Studies in the Philosophy of Biology: Reduction and Related Problems* (1974), p. 179.

[122] L. H. Hartwell et al. “From molecular to modular cell biology.” In: *Nature* 402.December (1999), pp. C47–C52.

[123] L. J. Old. “A testicular antigen aberrantly expressed in human cancers detected by autologous antibody screening”. In: *Proceedings of the National Academy of S* 94.March (1997), pp. 1914–1918.

[124] M. Aleksic et al. “Dependence of T cell antigen recognition on T cell receptor-peptide MHC confinement time.” In: *Immunity* 32.2 (Feb. 2010), pp. 163–74.

[125] J. M. Boulter et al. “Stable, soluble T-cell receptor molecules for crystallization and therapeutics”. In: *Protein Engineering Design and Selection* 16.9 (Sept. 2003), pp. 707–711.

[126] C. Berrevoets and Á. Szöor. “TCRs Genetically Linked to CD28 and CD3 ϵ Do Not Mispair with Endogenous TCR Chains and Mediate Enhanced T Cell Persistence and Anti-Melanoma Activity”. In: (2014).

[127] Y.-l. Chiu et al. “Sprouty-2 regulates HIV-specific T cell polyfunctionality”. In: 124.1 (2014), pp. 1–11.

[128] H. A. van den Berg et al. “Coreceptor CD8-driven modulation of T cell antigen receptor specificity.” In: *Journal of theoretical biology* 249.2 (Nov. 2007), pp. 395–408.

[129] M. Krogsgaard et al. “Evidence that structural rearrangements and/or flexibility during TCR binding can contribute to T cell activation.” In: *Molecular cell* 12.6 (Dec. 2003), pp. 1367–78.

[130] T. Ueno et al. “Functionally Impaired HIV-Specific CD8 T Cells Show High Affinity TCR-Ligand Interactions”. In: *The Journal of Immunology* 173.9 (Oct. 2004), pp. 5451–5457.

[131] E. Corse et al. “Attenuated T cell responses to a high-potency ligand in vivo.” In: *PLoS biology* 8.9 (Jan. 2010), pp. 1–12.

[132] J. D. Stone et al. “Opposite effects of endogenous peptide-MHC class I on T cell activity in the presence and absence of CD8.” In: *Journal of immunology (Baltimore, Md. : 1950)* 186.9 (May 2011), pp. 5193–200.

[133] C. C. Govern et al. “Fast on-rates allow short dwell time ligands to activate T cells”. In: *Proceedings of the N* (2010), pp. 1–6.

[134] S. Zhong et al. “T-cell receptor affinity and avidity defines antitumor response and autoimmunity in T-cell immunotherapy”. In: *Proceedings of the National Academy of Sciences* (Apr. 2013).

[135] R. H. McMahan et al. “Relating TCR-peptide-MHC affinity to immunogenicity for the design of tumor vaccines”. In: 116.9 (2006), pp. 2543–2551.

[136] M. Chmielewski et al. “T cell activation by antibody-like immunoreceptors: increase in affinity of the single-chain fragment domain above threshold does not increase T cell activation against antigen-positive target cells but decreases selectivity.” In: *Journal of immunology (Baltimore, Md. : 1950)* 173 (2004), pp. 7647–7653.

[137] R. Wolchinsky et al. “Antigen-Dependent Integration of Opposing Proximal TCR-Signaling Cascades Determines the Functional Fate of T Lymphocytes.” In: *Journal of immunology (Baltimore, Md. : 1950)* (Jan. 2014).

[138] D. Coombs et al. “Activated TCRs remain marked for internalization after dissociation from pMHC”. In: *Nature Immunology* 3.10 (2002), pp. 926–931.

[139] S. Valitutti, S. Müller, and M. Cella. “Serial triggering of many T-cell receptors by a few peptide MHC complexes”. In: *Nature* (1995).

[140] H. A. Van Den Berg, D. A. Rand, and N. J. Burroughs. “A reliable and safe T cell repertoire based on low-affinity T cell receptors.” In: *Journal of theoretical biology* 209.4 (Apr. 2001), pp. 465–86.

[141] N. J. Burroughs, Z. Lazic, and P. A. van der Merwe. “Ligand detection and discrimination by spatial relocalization: A kinase-phosphatase segregation model of TCR activation.” In: *Biophysical journal* 91.5 (Sept. 2006), pp. 1619–29.

[142] O. Dushek and D. Coombs. “Analysis of serial engagement and peptide-MHC transport in T cell receptor microclusters.” In: *Biophysical journal* 94.9 (May 2008), pp. 3447–60.

[143] S. Valitutti and A. Lanzavecchia. “Serial triggering of TCRs: A basis for the sensitivity and specificity of antigen recognition”. In: *Immunology Today* 18.1993 (1997), pp. 299–304.

[144] C. Wofsy, D. Coombs, and B. Goldstein. “Calculations show substantial serial engagement of T cell receptors.” In: *Biophysical journal* 80.February (2001), pp. 606–612.

[145] I. Stefanová et al. “TCR ligand discrimination is enforced by competing ERK positive and SHP-1 negative feedback pathways.” In: *Nature immunology* 4.3 (Mar. 2003), pp. 248–54.

[146] Q. J. Li et al. “miR-181a Is an Intrinsic Modulator of T Cell Sensitivity and Selection”. In: *Cell* 129 (2007), pp. 147–161.

[147] D. C. Wylie, J. Das, and A. K. Chakraborty. “Sensitivity of T cells to antigen and antagonism emerges from differential regulation of the same molecular signaling module.” In: *Proceedings of the National Academy of Sciences of the United States of America* 104.13 (Mar. 2007), pp. 5533–8.

[148] T. Lipniacki et al. “Stochastic effects and bistability in T cell receptor signaling.” In: *Journal of theoretical biology* 254.1 (Sept. 2008), pp. 110–22.

[149] P. Francois et al. “Phenotypic model for early T-cell activation displaying sensitivity, specificity, and antagonism”. In: *Proceedings of the National Academy of Sciences* (Feb. 2013).

[150] D. S. Lyons et al. “A TCR binds to antagonist ligands with lower affinities and faster dissociation rates than to agonists.” In: *Immunity* 5.1 (July 1996), pp. 53–61.

[151] C. Koniaras et al. “Inhibition of naïve class I-restricted T cells by altered peptide ligands.” In: *Immunology and cell biology* 77.4 (Aug. 1999), pp. 318–23.

[152] L. J. Carreño et al. “T-cell antagonism by short half-life pMHC ligands can be mediated by an efficient trapping of T-cell polarization toward the APC.” In: *Proceedings of the National Academy of Sciences of the United States of America* 107.1 (Jan. 2010), pp. 210–5.

[153] P. P. Yachi et al. “T cell activation enhancement by endogenous pMHC acts for both weak and strong agonists but varies with differentiation state.” In: *The Journal of Experimental Medicine* 204.11 (Oct. 2007), pp. 2747–57.

[154] M. Krogsgaard, J. Juang, and M. M. Davis. “A role for fffdselfffffd in T-cell activation”. In: *Semin Immunol.* 19.4 (2009), pp. 236–244.

[155] J. Sloan-Lancaster et al. “Partial T cell signaling: altered phospho-zeta and lack of zap70 recruitment in APL-induced T cell anergy.” In: *Cell* 79.5 (Dec. 1994), pp. 913–22.

[156] J. Madrenas et al. “Zeta phosphorylation without ZAP-70 activation induced by TCR antagonists or partial agonists.” In: *Science (New York, N.Y.)* 267.5197 (Jan. 1995), pp. 515–8.

[157] J. Madrenas et al. “The efficiency of CD4 recruitment to ligand-engaged TCR controls the agonist/partial agonist properties of peptide-MHC molecule ligands.” In: *The Journal of experimental medicine* 185.2 (Jan. 1997), pp. 219–29.

[158] S. H. Stotz et al. “T cell receptor (TCR) antagonism without a negative signal: evidence from T cell hybridomas expressing two independent TCRs.” In: *The Journal of experimental medicine* 189.2 (Jan. 1999), pp. 253–64.

[159] M. A. Daniels et al. “Cutting edge: a test of the dominant negative signal model for TCR antagonism.” In: *Journal of immunology (Baltimore, Md. : 1950)* 162.7 (Apr. 1999), pp. 3761–4.

[160] E. N. Kersh, G. J. Kersh, and P. M. Allen. “Partially phosphorylated T cell receptor zeta molecules can inhibit T cell activation.” In: *The Journal of experimental medicine* 190.11 (Dec. 1999), pp. 1627–36.

[161] A. Viola and A. Lanzavecchia. “T cell activation determined by T cell receptor number and tunable thresholds.” In: *Science (New York, N.Y.)* 273.5271 (July 1996), pp. 104–6.

[162] J. Das et al. “Digital signaling and hysteresis characterize ras activation in lymphoid cells.” In: *Cell* 136.2 (Jan. 2009), pp. 337–51.

[163] H. a. van den Berg et al. “Cellular-level versus receptor-level response threshold hierarchies in T-cell activation.” In: *Frontiers in immunology* 4.September (Jan. 2013), p. 250.

[164] J. J. Tyson, K. C. Chen, and B. Novák. “Sniffers, buzzers, toggles and blinkers: Dynamics of regulatory and signaling pathways in the cell”. In: *Current Opinion in Cell Biology* 15 (2003), pp. 221–231.

[165] K. E. Tkach et al. “T cells translate individual, quantal activation into collective, analog cytokine responses via time-integrated feedbacks”. In: *eLife* 2014 (2014), pp. 1–30.

[166] J. Gunawardena. “Multisite protein phosphorylation makes a good threshold but can be a poor switch.” In: *Proceedings of the National Academy of Sciences of the United States of America* 102.41 (Oct. 2005), pp. 14617–22.

[167] M. Chmielewski et al. “T cell activation by antibody-like immunoreceptors: increase in affinity of the single-chain fragment domain above threshold does not increase T cell activation against antigen-positive target cells but decreases selectivity.” In: *Journal of immunology (Baltimore, Md. : 1950)* 173 (2004), pp. 7647–7653.

[168] R. N. Germain and I. Stefanov. “The dynamics of T cell receptor signalling : Complex Orchestration and the Key Roles”. In: *Annual Reviews Immunology* (1999), pp. 467–522.

[169] E. Jäger et al. “Simultaneous humoral and cellular immune response against cancer-testis antigen NY-ESO-1: definition of human histocompatibility leukocyte antigen (HLA)-A2-binding peptide epitopes.” In: *The Journal of experimental medicine* 187.2 (1998), pp. 265–270.

[170] J. L. Chen et al. “Identification of NY-ESO-1 peptide analogues capable of improved stimulation of tumor-reactive CTL.” In: *Journal of immunology (Baltimore, Md. : 1950)* 165.2 (July 2000), pp. 948–55.

[171] J.-L. Chen et al. “Structural and kinetic basis for heightened immunogenicity of T cell vaccines.” In: *The Journal of experimental medicine* 201.8 (Apr. 2005), pp. 1243–55.

[172] S. Bownds et al. “Induction of tumor-reactive cytotoxic T-lymphocytes using a peptide from NY-ESO-1 modified at the carboxy-terminus to enhance HLA-A2.1 binding affinity and stability in solution.” In: *Journal of immunotherapy (Hagerstown, Md. : 1997)* 24.1 (2001), pp. 1–9.

[173] A. I. Webb et al. “Functional and structural characteristics of NY-ESO-1-related HLA A2-restricted epitopes and the design of a novel immunogenic analogue”. In: *Journal of Biological Chemistry* 279.22 (2004), pp. 23438–23446.

[174] E. McCormack et al. “Bi-specific TCR-anti CD3 redirected T-cell targeting of NY-ESO-1- and LAGE-1-positive tumors.” In: *Cancer immunology, immunotherapy : CII* 62.4 (Apr. 2013), pp. 773–85.

[175] M. A. Purbhoo et al. “Quantifying and imaging NY-ESO-1/LAGE-1-derived epitopes on tumor cells using high affinity T cell receptors.” In: *Journal of immunology (Baltimore, Md. : 1950)* 176 (2006), pp. 7308–7316.

[176] G. Stewart-Jones et al. “Rational development of high-affinity T-cell receptor-like antibodies”. In: *Proceedings of the National Academy of Sciences* 106.14 (2009), pp. 5784–5788.

[177] M. Sami et al. “Crystal structures of high affinity human T-cell receptors bound to peptide major histocompatibility complex reveal native diagonal binding geometry.” In: *Protein engineering, design & selection : PEDS* 20.8 (Aug. 2007), pp. 397–403.

[178] H. a. Young and K. J. Hardy. “Role of interferon-gamma in immune cell regulation.” In: *Journal of Leukocyte Biology* 58.October (1995), pp. 373–381.

[179] K. Schroder et al. “Interferon-γ: an overview of signals, mechanisms and functions”. In: *Journal of Leukocyte Biology* 75.2 (2004), pp. 163–189.

[180] M. Maurer and E. Von Stebut. “Macrophage inflammatory protein-1”. In: *International Journal of Biochemistry and Cell Biology* 36 (2004), pp. 1882–1886.

[181] C. Cells et al. “Identification the Major HIV-Suppressive Factors Produced by”. In: *Science* (1987).

[182] P. Menten, A. Wuyts, and J. Van Damme. “Macrophage inflammatory protein-1.” In: *Cytokine & growth factor reviews* 13 (2002), pp. 455–481.

[183] R. R. Bartelt et al. “Comparison of T cell receptor-induced proximal signaling and downstream functions in immortalized and primary T cells.” In: *PloS one* 4.5 (Jan. 2009), e5430.

[184] E. Hoffmann et al. “Multiple control of interleukin-8 gene expression.” In: *Journal of Leukocyte Biology* 72.November (2002), pp. 847–855.

[185] I. Vermes et al. “A novel assay for apoptosis. Flow cytometric detection of phosphatidylserine expression on early apoptotic cells using fluorescein labelled Annexin V”. In: *Journal of Immunological Methods* 184.95 (1995), pp. 39–51.

[186] L. Wooldridge et al. “Tricks with tetramers: how to get the most from multimeric peptide-MHC.” In: *Immunology* 126.2 (Mar. 2009), pp. 147–64.

[187] M. Hebeisen et al. “SHP-1 phosphatase activity counteracts increased T cell receptor affinity”. In: *The Journal of Clinical Investigation* 123.3 (2013).

[188] P. P. Yachi et al. “Nonstimulatory peptides contribute to antigen-induced CD8-T cell receptor interaction at the immunological synapse.” In: *Nature immunology* 6.8 (Aug. 2005), pp. 785–92.

[189] H. Liu et al. “On the dynamics of TCR:CD3 complex cell surface expression and downmodulation.” In: *Immunity* 13.5 (Nov. 2000), pp. 665–75.

[190] U. Alon. “Network motifs: theory and experimental approaches.” In: *Nature Reviews. Genetics* 8.June (2007), pp. 450–461.

[191] D. Kim, Y. K. Kwon, and K. H. Cho. “The biphasic behavior of incoherent feed-forward loops in biomolecular regulatory networks”. In: *BioEssays* 30 (2008), pp. 1204–1211.

[192] S.-H. Chen et al. “Incoherent feed-forward regulatory logic underpinning glucocorticoid receptor action.” In: *Proceedings of the National Academy of Sciences of the United States of America* 110.5 (2013), pp. 1964–9.

[193] S. S. Shen-Orr et al. “Network motifs in the transcriptional regulation network of Escherichia coli.” In: *Nature genetics* 31.April (2002), pp. 64–68.

[194] K. Takeda et al. “Incoherent Feedforward Control Governs Adaptation of Activated Ras in a Eukaryotic Chemotaxis Pathway”. In: *Science Signaling* 5.205 (2012), ra2–ra2.

[195] R. Entus, B. Aufderheide, and H. M. Sauro. “Design and implementation of three incoherent feed-forward motif based biological concentration sensors”. In: *Systems and Synthetic Biology* 1 (2007), pp. 119–128.

[196] S. Kaplan et al. “The incoherent feed-forward loop can generate non-monotonic input functions for genes.” In: *Molecular systems biology* 4.203 (2008), p. 203.

[197] F. G. Tadesse et al. “Unpredicted phenotypes of two mutants of the TcR DMF5”. In: *Journal of Immunological Methods* (2015).

[198] P. E. Love and S. M. Hayes. “ITAM-mediated Signaling by the T-Cell Antigen Receptor”. In: (2010), pp. 1–11.

[199] P. D. Holler et al. “CD8(-) T cell transfectants that express a high affinity T cell receptor exhibit enhanced peptide-dependent activation.” In: *The Journal of experimental medicine* 194.8 (2001), pp. 1043–1052.

[200] M. Naramura et al. “c-Cbl and Cbl-b regulate T cell responsiveness by promoting ligand-induced TCR down-modulation”. In: 3.12 (2002).

[201] D. Escors et al. “On the Mechanism of T cell receptor down-modulation and its physiological significance.” In: 1.1 (2011), pp. 1–9.

[202] U. Lorenz. “SHP-1 and SHP-2 in T cells: two phosphatases functioning at many levels.” In: *Immunological reviews* 228.1 (Mar. 2009), pp. 342–59.

[203] W. Paster et al. “A THEMIS : SHP 1 complex promotes T-cell survival”. In: 34.3 (2015), pp. 393–409.

[204] C. L. Poirel et al. “Top-Down Network Analysis to Drive Bottom-Up Modeling of Physiological Processes”. In: *Journal of Computational Biology* 20.5 (2013), pp. 409–418.

[205] J. J. Hornberg et al. “Cancer: A Systems Biology disease”. In: *BioSystems* 83 (2006), pp. 81–90.

[206] F. J. Bruggeman and H. V. Westerhoff. “The nature of systems biology”. In: *Trends in Microbiology* 15.1 (2007), pp. 45–50.

[207] W. Ma et al. “Defining network topologies that can achieve biochemical adaptation.” In: *Cell* 138.4 (Aug. 2009), pp. 760–73.

[208] O. Brandman et al. “Interlinked fast and slow positive feedback loops drive reliable cell decisions.” In: *Science (New York, N.Y.)* 310.October (2005), pp. 496–498.

[209] T. Y.-C. Tsai et al. “Robust, tunable biological oscillations from interlinked positive and negative feedback loops”. In: *Science* 321.5885 (2008), pp. 126–129.

[210] H. Mayer, K. S. Zaenker, and U. An Der Heiden. “A basic mathematical model of the immune response.” In: *Chaos (Woodbury, N.Y.)* 5.1995 (1995), pp. 155–161.

[211] D. M. Hawkins. “The Problem of Overfitting”. In: *Journal of Chemical Information and Computer Sciences* 44 (2004), pp. 1–12.

[212] B. Novák and J. J. Tyson. *Modeling the Cell Division Cycle: M-phase Trigger, Oscillations, and Size Control*. 1993.

[213] J. J. Tyson and B. Novák. “Models in biology: lessons from modeling regulation of the eukaryotic cell cycle”. In: *BMC Biology* 13 (2015), p. 46.

[214] A. Goldbeter and D. E. Koshland. “An amplified sensitivity arising from covalent modification in biological systems.” In: *Proceedings of the National Academy of Sciences of the United States of America* 78.11 (1981), pp. 6840–6844.

[215] C. Y. Huang and J. E. Ferrell. “Ultrasensitivity in the mitogen-activated protein kinase cascade.” In: *Proceedings of the National Academy of Sciences of the United States of America* 93.September (1996), pp. 10078–10083.

[216] J. J. Tyson and B. Novák. “Functional motifs in biochemical reaction networks.” In: *Annual Review of physical chemistry* 61 (Mar. 2010), pp. 219–40.

[217] U. Alon et al. “Robustness in bacterial chemotaxis.” In: *Nature* 397.January (1999), pp. 168–171.

[218] A. Hoffmann et al. “The IkappaB-NF-kappaB signaling module: temporal control and selective gene activation.” In: *Science (New York, N.Y.)* 298.December (2002), pp. 1241–1245.

[219] J. J. Tyson, A. Csikasz-Nagy, and B. Novák. “The dynamics of cell cycle regulation”. In: *BioEssays* 24 (2002), pp. 1095–1109.

[220] M. Hebeisen and L. Baitsch. “SHP-1 phosphatase activity counteracts increased T cell receptor affinity”. In: *The Journal of clinical ...* (2013).

[221] M. Aleksic et al. “Different affinity windows for virus and cancer-specific T-cell receptors: Implications for therapeutic strategies”. In: *European Journal of Immunology* 42.12 (2012), pp. 3174–3179. arXiv: NIHMS150003.

[222] J. Oates, N. J. Hassan, and B. K. Jakobsen. “ImmTACs for targeted cancer therapy: Why, what, how, and which”. In: *Molecular Immunology* (2015), pp. 1–8.

[223] N. P. Restifo, M. E. Dudley, and S. a. Rosenberg. “Adoptive immunotherapy for cancer: harnessing the T cell response.” In: *Nature Reviews. Immunology* 12.4 (Jan. 2012), pp. 269–81.

[224] S. Srivastava and S. R. Riddell. “Engineering CAR-T Cells: Design Concepts”. In: *Trends in Immunology* signal 1 (2015), pp. 1–9.

[225] M. Sadelain, R. Brentjens, and I. Rivière. “The promise and potential pitfalls of chimeric antigen receptors”. In: *Current Opinion in Immunology* 21 (2009), pp. 215–223.

[226] M. Chmielewski et al. “T cell activation by antibody-like immunoreceptors: increase in affinity of the single-chain fragment domain above threshold does not increase T cell activation against antigen-positive target cells but decreases selectivity”. In: *The Journal of Immunology* 173.12 (2004), pp. 7647–7653.

[227] R. Oren et al. “Functional Comparison of Engineered T Cells Carrying a Native TCR versus TCR-like Antibody-Based Chimeric Antigen Receptors Indicates Affinity/Avidity Thresholds”. In: *The Journal of Immunology* 193 (2014), pp. 5733–5743.

[228] S. Thomas et al. “Human T cells expressing affinity-matured TCR display accelerated responses but fail to recognize low density of MHC-peptide antigen.” In: *Blood* 118.2 (July 2011), pp. 319–29.

[229] K. N. Pollizzi and J. D. Powell. “Regulation of T cells by mTOR: the known knowns and the known unknowns.” In: *Trends in immunology* 36.1 (2015), pp. 13–20.

[230] B. Malissen and P. Bongrand. “Early T Cell Activation: Integrating Biochemical, Structural, and Biophysical Cues”. In: *Annual Review of Immunology* 33 (2015), pp. 539–561.

[231] S. M. Kaech and R. Ahmed. “Memory CD8+ T cell differentiation: initial antigen encounter triggers a developmental program in naïve cells.” In: *Nature immunology* 2.5 (2001), pp. 415–22. arXiv: NIHMS150003.

[232] M. K. Slifka and J. L. Whitton. “Functional avidity maturation of CD8(+) T cells without selection of higher affinity TCR.” In: *Nature immunology* 2.8 (Aug. 2001), pp. 711–7.